The Thesis Committee for Luis Enrique Arce Perez
Certifies that this is the approved version of the following thesis:

Neogene Current-Modified Submarine Fans and Associated Bed Forms in Mexican Deep-water Areas

APPROVED BY
SUPERVISING COMMITTEE:

Co-Supervisor:

John W. Snedden

Co-Supervisor:

William L. Fisher

Richard J. Chuchla

Neogene Current-Modified Submarine Fans and Associated Bed Forms in Mexican Deep-water Areas

by

Luis Enrique Arce Perez, B.E.

Thesis

Presented to the Faculty of the Graduate School of

The University of Texas at Austin

in Partial Fulfillment

of the Requirements

for the Degree of

Master of Science in Energy and Earth Resources

The University of Texas at Austin

May 2017

Dedication

To my mother, father and brother.

Acknowledgements

I would first like to thank my advisor Dr. John W. Snedden, for his patience, encouragement, his endless help and being an outstanding advisor. He consistently allowed this paper to be my own work, but steered me in the right direction whenever he thought I needed it. He also has been a source of inspiration as geoscientist.

Thanks to my co-advisor, Dr. William L. Fisher for his support during the master's program and for being a role model. I would also like to acknowledge Mr. Richard J. Chuchla for his valuable comments on this thesis.

I also thank all the members of the Gulf Basin Depositional Synthesis (GBDS) Industrial Associates research project for their support during my graduate education. I especially thank Jon Virdell for helping me create many images for this thesis. I also appreciate Patricia Ganey-Curry for her comments on this thesis and other graduate students Jie Xu, Luciana de la Rocha, and Mario Gutierrez for their support and making me feel at home in this group.

PGS and ION provided seismic data used in this study, which were key element for this thesis. I particularly appreciate the supporting efforts of Don Herron (PGS) who facilitated measurement of bedform dimensions and the PGS data access overall.

Finally, I must express my very profound gratitude to my parents and brother for providing me with unfailing support and continuous encouragement throughout my years of study and through the process of researching and writing this thesis. This accomplishment would not have been possible without them. Thank you.

Abstract

Neogene Current-Modified Submarine Fans and Associated Bed Forms in Mexican Deep-water Areas

Luis Enrique Arce Perez, M.S.E.E.R.

The University of Texas at Austin, 2017

Supervisors: John W. Snedden
William L. Fisher

The Mexico's Gulf of Mexico Neogene record reflects the dynamic interaction between high rates of sedimentation and tectonic processes. Distinctive Pliocene to Miocene-age shingled seismic clinoforms reflections were identified in a previous study using older data and interpreted as contourite drift deposits located east of the Mexican Ridges in paleowater depths exceeding 400 meters. The database for this thesis includes new and recently reprocessed seismic data, well logs and core information. Large scale bedforms with seaward-dipping accretion sets (SDAS) are documented in several geobodies mapped in the study area.

The objectives of this research are to evaluate the paleogeographic evolution of the southwestern Gulf of Mexico and deepwater systems during Neogene, evaluating several hypotheses for development of these unique SDAS deepwater bedforms, placing observations in a regional context, and interpreting likely sediment sources and transport pathways.

The SDAS were present in four geobodies, two of Upper Miocene (UM) age, one in the Mio-Pliocene (PL1) and another in the Pliocene (PGa) genetic sequence. Time structure maps show progressive infill of the deep-water Veracruz Trough from the southwest. Isochron maps show individual SDAS geobodies thinning basinwards, paralleling trends of adjacent submarine fans. The geobodies were likely formed during an episode of high precipitation and river discharge, modulated by tectonics, and a steep slope that may have allowed frequent bypass of sediments to the basin. SDAS show a series of internal structures climbing upward and landward that are interpreted as cyclic steps bedforms deposited by high-velocity, supercritical turbidity flows. Geobody 2 is associated with an adjacent channel complex and may be a product of unconfined, levee overbanking flows. Other geobodies are associated with submarine fan mounds.

The Mexican Ridges foldbelt may have steered southerly longshore and along slope flow into the nearby Cañonero Canyon, then diverting turbidity flows to the east. The early forming Mexican Ridges may also have created a steep slope gradient and bottom roughness that facilitated local development of hydraulic jumps, a prerequisite for generation of cyclic steps bedforms. Identification of these unusual bedforms in Pliocene and Miocene strata of deepwater Mexico represents one of first documented occurrence in subsurface settings.

Table of Contents

List of Tables

List of Figures

CHAPTER 1: INTRODUCTION

Overview

The Mexican Gulf of Mexico is one of the most tectonically and sedimentologically complex areas in the world. Multiple tectonics events have created a diverse set of structural trends. Convergence of the North American, Caribbean and Cocos plates has continued in this region since the Late Oligocene (Moran-Zenteno et al., 2000). The Gulf of Mexico basin also has been marked by high rates of sedimentation and subsidence accompanied with long term accommodation. The Neogene basin record therefore reflects a dynamic interaction of tectonic and sedimentary processes which are driven not only by local tectonics but also by the larger scale regional tectonics.

This study is designed to contribute to the overall understanding of the Gulf of Mexico, one of the most prominent hydrocarbon bearing basins in the world. Recent Mexican Energy Reform has increased interest in this area, with new seismic data acquired that a form a large part of the database used to interpret the Neogene geologic history in the study area.

The goal of this thesis is to investigate the deep marine sedimentary evolution of a lightly explored frontier area located in deep waters of the southwestern Gulf of Mexico. The main stratigraphic intervals studied are the Miocene and Pliocene; other stratigraphic intervals above and below are also included in some stages of the project in order to constrain interpreted evolutionary patterns.

My database includes new and recently reprocessed seismic data, well logs and core information for systematic analysis of a series of large, seaward dipping accretion sets (SDAS) in this deep-water system located east of the Mexican Ridges (Figure 1.1). What is unknown is the extension and geometry of these SDAS geobodies and the

sedimentological processes that that may have caused deposition of these unique geobodies.

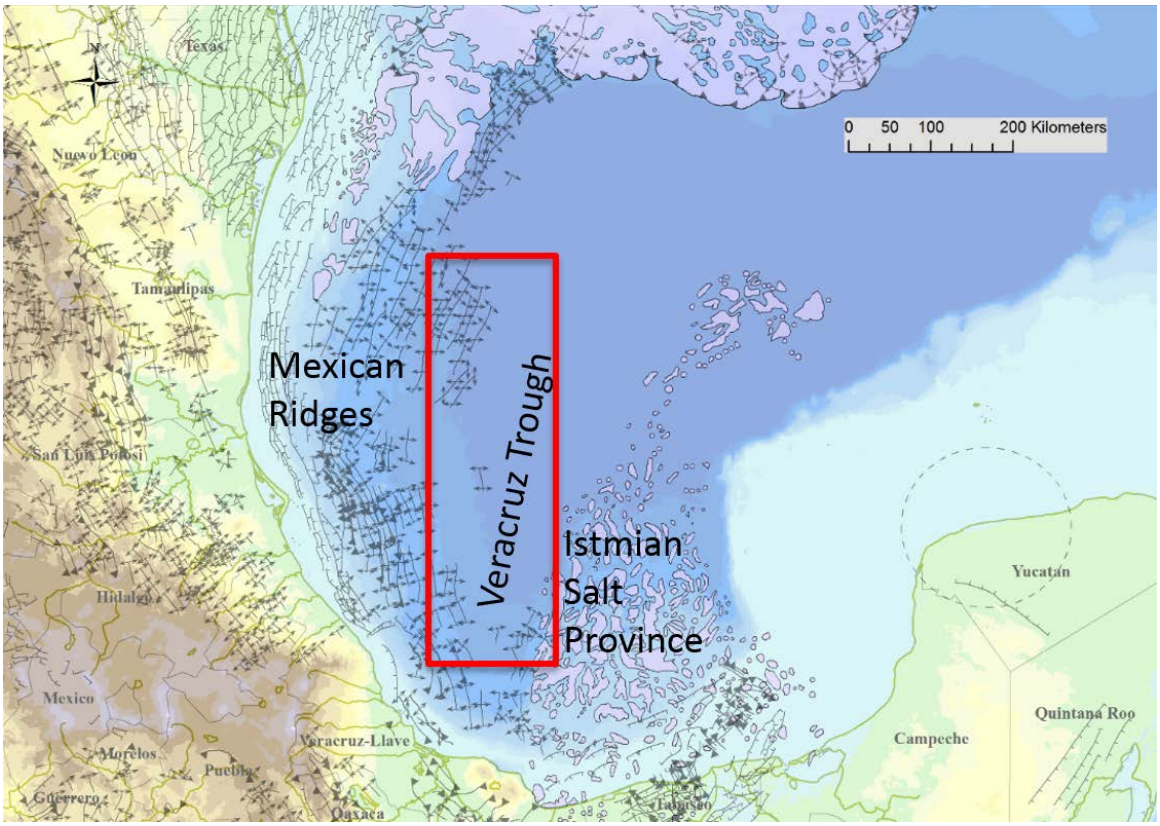

Figure 1.1. Location of the study area. (Modified from Padilla, 2007)

In detail, this study includes a new seismic facies scheme for the Miocene-Pliocene of the study area and a map of the extent of those seismic facies geobodies. Development of a sequence stratigraphic framework will illuminate external and internal controls on the architecture of these deep water depositional sequences. These are placed into a regional to basin-scale context including considerations of possible sediment provenance, tectonic, and climatic influences. A modern analog (Sea of Japan) representing a high relief, high precipitation system is also discussed.

This research is important not only to understand more about a frontier area in the southern Gulf of Mexico but also the Miocene-Pliocene timeframe, a key transitional phase in the earth's history. The role of the changes in bottom water flow during progressive closure of the equatorial seaway separating North and South America will also be discussed. The relationship to high density turbidity flows and associated landward accreting bed forms and cyclic steps (Cartigny et al., 2011) is also considered.

Geologic Background

The Gulf of Mexico basin has undergone a long and complex tectonic and depositional evolution since it began in the Late Triassic as part of the breakup of the supercontinent Pangea (Figure 1.2A). The general structural framework of the southwestern Gulf of Mexico comprises four main stages:

1) Rifting and post-salt crustal stretching from 210 to 155 Ma, Late Triassic to Late Jurassic. In this stage, rifting between the North American plate and the Yucatan microplate resulted in tectonically active basins that were initially filled by syn-rift continental fluvial and lacustrine red beds and volcanic rocks (Salvador, 1987). The Gulf of Mexico salt was deposited between 170 and 156 Ma ago (Figures 1.2B, 3A) followed by a post salt crustal stretching (Figures 1.2C, 3B) phase that in turn was succeeded by the continental rifting that continued for another 7 to 12 m.y. (Hudec et al., 2013).

2) Sea floor spreading from 155 to 137 Ma, Late Jurassic to Early Cretaceous. During Jurassic opening of the Gulf of Mexico, sea floor spreading caused separation of the salt into two major provinces (Louann and Campeche Isthmian Salt). Oceanic crust emplacement started first in the east and west of the basin and then the center separated

Figure 2D, E). This was followed immediately by a period of subsidence due to oceanic crustal cooling (Figures 3C, D; Hudec et al. 2013).

3) Laramide shortening from the Late Cretaceous to the Middle Eocene. During the Late Cretaceous, an acceleration of the Farallon Plate subduction beneath the North American plate set up thin skin deformation in Mexico, resulting in the uplift of the Sierra Madre Oriental (Guzman and Cserna 1963). This Hidalgoan tectonic event, as is called in Mexico, changed sedimentation from carbonate to terrigenous siliciclastic as large volumes of siliciclastics were transported by active fluvial systems into the southern Gulf of Mexico. On the nearby Yucatan block, carbonate sedimentation, however, continued uninterrupted. The Hidalgoan deformation continued until Middle Miocene and migrated progressively from west to east. Deposition east of the Sierra Madre Oriental was in developing foreland basins along the present leading edge of the fold belt in the Parras-San Carlos, Tampico-Misantla and Veracruz basins (Cserna, 1989). Volcanic activity in western Mexico increased during this period (Padilla, 2007).

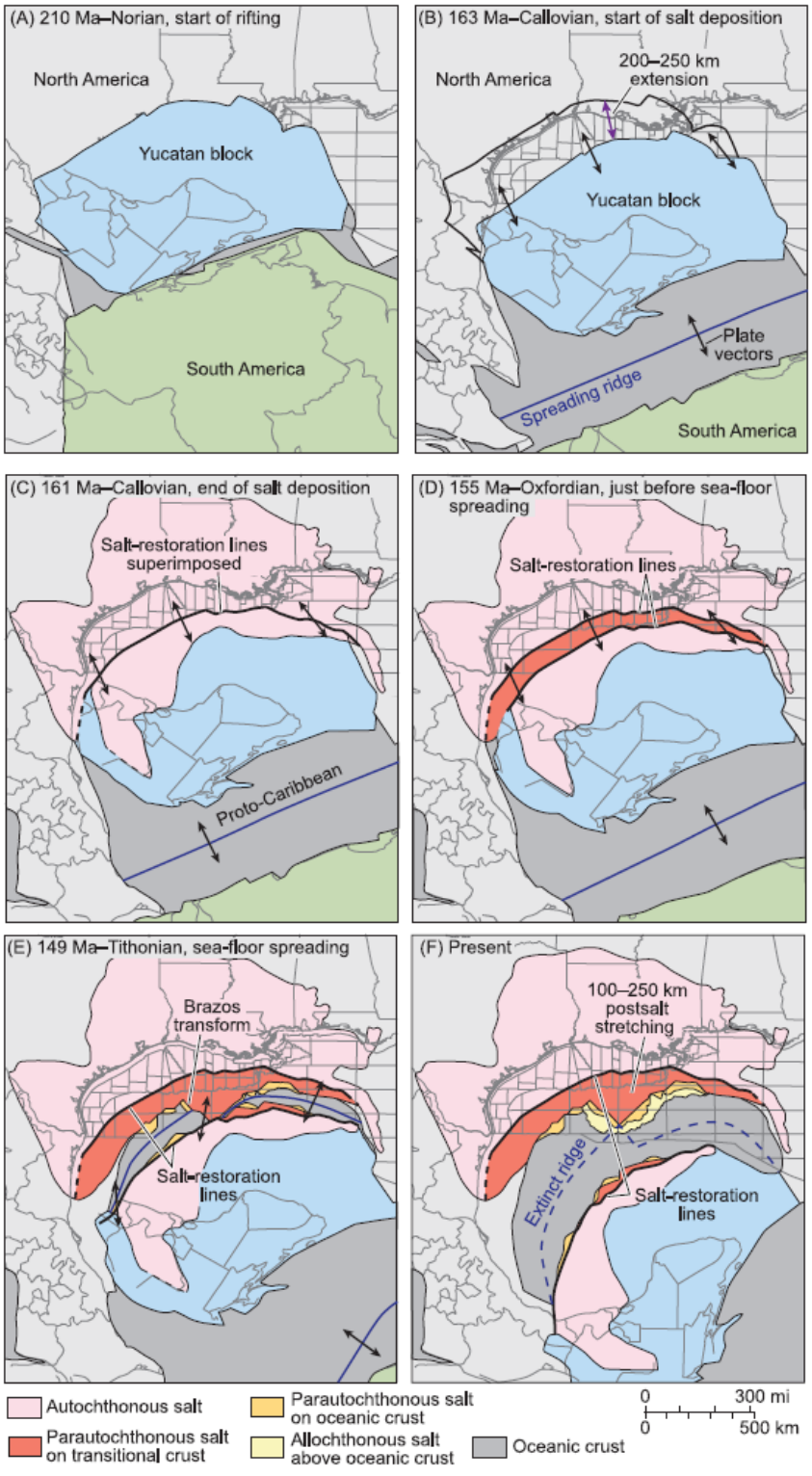

Figure 1.2. Sequential plate restoration from Hudec et al., 2013.

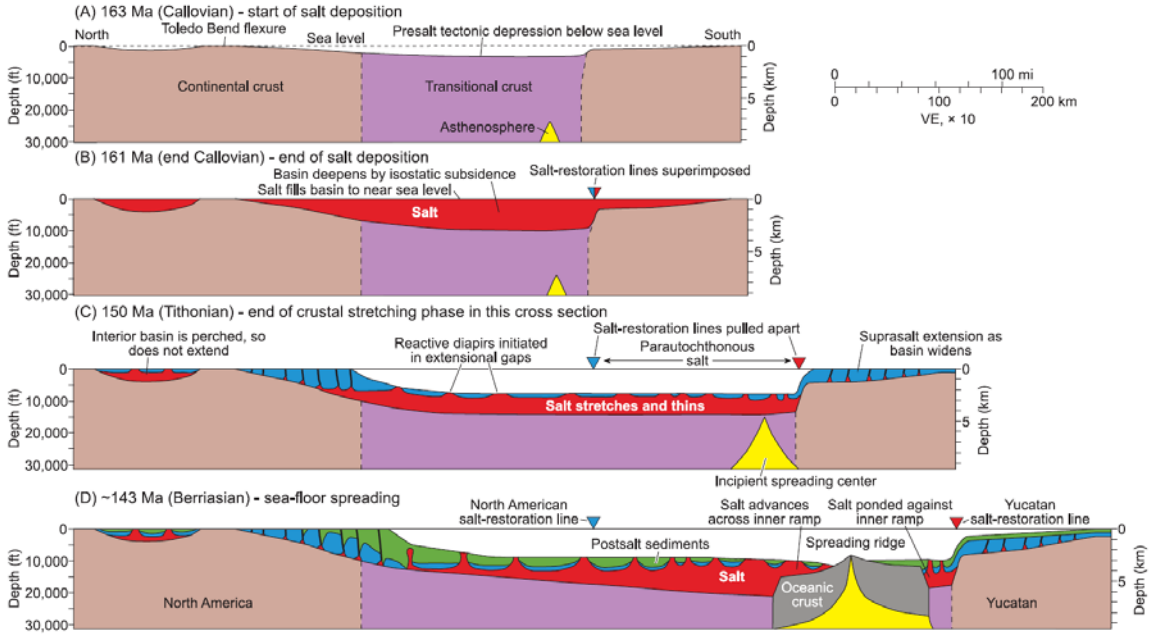

Figure 1.3. Schematic section restoration of basin evolution. (Hudec et al., 2013).

4) Late Eocene to the present day post-orogenic and divergent margin development, (Figure 1.2F). The post-orogenic stage started as a decrease of relative motion between North American and Caribbean plate, resulting in development of rapidly subsiding basins that were filled with detritus supplied from local uplifts (Padilla, 2007). This was sediment-load driven subsidence that resulted from the uplift and denudation of the Laramide fold and thrust belt onshore to the west of the present day divergent margin (Vazquez-Meneses, 2005).

At nearly the same time, southeastern Mexico was strongly influenced by the migration of the Chortis Block in the Chiapas region, accompanied by development of volcanism, contraction and lateral faulting. Displacement of the Chortis Block was driven by eastward magmatic migration along the Pacific margin. The oldest magmatic record around the Southwestern Gulf of Mexico is the volcanic and plutonic rocks of the Sierra Madre del Sur during the Oligocene. Then there is a time gap between the magmatism of

the Sierra Madre del Sur and the Trans-Mexican Volcanic Belt. This is thought to be a response to the geometry of the subducted plate, related to migration of a triple junction trench-trench-transform that accompanied the movement of the Chortis Block (Schaaf et al., 1995).

During Middle Miocene, the Trans-Mexican Volcanic Belt (TMVB) was established as an independent tectonic province (Ferrari et al., 2012), as a result of the counterclockwise rotation of the volcanic axis from the NNW-oriented Oligocene Sierra Madre Occidental (SMO). The geologic evolution of the TMVB has been divided into four main episodes (Figure 1.4).

1) Early to mid-Miocene, initiation of a volcanic arc of intermediate composition.

2) A late Miocene episode of eastward migration mafic volcanism located at the north of the previous arc.

3) Latest Miocene and early Pliocene time volcanism changed along the arc to more bimodal composition and started to migrate toward the trench.

4) Late Pliocene and Pleistocene development of an arc with variable composition magmas.

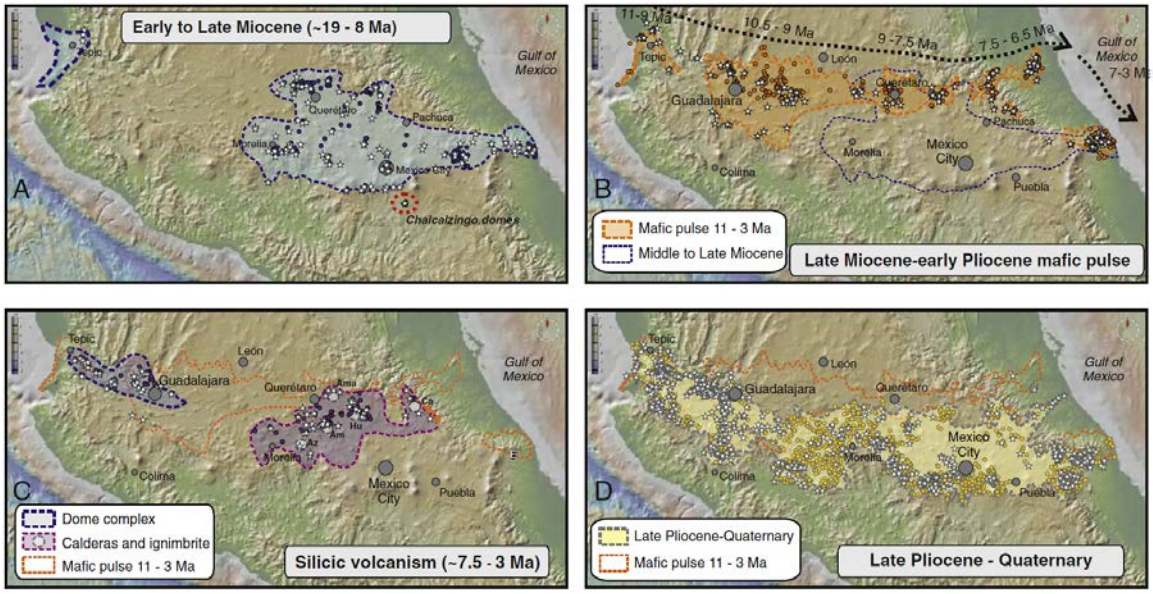

Figure 1.4. The four magmatic episodes of the Trans-Mexican volcanic belt (Ferrari et al., 2012).

There is another important Neogene volcanic province, called the Eastern Alkaline Province, a belt that is composed by five volcanic fields (Ferrari et al., 2005). The most recent arc volcanism in southeastern Mexico is the Chiapanecan Volcanic Arc, operating since the Pliocene (Figure 1.5).

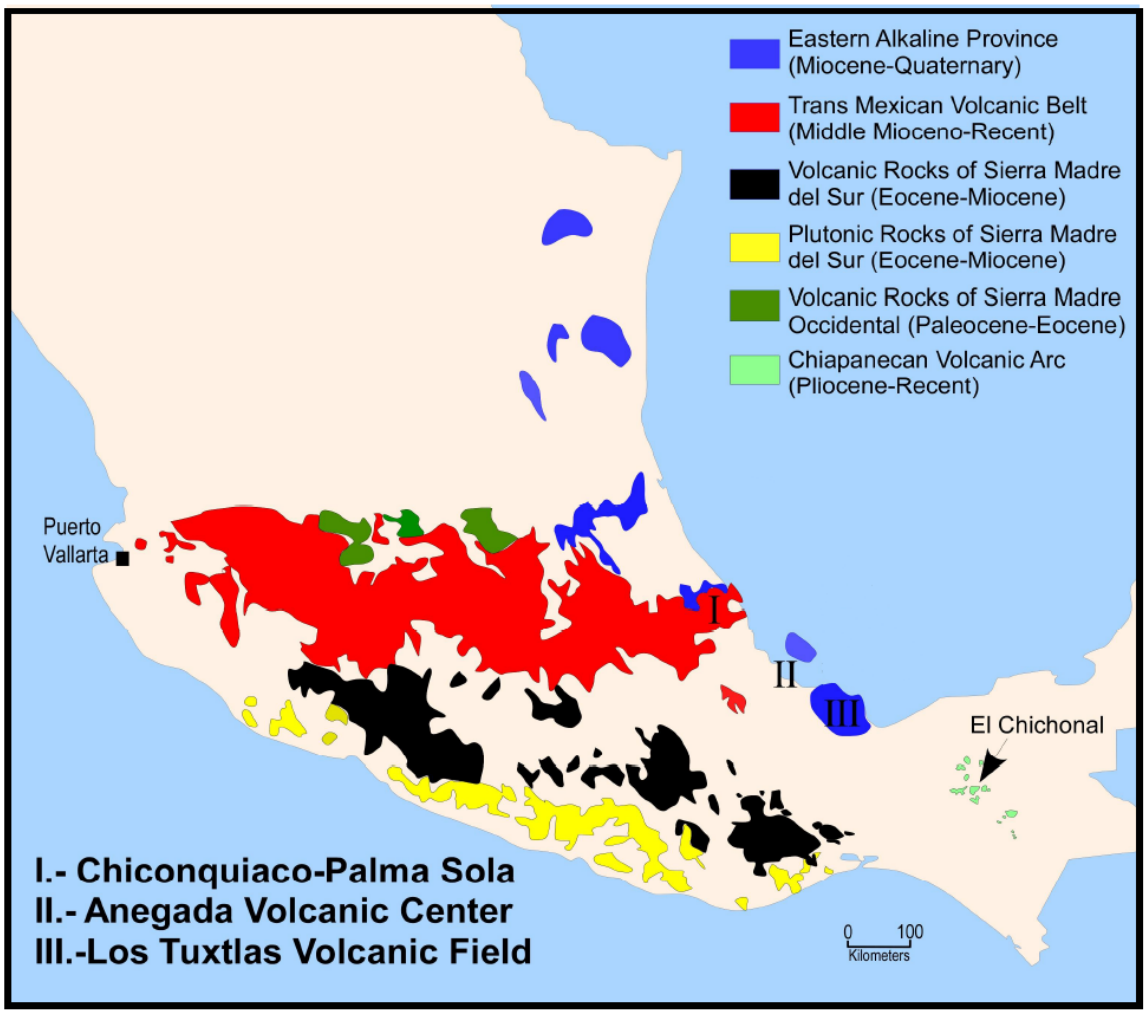

Figure 1.5. Volcanic provinces of the South Central and Southeastern Mexico (Ferrari, et al. 2005).

Migration of the Chortis Block not only produced a magmatic displacement but also a shift of the deformational zone, creating the Chiapaneca orogeny in the Middle Miocene. The Chiapaneca orogeny created northward salt evacuation in the Isthmian salt basin that resulted in a linked extension-compressional gravity driven system with tectonic transport toward the northwest known as Catemaco fold belt (Gomez-Cabrera

and Jackson, 2009). By Middle Miocene, deformation of the Veracruz Basin occurred, closely followed by uplift of the Anegada High and Los Tuxtlas (Jacobo et al., 1992)

There is another extensional-contractional linked system that initially formed in the western margin of the Gulf of Mexico during the Middle Miocene, known widely as the Mexican Ridges. The migrating Cocos Plate shifted its direction to the northeast, generating compression in the continental slope, east of Burgos, Tampico Misantla, and Veracruz Basins. This in turn created a tectonic gradient for the slope sediments tilted toward the Gulf of Mexico basin. Structural boundaries in the western area are a series of parallel, north-trending growth faults and further seaward show a parallel set of north-trending folds and low-angle thrust faults that cut the Paleogene and Neogene section. The Miocene to Pleistocene section in eastern areas is deformed into a series of large folds with wavelengths of 10 to 12 km and amplitude from 300 m to 1 km (Padilla, 2007).

The Mexican Ridges (Figure 1.6) thus developed as a consequence of gravitational spreading processes, synchronous with growth faulting of the western onshore and continental shelf areas. The extensional-contraction linked system is thought to detach on overpressured Upper Eocene shales, with an additional detachment surface in the Oligocene section. The main deformational mechanism is by limb rotation (Salomon-Mora, 2011). Deformation occurred in several stages from middle Miocene to the present day (Salomon-Mora, 2011). This deformation correlates with highly active petroleum systems, including migration and trapping of hydrocarbons, in turn forming direct hydrocarbon indicators, overpressured traps, gas chimneys, gas hydrates, and sea floor hydrocarbon seeps that are being investigated as part of new regional exploration efforts.

Development of high amplitude folds and a pronounced tilt toward the basin may have also played a role in facilitated acceleration of high-energy turbidity flows from western sources, either through canyons or deltaic input points. The sea floor gradient was likely much higher than most passive or divergent margins, providing potential energy to sediment gravity flows coming into the basin. The tectonic features may have also provided a degree of "bottom roughness" that is essential to formation of hydraulic jumps and cyclic step bedforms in Mexican deepwater areas.

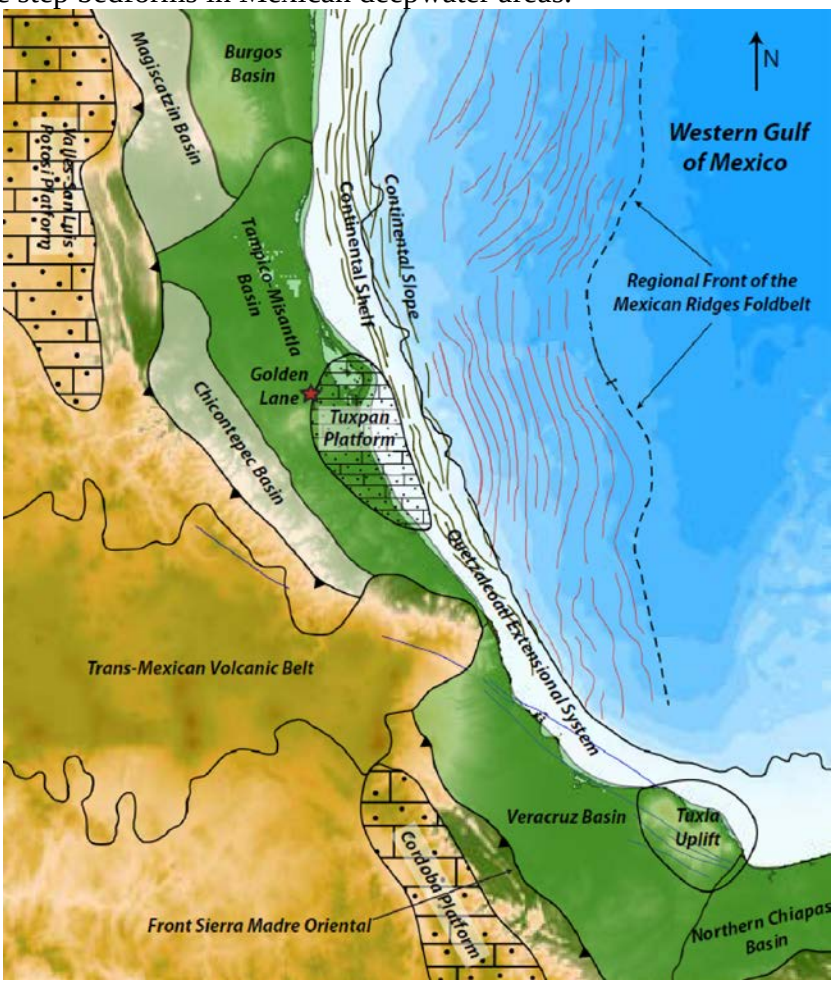

Figure 1.6. Map of the main structural elements of the southwestern Gulf of Mexico, showing the structural trend of the Mexican Ridges (Yarbuh and Contreras, 2015)

Neogene Depositional History

In the Gulf of Mexico, a great deal of sediment bypassed the shelf margin to be deposited in slope and basin floor systems during the Neogene (Galloway et al, 2000). Gulf Basin Depositional Synthesis Project (GBDS) established seismic sequences based on those first delineated by Feng (1995). Those genetic sequences record major episodes of sediment infill and are bounded by prominent marine flooding horizons, as well provide a stratigraphic and depositional framework for the basin floor (Figure 1.7).

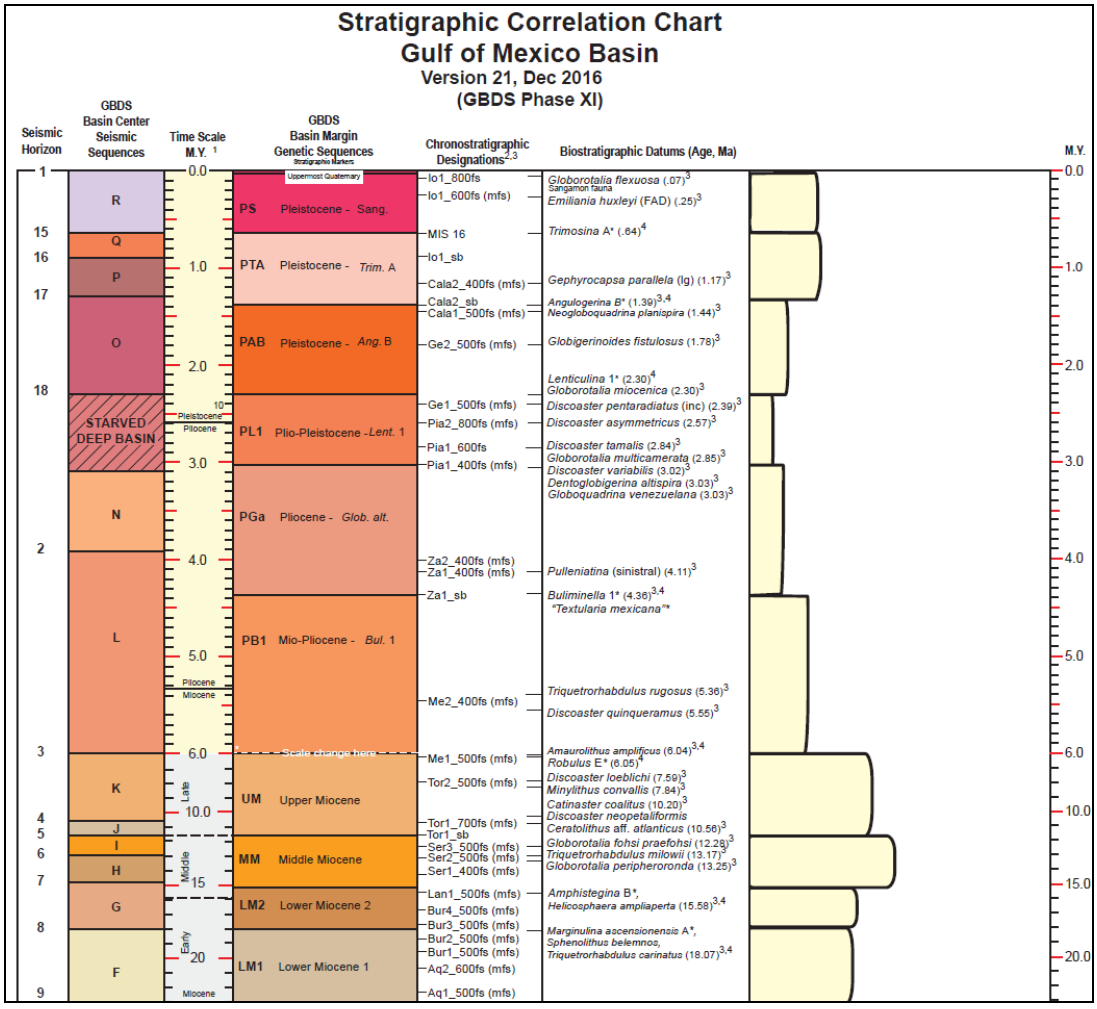

Figure 1.7. Chronology of Gulf of Mexico Neogene genetic sequences.

The Cenozoic history of Gulf of Mexico sediment filling can be summarized by the pattern of shelf-margin progradation (Figure 1.8). For this study where the western margin is our focus, this pattern reflects volcanism, and consequent uplift and erosion of much of central Mexico and the southwest United States that flooded the southwestern basin with siliciclastic sediments. The western margin was initially displaced basinward as much as 80 mi (125 km) by late Mesozoic and Paleocene tectonic uplift of eastern Mexico and the adjacent basins. Further Paleogene deformation and concomitant deposition advanced the margin to a position near the present coastline. Subsequent Neogene depositional offlap has been modest, dominated by slope bypass.

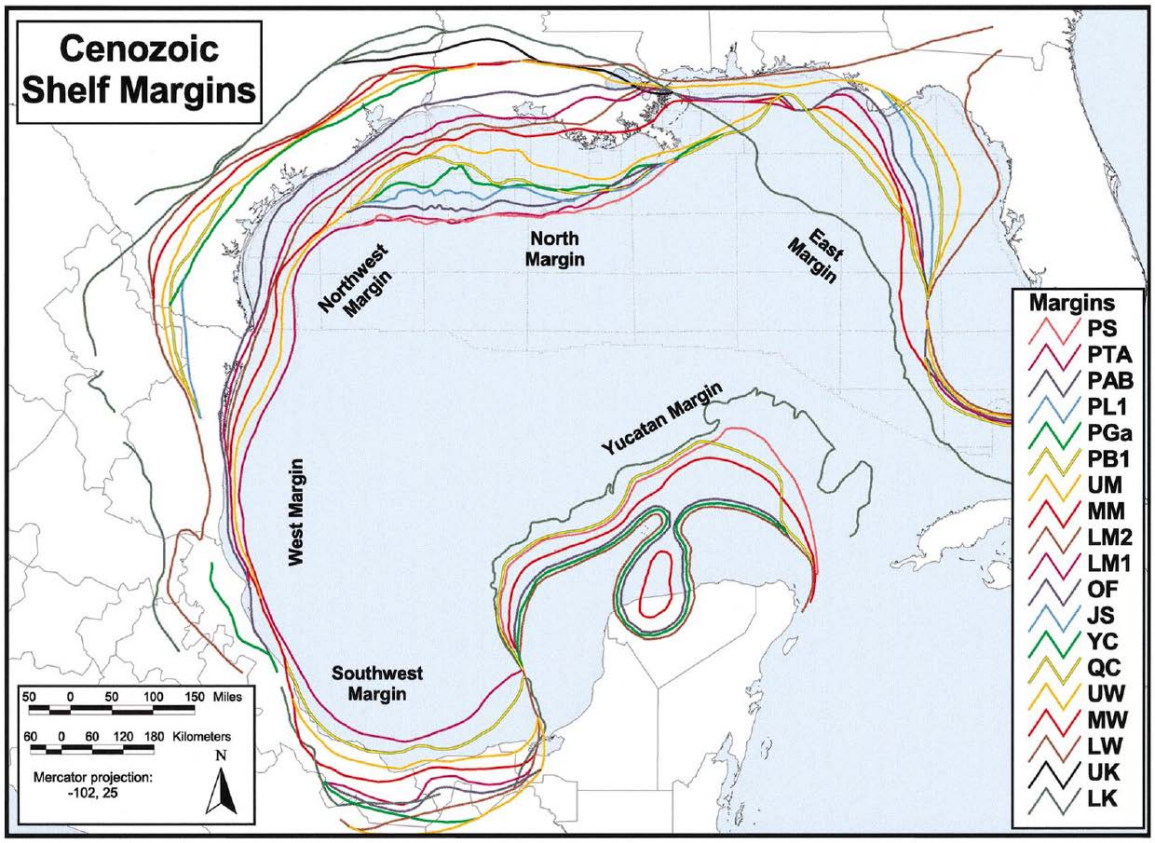

Figure 1.8. Cenozoic shelf break positions at top of successive GBDS deposodes. From Galloway et al. 2000.

The depositional timeframe of interest for this study is the Neogene, centered on the Upper Miocene (UM), Mio-Pliocene (PB1) and Pliocene (PGa). Galloway et al. (2000) determined that the early Miocene (LM1 and LM2) was a period of relative paleogeographic stability of the Gulf of Mexico (Figure 1.9A). Snedden et al. 2012 interpreted Lower Miocene submarine fans formed in eastern Mexico, possibly related to sediment influx generated by renewed orogenic activity in Mexico. At that time, the northeastern Mexico shelf had a wave-dominated shore zone system (Rodriguez, 2011). Within the Lower Miocene 2 (LM2) deposode (Galloway et al. 2000), a submarine fan system with mounding in its inner fairway developed with a northeasterly trend (Galloway et al., 2000). Submarine fans can be related to increased uplift and erosion of the Mexican landmass, along with loading and destabilization of the narrow eastern Mexican shelf (Rodriguez, 2011).

Galloway et al. (2000) suggested that the middle Miocene (MM) basin-margin sequence only records about 3 m.y. of deposition of the 5.5 m.y. interval (Figure 1.9B). The basin-margin sequence is bounded by regional marine transgressive shale units. The upper Miocene (UM) is a genetic sequence reflecting relatively stable sediment dispersal and paleogeography (Figure 1.9C). It records sediment dispersal systems that persisted with little modification for nearly 7 m.y. In eastern Mexico, slow rates of supply and high wave energy locally swept sand along the narrow shelf and slope. Thick contourite drift complexes are thought to have accumulated in deepwater areas, (Snedden et al., 2012), anchored on its southern end by a submarine mound perhaps related to sediment generated during uplift and erosion of the Trans-Mexican volcanic belt (Rodriguez and Mann, 2011) .

By the end of Upper Miocene to early Pliocene (PB1 contourite drift accumulations were interpreted on the basin floor areas of the west and southwest basin.

(Figure 1.9D), a large mass transport complex originated from the Veracruz margin, and a north-extending tongue of sandy basin-floor turbidites of the Campeche apron. Figure 1.9E shows the early to early late Pliocene deposode (PGa) was interpreted to indicate presence of local areas of drift complexes, muddy turbidites and hemipelagics, and a tongue-shaped mass-transport complex accumulated along the southwestern Gulf of Mexico. During the late Pliocene (PL1) most of the southwest Gulf floor was sediment starved, only a local drift accumulation occurs in the area (Figure 1.9F). Also a mass transport complex is interpreted to be derived from the Texan margin Galloway et al., 2000.

Although the fluvio-deltaic transport pathways are well documented for the basin as a whole, the apparent along slope transport and bypass to the east, up to 150 km from the deltaic depocenters, is striking. The explanation from Snedden et al. (2012) for this apparent eastern offset of the source to sink system relates to strong near-bottom contour currents generated during progressive closure of the equatorial seaway between North and South America.

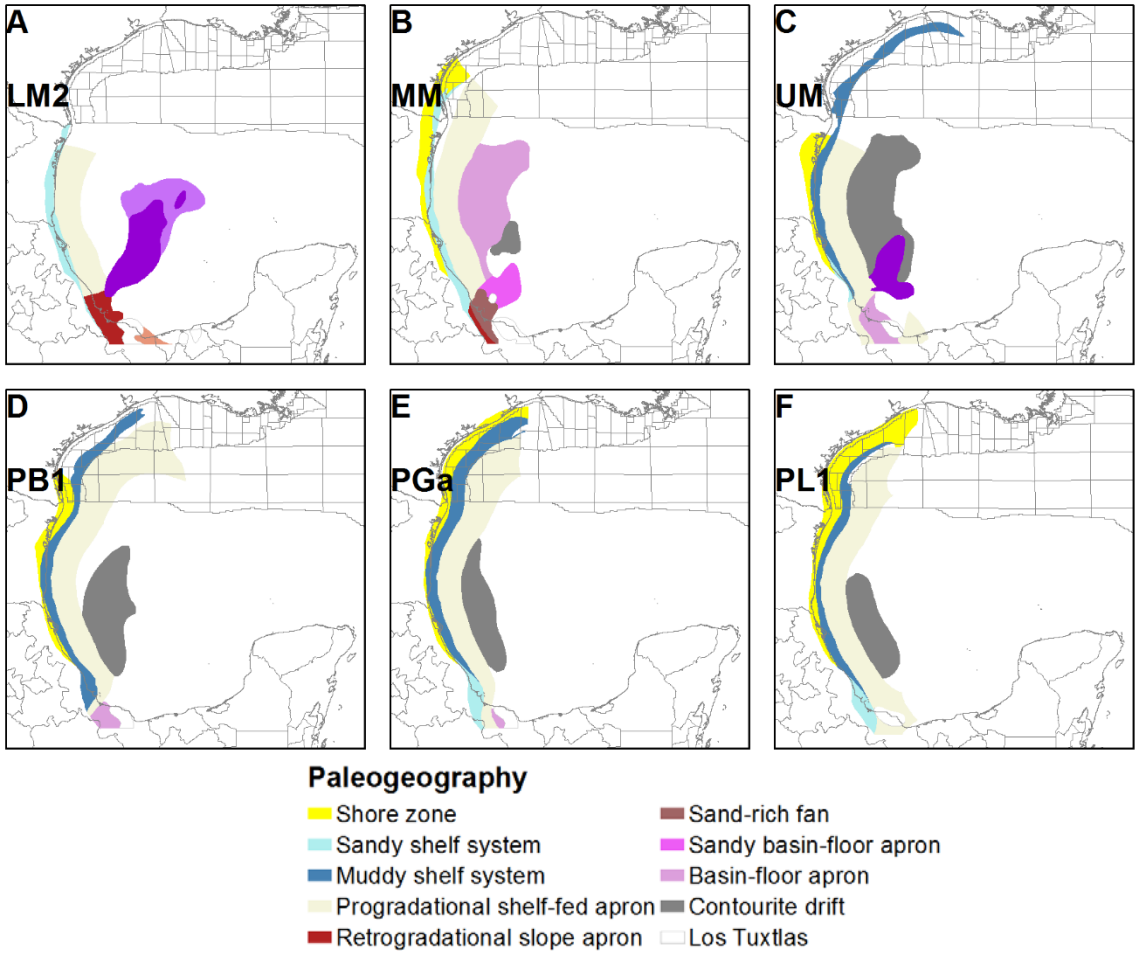

Figure 1.9. GBDS Paleogeographic reconstructions of the Gulf of Mexico Basin.

The seismic facies that are a focus of this study are seaward dipping reflections at the east of the Mexican Ridges. These were originally analyzed by Snedden et al. (2012) (Figure 1). These were described as a series of hummocky, oblique, and shingled to parallel seismic clinoform reflections (Figure 1.10) and were interpreted as contourite drifts and current modified deepwater deposits. Original widely spaced UTIG seismic lines, suggest that these shingled clinoforms dip to the north and northeast (Snedden et al., 2012).

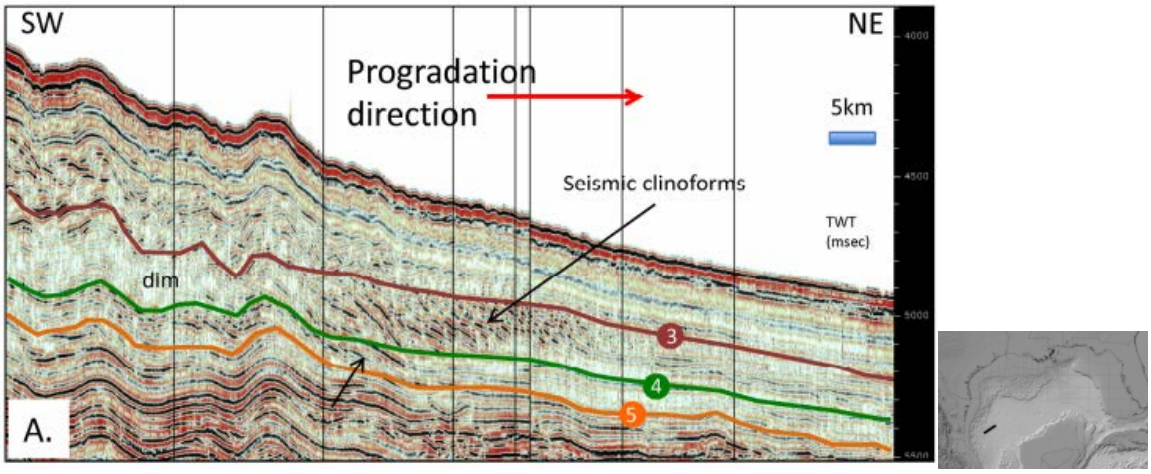

Figure 1.10. UTIG seismic line showing the seismic clinoforms from Snedden et al., 2012.

These reflections terminate eastward (paleoseaward), as dips decrease, into a series of horizontal, parallel, and continuous reflections. To the west, the key seismic interval continues into the folds of the Mexican Ridges, thinning progressively landward. The clinoform or shingled reflection packages are bounded at the base by GBDS basin center seismic sequence MM–I, thought to be Late Middle Miocene in age (Snedden et al., 2012). These were preliminary age assignments, based on older seismic data with few well-ties for calibration. The upper surface, where clinoforms change to wavy-bedded reflections, was interpreted to coincide with the GBDS Basin center sequence UM–K, thought to Latest Miocene in age (Galloway et al., 2000).

As mentioned, these seaward dipping, shingled to clinoforming reflection sets were interpreted as contourite deposits built by the strong bottom currents as function of the closure of the Panama gateway (Snedden et al. 2012). It was hypothesized that strong bottom currents could have eroded the newly formed Miocene submarine fans and transported the material to the north, creating these deep marine deposits.

As will be discussed below, access to both reprocessed UTIG data as well as newly acquired seismic data from PGS allows for better imaging to understand these unique seaward dipping seismic reflection sets. Calibration with local well control (e.g. Kunah-1 and DSDP Site 90) also improves the interpretation and supports a new genetic hypothesis.

CHAPTER 2: DATA AND METHODOLOGY

In the southwestern Gulf of Mexico deep-water area, new and recently reprocessed seismic data reveal a series of large, bed form dominated Seaward Dipping Accretion Sets (SDAS; Figure 2.1). These Miocene to Pleistocene age seismic packages are interpreted to have been deposited in paleo water depths exceeding 400 meters (Snedden et al., 2012).

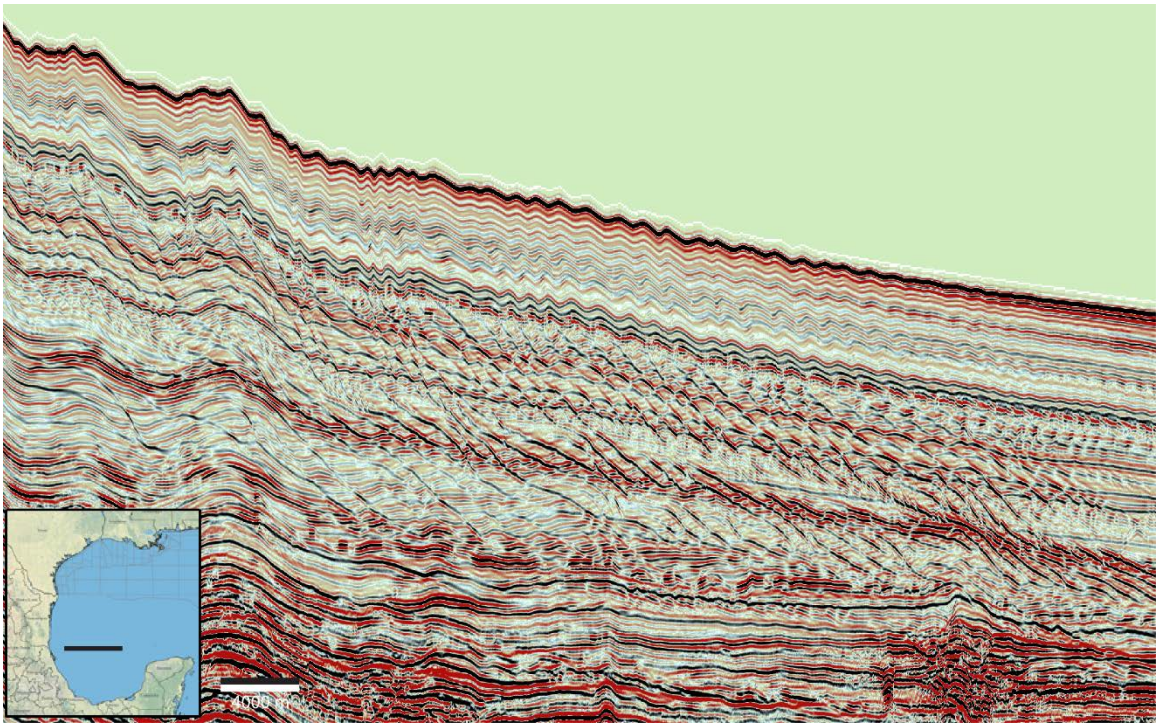

Figure 2.1 PGS seismic survey line 19. Uninterpreted time section showing seaward dipping accretion sets (SDAS) in the eastern Mexico deepwater. Inset shows approximate location of seismic line.

Research Objectives:

The objectives of this research are to evaluate the paleogeographic evolution of the southwestern Gulf of Mexico and associated deepwater systems during Neogene, including:

1- Evaluating several hypotheses for development of these deepwater bedforms in the Mexico's Gulf of Mexico

2- Placing observations in a regional context and interpreting likely sediment sources and transport pathways

In order to understand the origin of the Seaward Dipping Accretion Sets (SDAS) in Mexico, isochore and structural maps from the Neogene interval were constructed using well logs, published cross-sections from interpreted seismic lines, biostratigraphic information and marine seismic data (Figure 2.2). The primary datasets for the southern Gulf of Mexico interpretation are PGS data and ION's YucatanSPAN, which contains 17,742 km of 2D seismic lines within the southern Gulf of Mexico. Three maps of the SDAS facies in different intervals from all the available lines were made to assess the extent and, the origin of these features. Wells used for this study were obtained from the GBDS database, DSDP well reports, and from published Mexican reports and literature. Well logs and biostratigraphic information were used to determine the top and bottom of each chronostratigraphic interval studied. Six top deposode genetic sequence, (Galloway et al., 2000) surfaces were interpreted: Lower Miocene 2 (LM2), Middle Miocene (MM), Upper Miocene (UM), Mio-Pliocene (PB1), Pliocene (PGa) and Plio-Pleistocene (PL1).

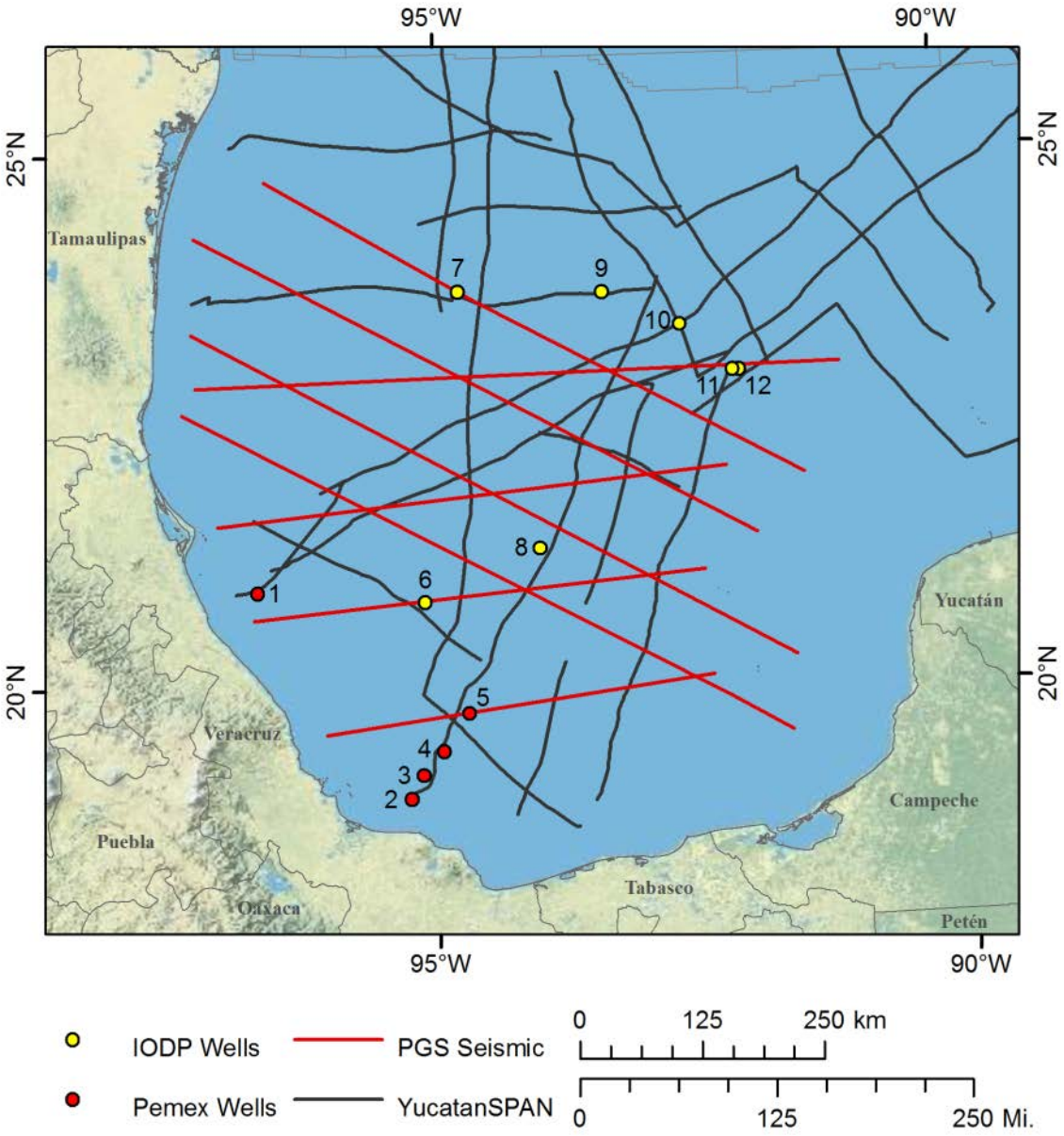

Figure 2.2 Location of all well and seismic data that were used for this project.

The primary wells with lithology and age information that were used to calibrate the seismic were from PEMEX Kunah-1 and DSDP Leg 10 Site 90. Pemex wells Yoka-1, Pushkon-1, Piklis-1 and Lakach-1 also provided some constrain on seismic correlation of

surfaces but no lithology data was publically available. Other DSDP sites providing some local ties were sites 2, 3, 87, 88, 89, and 91. Seismic interpretation was carried out using a combination of 2D pre-stack, time-migrated seismic (PGS) and 2D depth imaged seismic data sets (YucatanSPAN), which were provided to GBDS by these seismic companies. Due to the structural complexity and pronounced changes in thickness in the Mexican Ridges and Campeche salt-cored structures, seismic correlation could be locally difficult but did not materially affect regional seismic correlations.

Newly acquired PGS seismic lines in the study area had not yet been converted from time to depth when provided. Therefore, new velocity time/depth curves were generated for key structural provinces of this study area in order to better tie wells into PGS seismic lines. Velocity data were calculated by obtaining several time and depth values from a time-and depth versions of YucatanSPAN™ at each specific location. Best-fit second-order polynomial equations were used for subsequent conversions of time to depth (Figure 2.3). These were later checked against fast-track depth-imaged versions of the PGS lines at key locations (e.g. Leg 10 Site 90 in Figure 2.3).

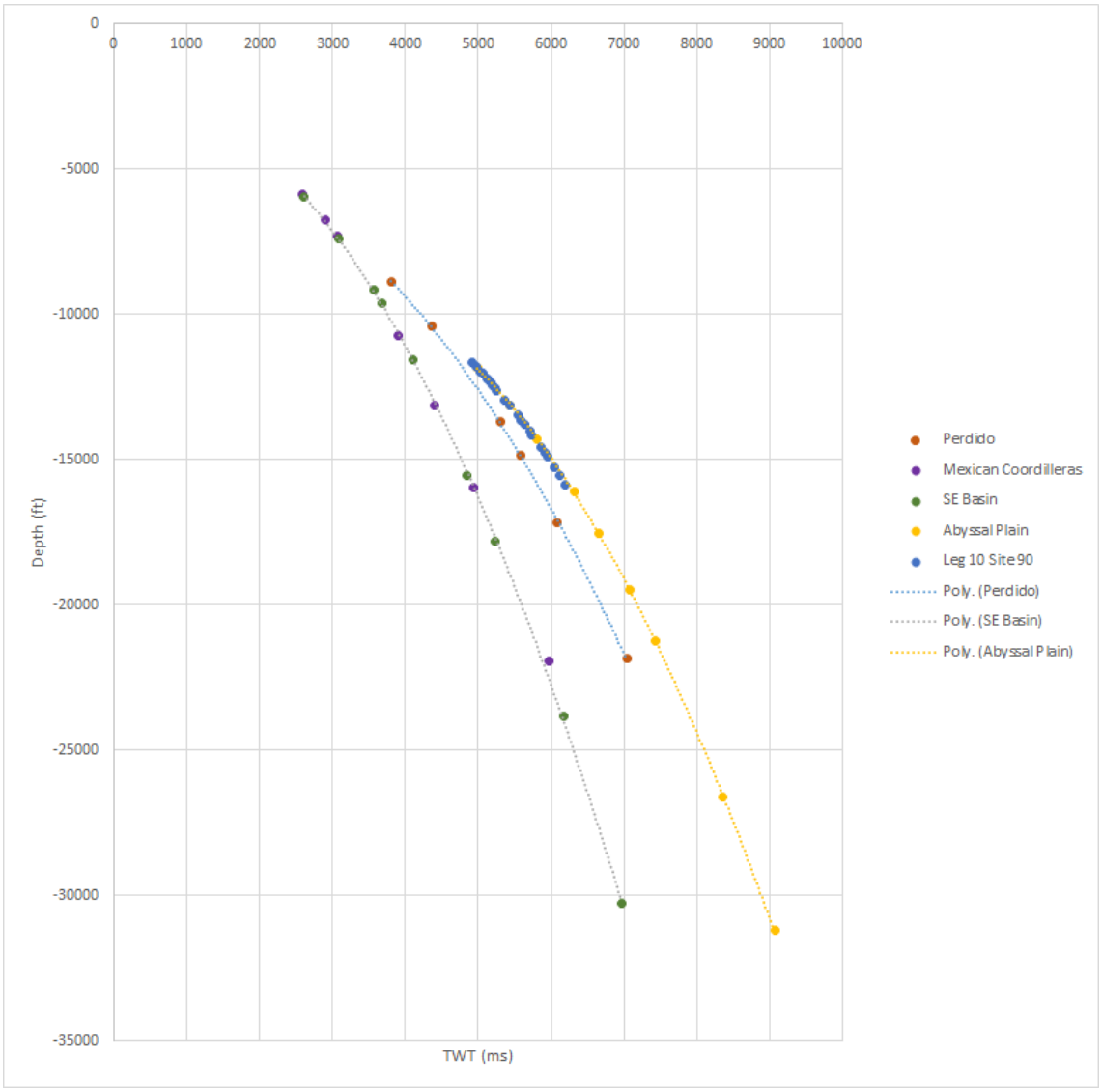

Figure 2.3 Time/depth curves for various areas of offshore Mexico.

Limitations

The southern Gulf of Mexico has significantly less publicly available data than the northern Gulf of Mexico (Fig. 2.1). This project had no access to 3D seismic data in the south nor to CNIH Mexico deep-water well control, until late in this work when Kunah-1 was provided. Deep-water interpretation in Mexico is largely based on 2D regional lines. This research was not intended to define detailed depositional environments at specific locations in Mexican deep-water areas. Instead, the purpose of this research is to inform the reader about the general trends of sedimentation of unique bedforms (sediment waves) of the SDAS seismic facies in the southern Gulf of Mexico. It also important to note the geographic limits of this project, which are focused on the southwestern Gulf of Mexico where the bathymetry of the region is complex and source to sink transport pathways not well understood. Some areas have different and complex structural domains that would require structural reconstructions that are beyond the scope of this project.

Examination of depth-imaged 2D seismic data provided by PGS

Late in this study (March 2017), PGS facilitated collection of measurements from depth-imaged 2D seismic data of the SDAS. From this data, height (D) and length (L) of the leeside were measured and from simple trigonometry, and angle (α) was calculated. From the stoss side, height (D') and the length (L') were measured, yielding the angle (β). The figure 2.4 shows how the angles and the thickness of the stoss and lee were determined.

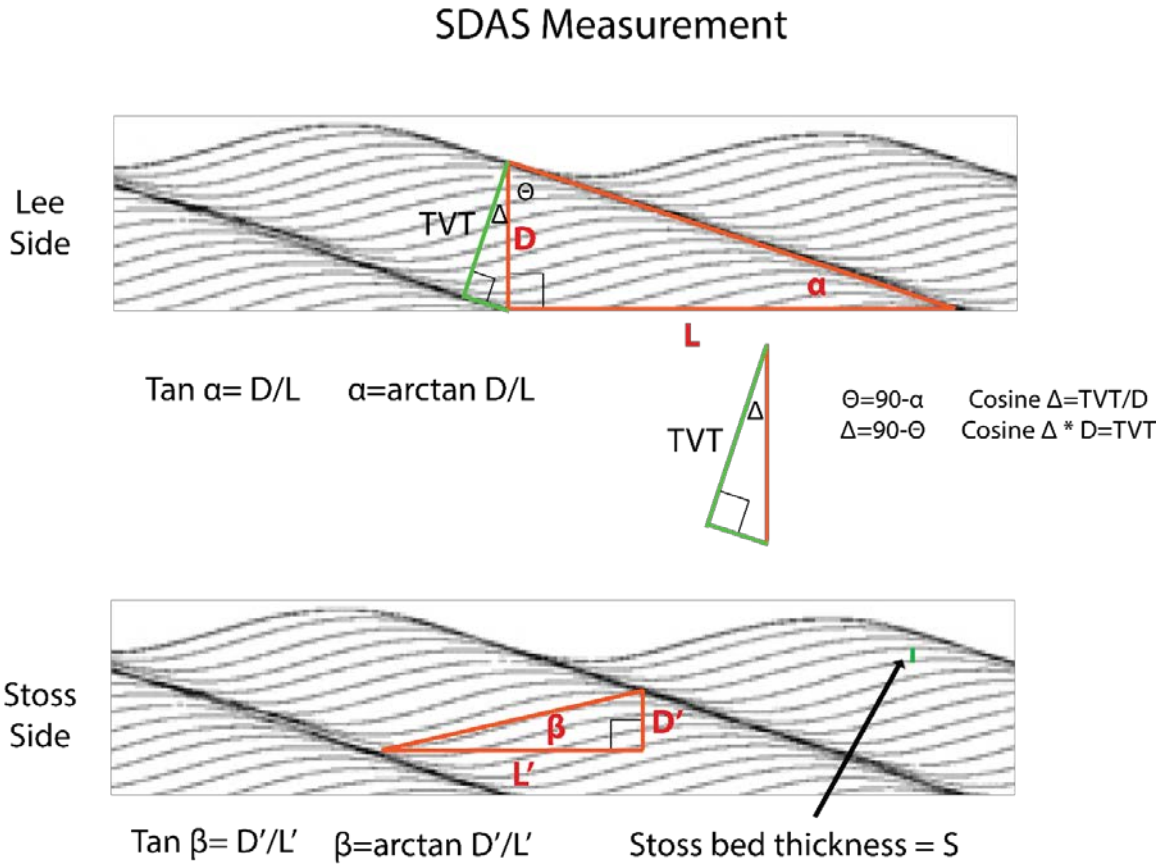

Figure 2.4. Schematic drawing of trigonometric relationships used to measure the angles and thickness of the stoss and lee sides of the SDAS bedforms.

Thickness of the SDAS sets, were measured by unit. (Figure 2.5). For the wavy sets the wavelength was measured from crest to crest, while the amplitude is measured from trough to crest and complete thickness of the wavy sets is from the bottom to the top of the body as shown in Figure 2.6.

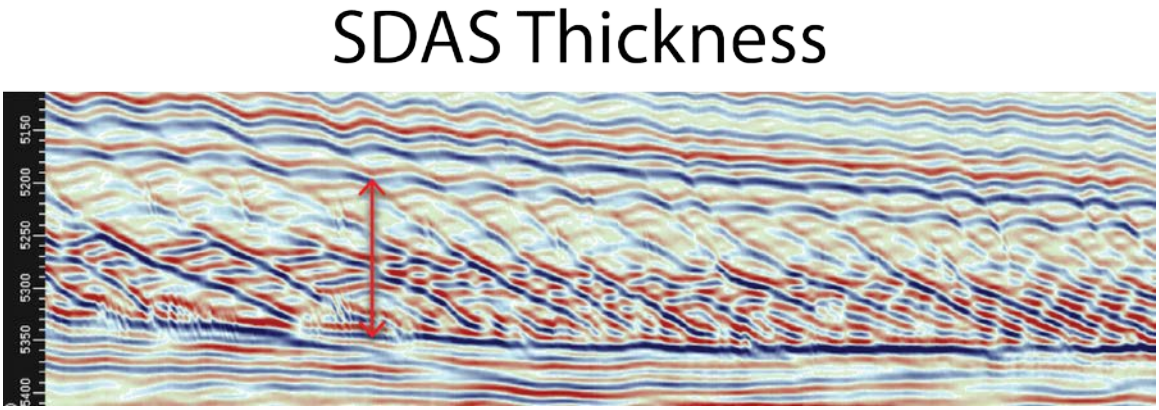

Figure 2.5. Seismic section showing the measurement of the SDAS

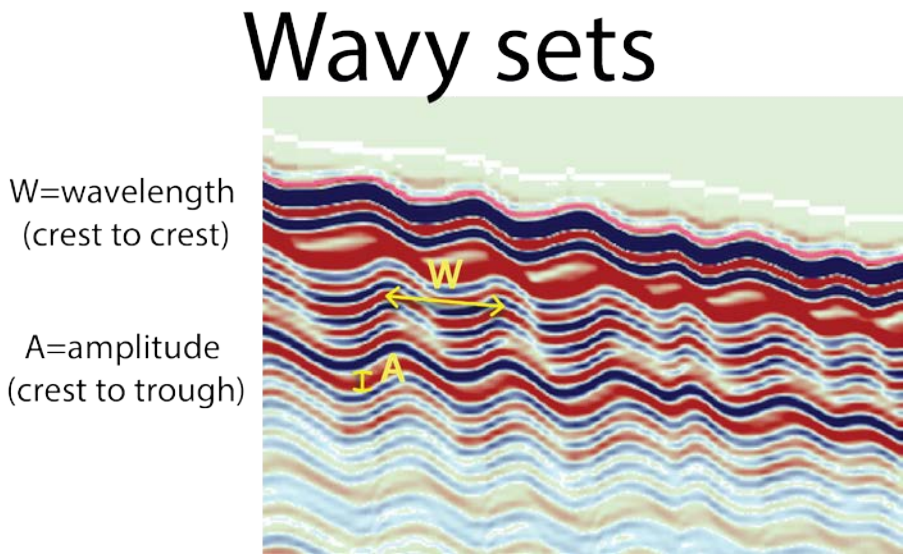

Figure 2.6. Seismic section showing the measurements in the wavy sets

Well Data Analysis

As mentioned above, Lower Miocene to Pleistocene stratigraphic intervals were analyzed on all Mexican wells available. The study area wells were analyzed using gamma ray logs from Pemex wells located in Mexican waters and the core logs from DSDP sites. Few wells penetrate the study interval and only Site 90 penetrates the seismic facies SDAS body # 2 (Figure 2.7). Kunah-1 penetrated the Lower Pliocene SDAS facies south of our main study area.

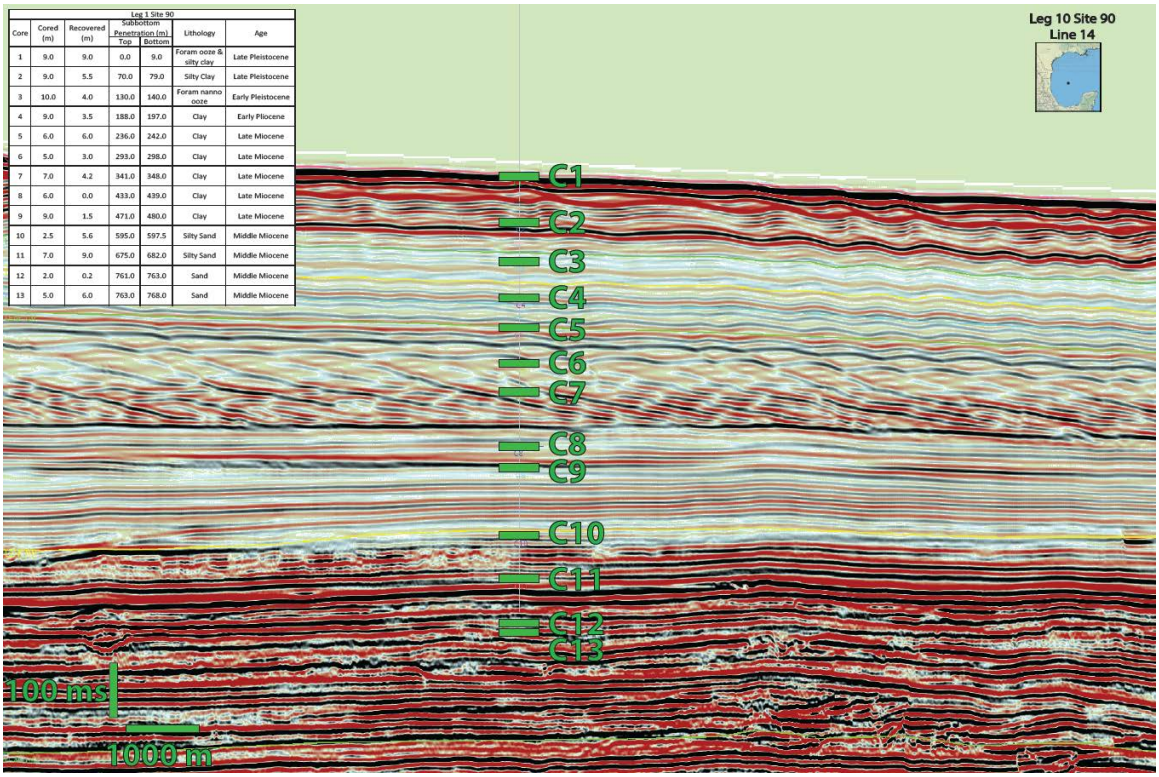

Figure 2.7 Seismic tie with DSDP site 90. Dominance of clay in the intervals that cross the SDAS body could relate to failure in recovery of unconsolidated sand as noted in the DSDP Volume X.

In the Leg 10 Site 90, cores 6 and 7 cut across the SDAS interval in the Upper Miocene. Both cores record largely a clay lithology but they only recovered sixty percent

of the sample (Table 2.1). It is possible the 40% lost section was unconsolidated sand that was difficult to recover with older coring technology. Sand-clay intercalation is expected in the SDAS based on seismic response showing alternating peak and trough reflections.

Table 2.1. The thirteen cores that were acquired in site 90 (DSDP Volume X).

Leg 1 Site 90						
Core	Cored (m)	Recovered (m)	Subbottom Penetration (m)		Lithology	Age
			Top	Bottom		
1	9.0	9.0	0.0	9.0	Foram ooze & silty clay	Late Pleistocene
2	9.0	5.5	70.0	79.0	Silty Clay	Late Pleistocene
3	10.0	4.0	130.0	140.0	Foram nanno ooze	Early Pleistocene
4	9.0	3.5	188.0	197.0	Clay	Early Pliocene
5	6.0	6.0	236.0	242.0	Clay	Late Miocene
6	5.0	3.0	293.0	298.0	Clay	Late Miocene
7	7.0	4.2	341.0	348.0	Clay	Late Miocene
8	6.0	0.0	433.0	439.0	Clay	Late Miocene
9	9.0	1.5	471.0	480.0	Clay	Late Miocene
10	2.5	5.6	595.0	597.5	Silty Sand	Middle Miocene
11	7.0	9.0	675.0	682.0	Silty Sand	Middle Miocene
12	2.0	0.2	761.0	763.0	Sand	Middle Miocene
13	5.0	6.0	763.0	768.0	Sand	Middle Miocene

Kunah-1 is other well that was used for calibration and also had lithological data. This well is located at the south of the study area (Figure 2.2, well 4). Mud log data in the Lower Pliocene in the distal portion of the SDAS seismic facies show an intercalation of fine sand and clay, consistent with the varying seismic amplitudes that are observable at the well to seismic tie (Figure 2.8).

The GBDS basin margin genetic sequences were correlated on the 2D seismic across the study area, tying wells where possible. In structurally complex areas like the

Mexican Ridges, the intervals of interest greatly thin and condense (Figure 2.9). The SDAS body 1, 3 and 4 are located just east of the Mexican ridges while the SDAS body 2 is located several kilometers away from the fold belt. Also in the image shown in Figure 2.9, one can observe how the SDAS initiate immediately east of the fold belt.

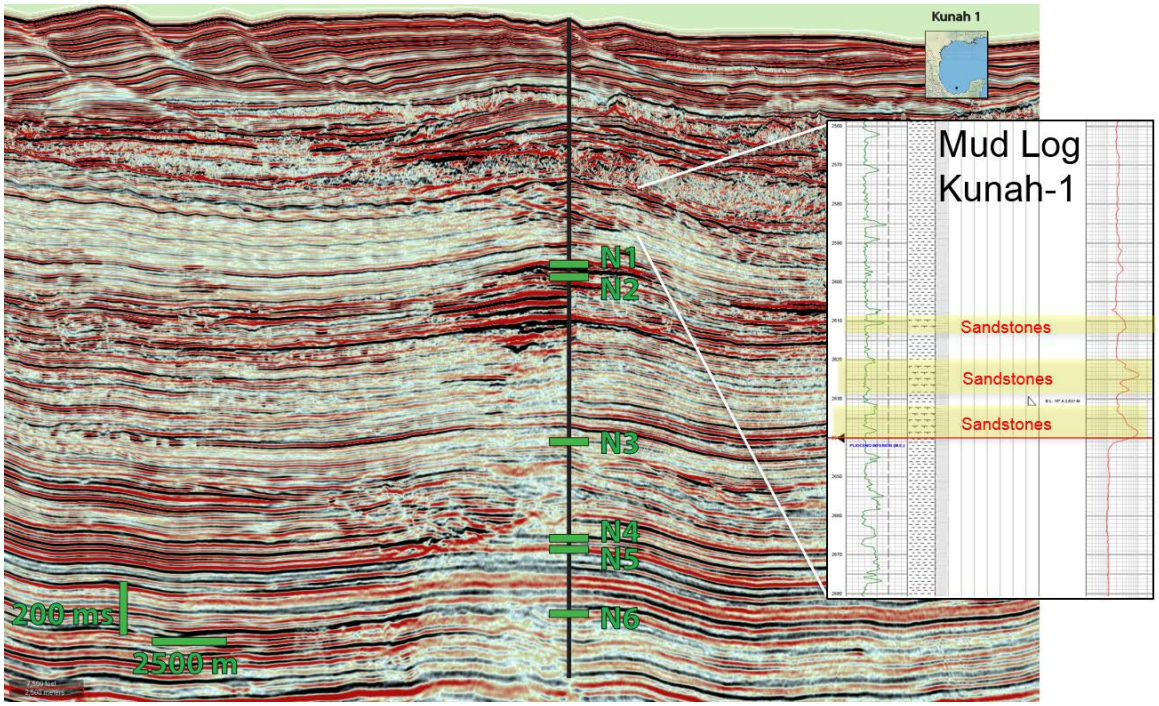

Figure 2.8 Seismic tie with Kunah 1. Well is located about 8km southeast of the seismic line.

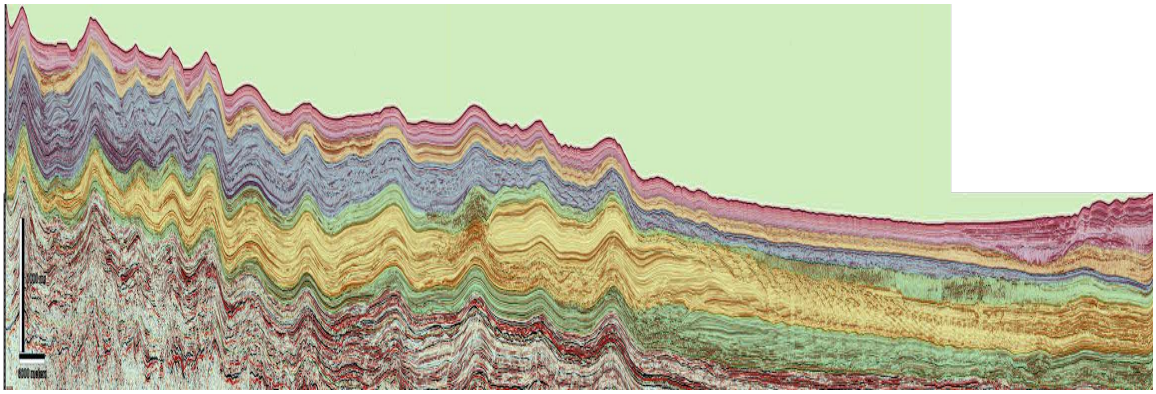

Figure 2.9 Cross-section Line 23. Shows the different interval thickness from the Mexican Ridges to the Study Area.

CHAPTER 3: RESULTS

Seismic Data Analysis

Four GBDS Basin Margin Genetic Sequences were interpreted on the seismic data and tied to wells available for calibration. Time structure and isochron maps were generated for each mapped horizon (Figures 3.1-3.4). From the time structure maps, one can infer that the Veracruz trough was well-developed by the Middle Miocene, between the Campeche salt province on the SE and the Mexican Ridges to the west.

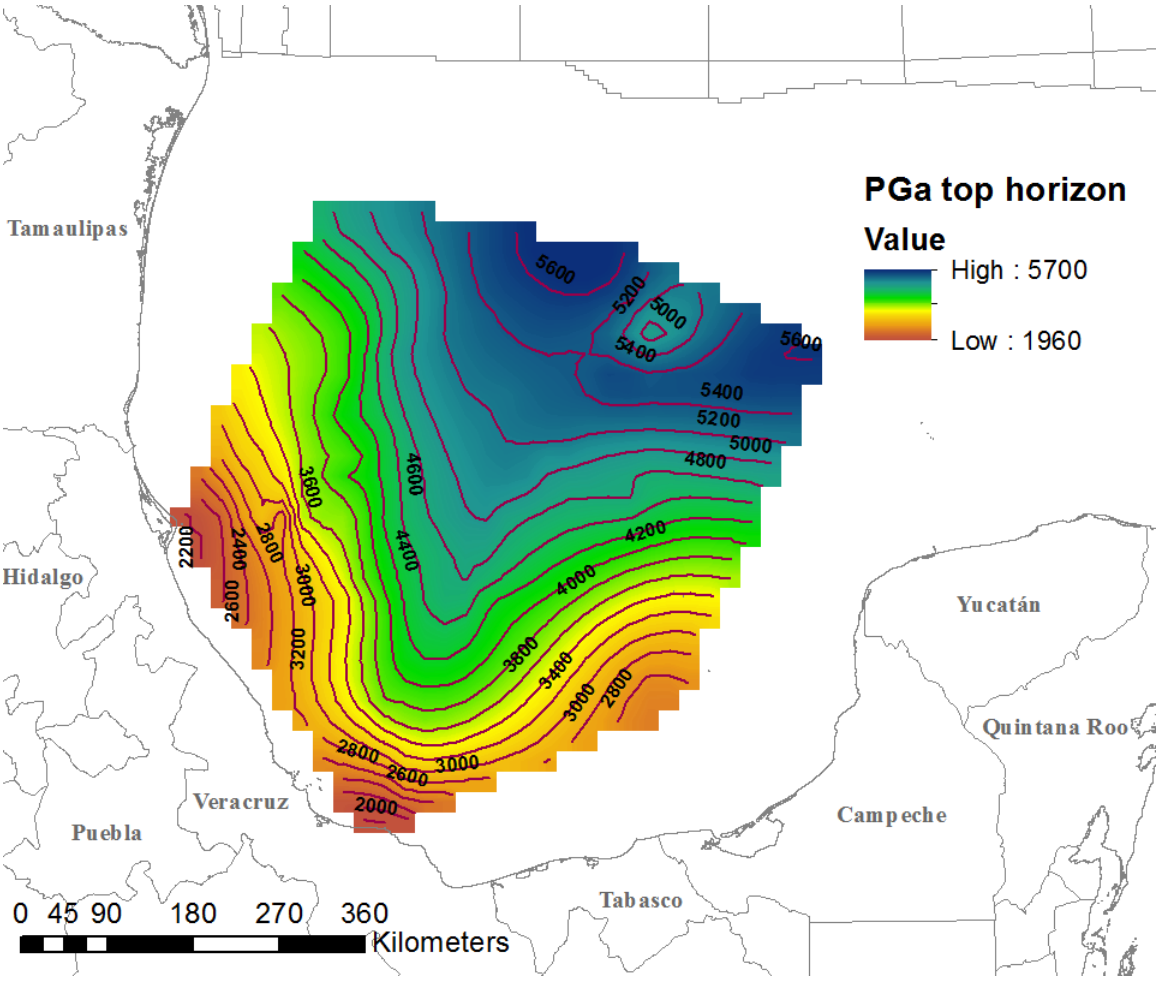

Figure 3.1 PGa time structure map, milliseconds (TWT).

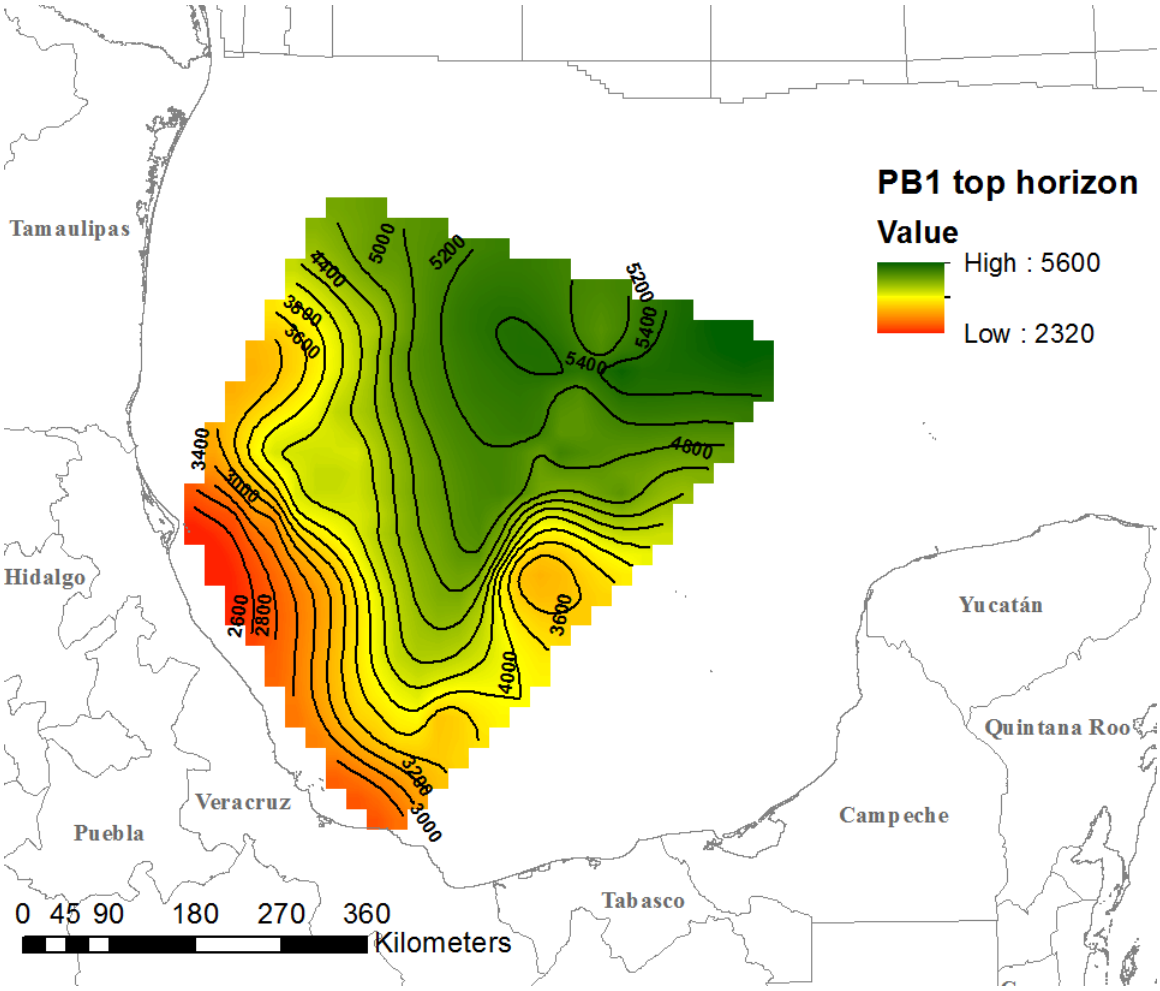

Figure 3.2 PB1 time structure map, milliseconds (TWT).

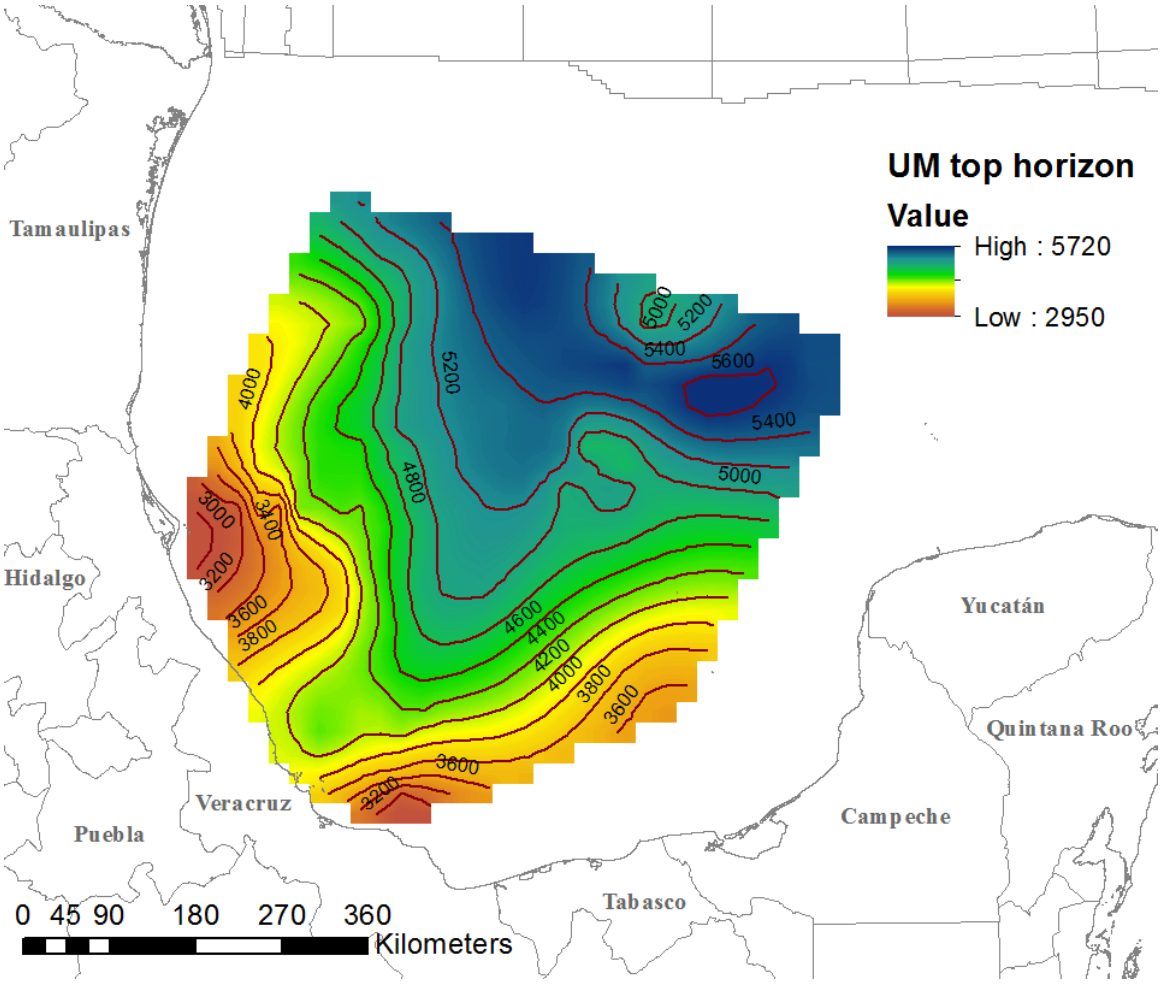

Figure 3.3 UM time structure map, milliseconds (TWT).

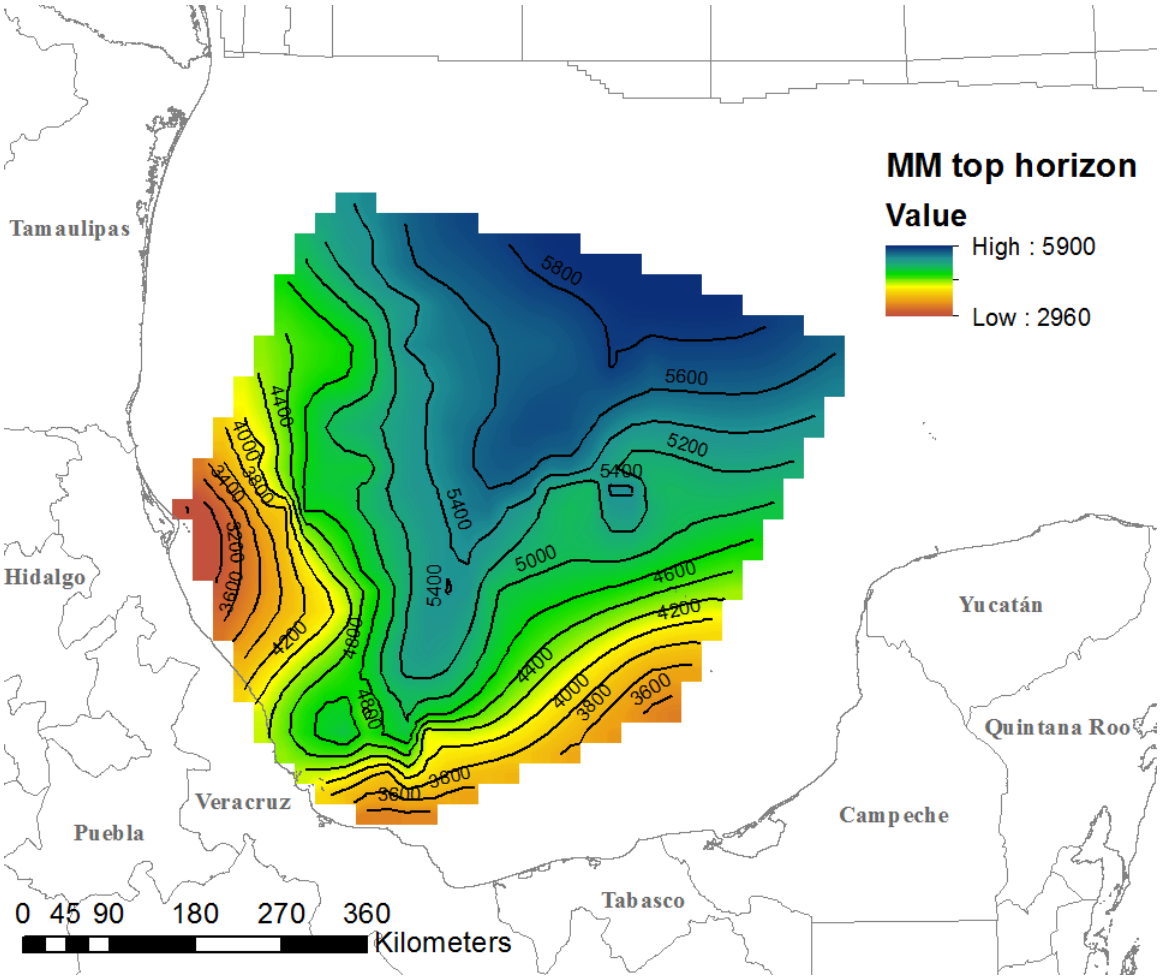

Figure 3.4 MM time structure map, milliseconds (TWT).

Isochron maps were generated by subtracting time structure surfaces for two horizons (Figures 3.5, 3.6 and 3.7). From those maps it is clear that that the sediment accommodation is progressively shifting from the south to the west, reflecting progressive source terrain uplift and generation of terrigenous sediments for the high gradient rivers of the Sierra Madre and the Trans-Mexican Volcanic Belt.

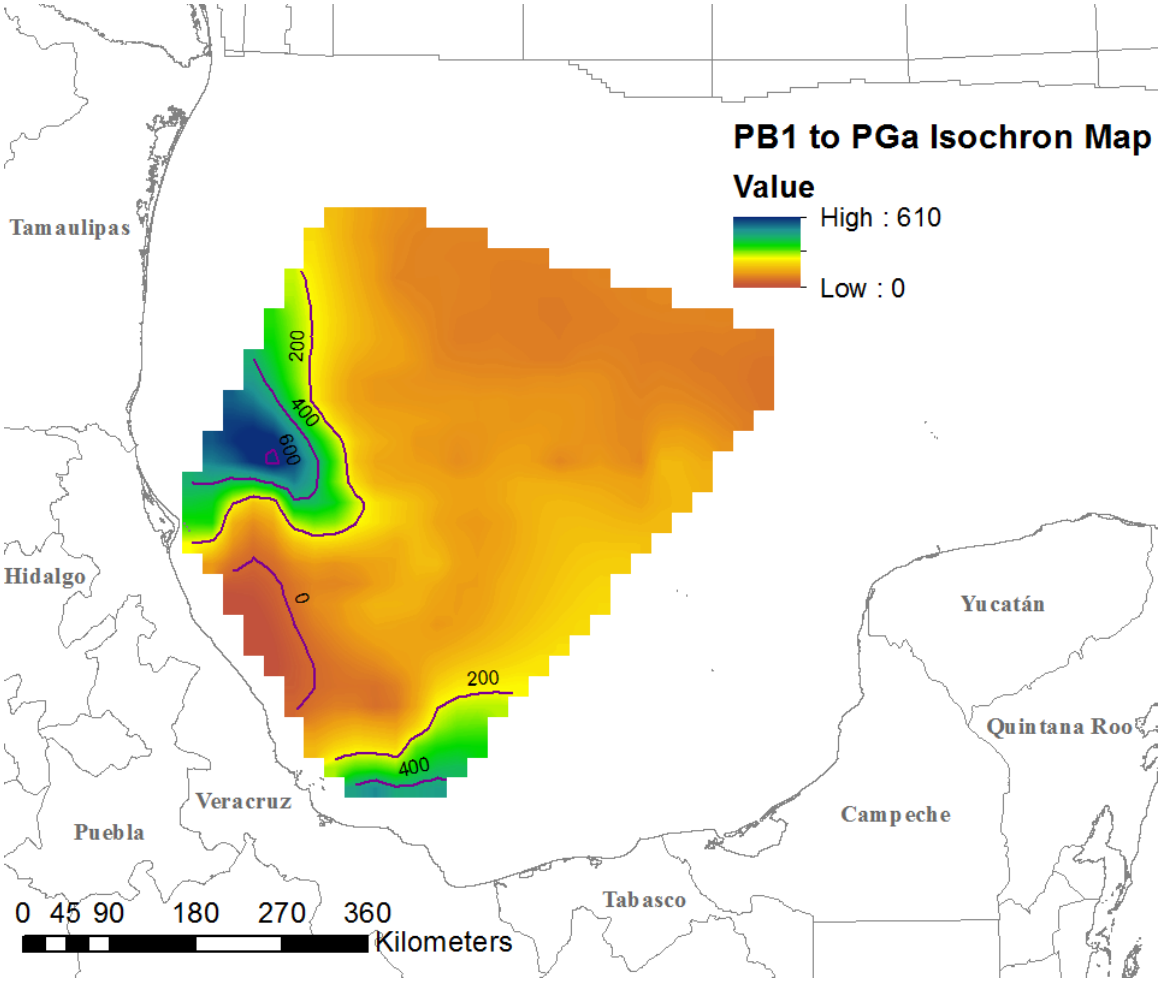

Figure 3.5 PB1 to PGa Isochron Map, milliseconds (TWT).

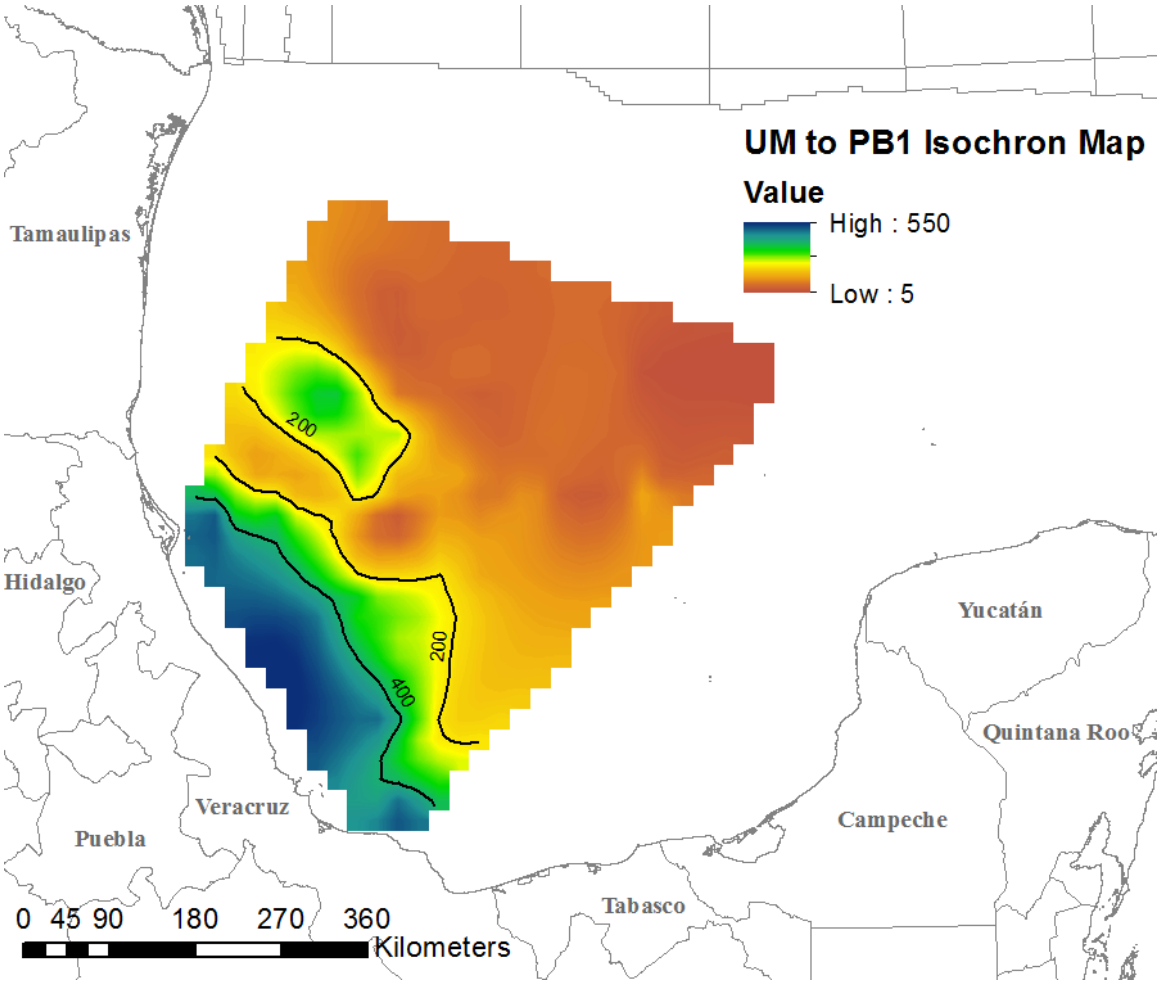

Figure 3.6 UM to PB1 Isochron Map, milliseconds (TWT).

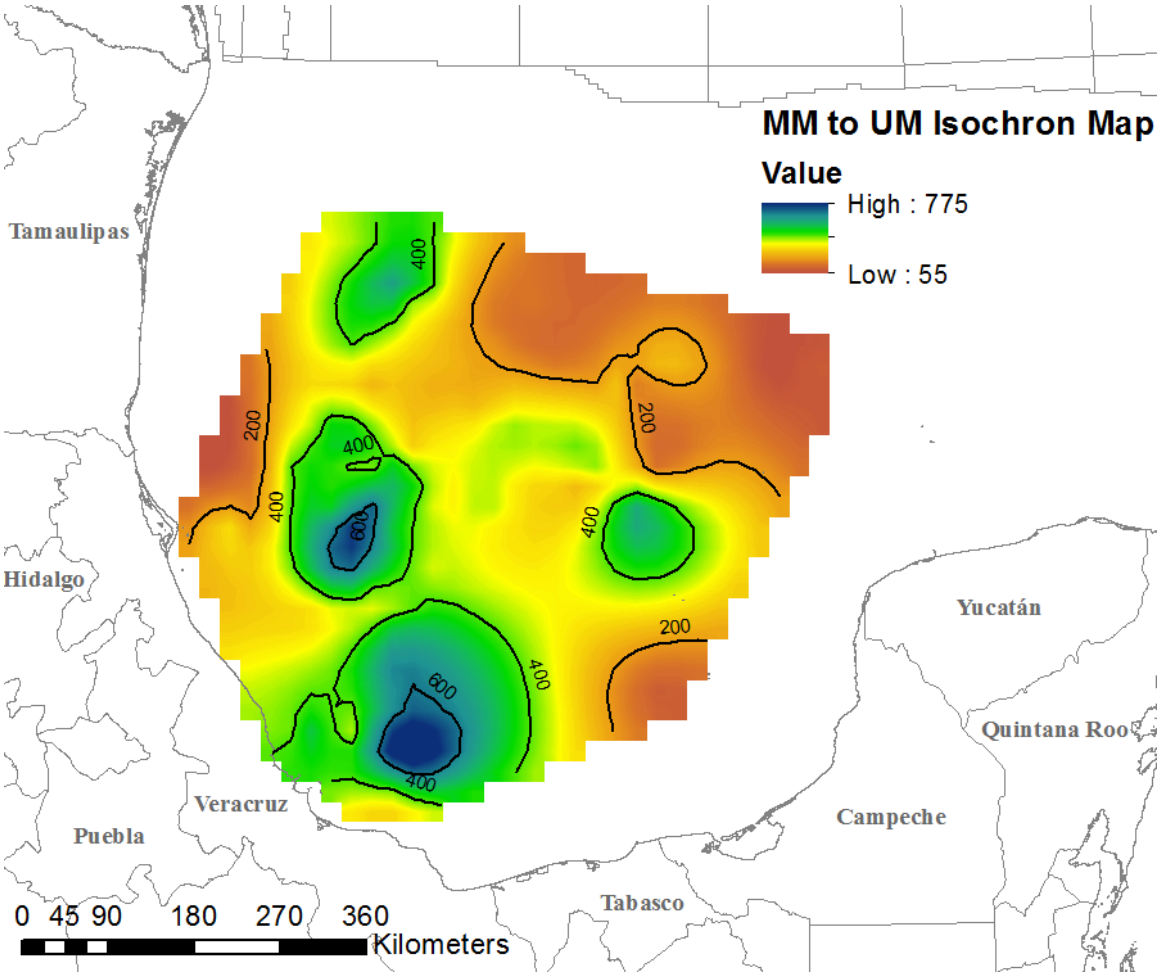

Figure 3.7 MM to UM Isochron Map, milliseconds (TWT).

Seismic Facies Analysis

Seismic intervals include eleven distinct seismic facies (Figure 3.8). Efforts were focused on a unique seismic facies that is referred to as the Seaward Dipping Accretion Surfaces (SDAS). Geobodies dominated by this SDAS seismic facies are present in four areas and in three time intervals, two in the UM, one in the PB1 and one in the PGa basin margin sequence

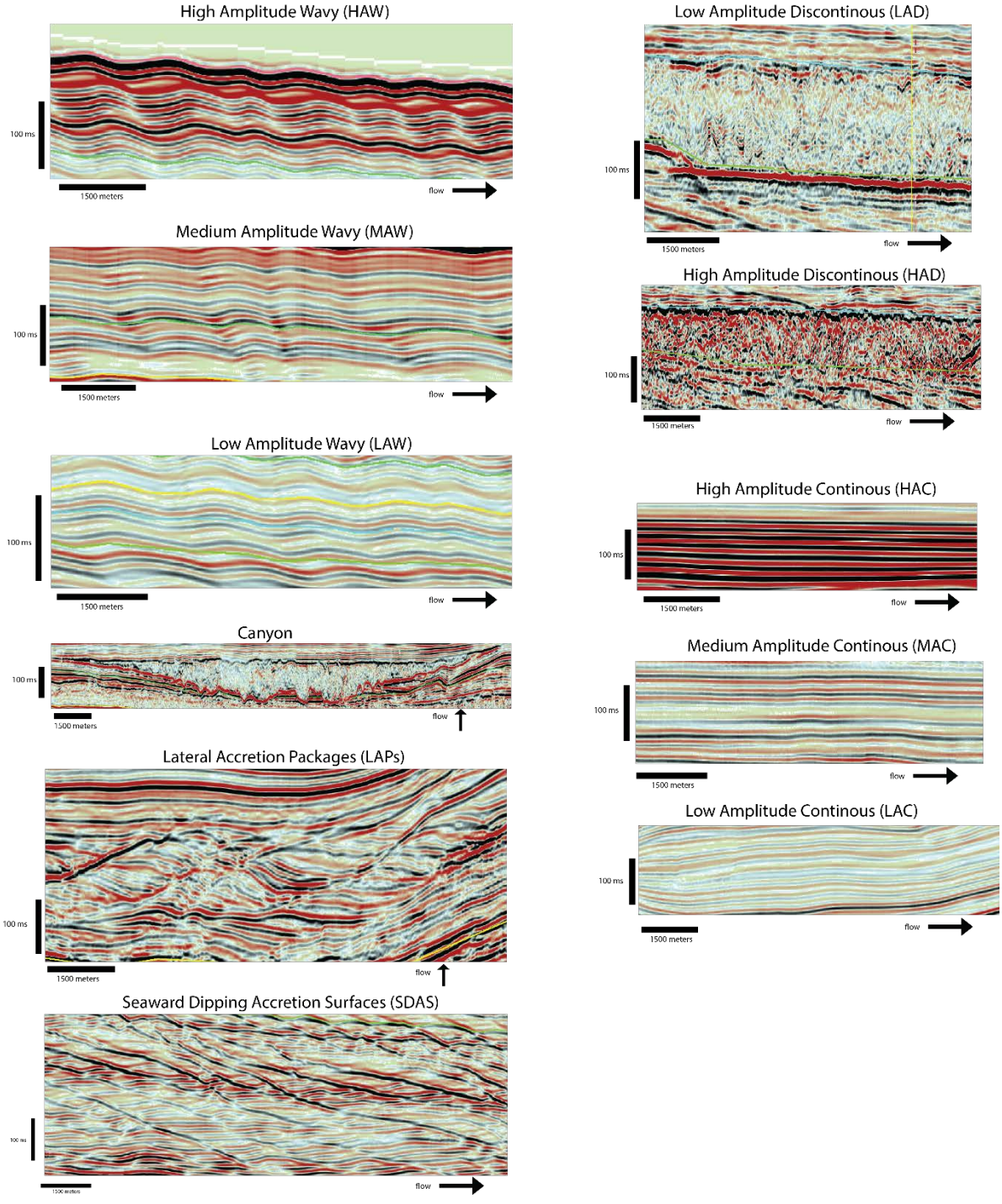

Figure 3.8 Examples of different seismic facies identified in this study.

Snedden et al., (2012) used interval velocities derived from analogous near-surface sediments (1848 m/sec) to give an estimated thickness range for the SDAS facies from 130 to 250 m, thinning both landward and seaward. Examination of depth-imaged 2D seismic data provided by PGS indicates reduced set thicknesses, more in the range of 17 to 144 meters (Table 3.1). The lee-side set length can be as long as 4.5 km while the stoss can be as long as 7.5 km (Figure 2.4). The leeside accretion sets are typically asymmetrical and dip seaward.

SDAS facies bodies analysis

East of the Mexican Ridges and centered on the Veracruz trough, a series of geobodies of the Upper Miocene SDAS facies were identified and mapped (Figures 3.9-3.12). These are described and discussed below.

SDAS UPPER MIOCENE BODY # 1

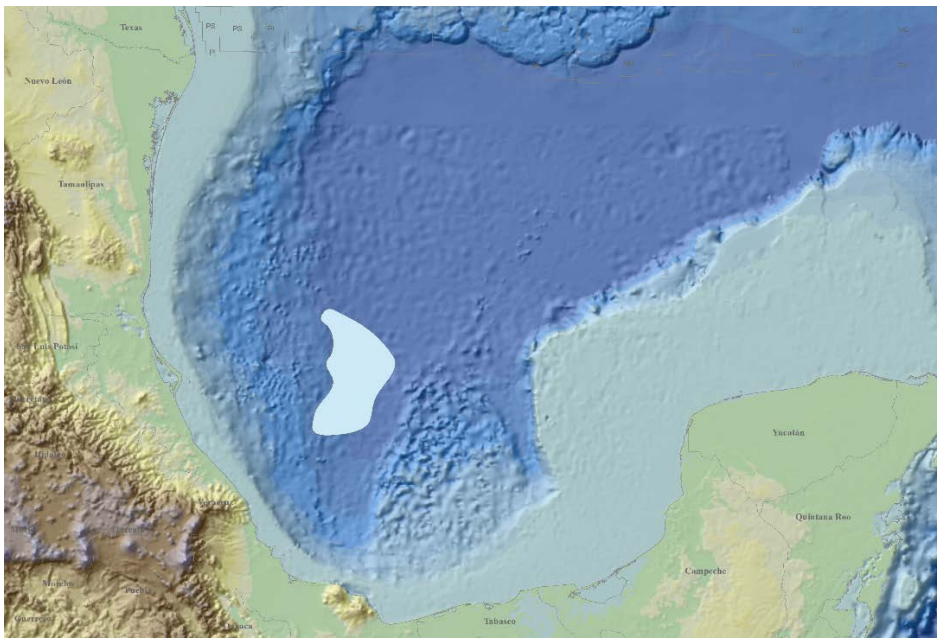

Figure 3.9. Showing the location of the UM SDAS package number 1.

Table 3.1. Measurements from the PGS seismic depth-imaged

Geobody	Line #	Lee side			Stoss side			SDAS Thickness [m]	Interval Thickness [m]
		D [m]	L [m]	α [degrees]	D' [m]	L' [m]	β [degrees]	TVT from D and α	
1	23	122.0	2900.0	2.4	32.0	1018.3	1.8	121.9	399.0
1	23	88.0	1800.0	2.8	48.0	1470.2	1.9	87.9	127.0
1	23	120.0	2600.0	2.6	53.0	2249.0	1.4	119.9	390.0
1	23	67.0	1500.0	2.6	52.0	1985.8	1.5	66.9	246.0
1	5	139.0	3500.0	2.3	80.0	1850.0	2.5	138.9	
1	5	144.0	4000.0	2.1	42.0	2300.0	1.0	143.9	
1	5				36.0	1000.0	2.1		
1	20								370.0
1	19	98.0	3500.0	1.6				98.0	
Average		111.1	2828.6	2.3	49.0	1696.2	1.7	111.1	306.4
2	3	20.0	1000.0	1.1				20.0	
2	3	17.0	900.0	1.1				17.0	
2	3	29.0	1000.0	1.7				29.0	
Average		22.0	966.7	1.3				22.0	
3	19	50.0	2866.0	1.0				50.0	
3	23	33.0	1000.0	1.9				33.0	
3	23	33.0	1000.0	1.9				33.0	
3	19	70.0	3900.0	1.0				70.0	
3	19	48.0	1200.0	2.3				48.0	
3	20								463.0
3	20	84.0	1650.0	2.9	22.0	850.0	1.5	83.9	125.0
3	20	55.0	1000.0	3.1				54.9	324.0
3	4	61.0	2000.0	1.7	23.0	1500.0	0.9	61.0	
Average		54.3	1827.0	2.0	22.5	1175.0	1.2	54.2	304.0
4	3	82.0	1500.0	3.1	30.0	7500.0	0.2	81.9	135.0
4	3	77.0	2000.0	2.2	35.0	7427.0	0.3	76.9	
4	4	74.0	4500.0	0.9	39.0	1000.0	2.2	74.0	
4	4	57.0	2500.0	1.3	20.0	1100.0	1.0	57.0	
4	4	57.0	1950.0	1.7				57.0	
4	4	78.0	2500.0	1.8				78.0	
Average		70.8	2491.7	1.8	31.0	4256.8	0.9	70.8	135.0
Average		71.0	2177.8	2.0	39.4	2403.9	1.4	70.9	286.6
MIN		17.0	900.0	0.9	20.0	850.0	0.2	17.0	125.0
MAX		144.0	4500.0	3.1	80.0	7500.0	2.5	143.9	463.0

Table 3.2 Measurements of SDAS UM geobody 1

SDAS UM Geobody 1			
Vendor	**Lines**	**North to South**	**West to East**
PGS	19, 20, 22, 23	192 Km	97 Km
YucatanSPAN™	150, 3000, 3500, 4000	20.7° to 22.4°	94.4° to 95.5°

This first geobody is located on the western edge of a long chain of tectonic folds that are themselves visible in the modern seabed. These structures are more numerous at the north end of the geobody, showing 17 structures in the most northern seismic line and become smaller until six structures are observable on the southern line. The north and central part of the geobody is limited to the west by a MAC facies that has a smooth transition to SDAS while in the southern part of the body is limited to the west by a MAW facies with a gradual change to SDAS. The SDAS transitions to MAC seismic facies to the east.

The SDAS package is generally thicker at the north end, reaching 300 ms (TWT) and thinning to the south, ranging from 260 ms in the central part and decreasing to 150 ms in the southernmost part (Figure 3.10). The SDAS geobody is thinning to the east until it terminates laterally (Figure 3.11).

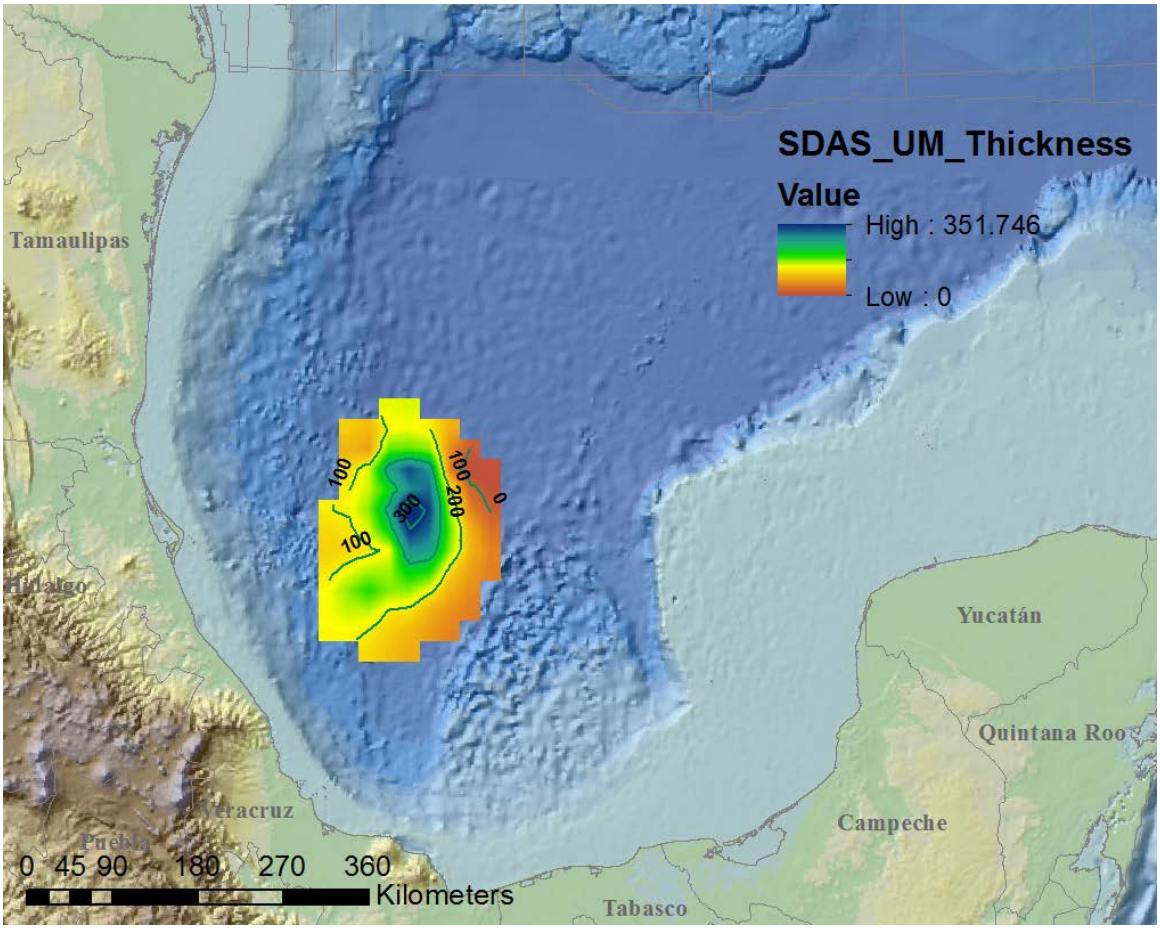

Figure 3.10 Isochron Map of the SDAS geobody 1, milliseconds (TWT).

The northern and southern parts of the SDAS package are located over Medium Amplitude Continuous (MAC) seismic facies while the central part overlays Medium Amplitude Wavy (MAW) seismic facies.

Under the geobody 1 are MAC facies in the northern and southern part while in the central part the geobody is over a MAW facies. Above this geobody the central part has High Amplitude Discontinuous (HAD) facies (Figure 3.11). In the north and south, geobody 1 is below the geobody 3 from the PB1 interval.

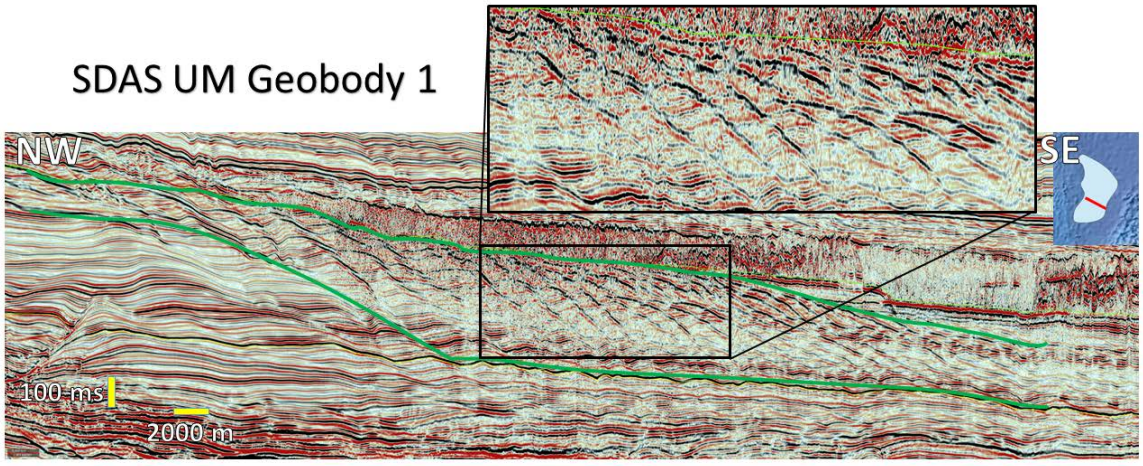

Figure 3.11. Seismic line showing SDAS geobody number one.

SDAS UPPER MIOCENE BODY # 2

A second Upper Miocene geobody of SDAS seismic facies was identified and mapped (Figure 3.12). This geobody 2 is located about 120 km to the north of the SDAS geobody number 1.

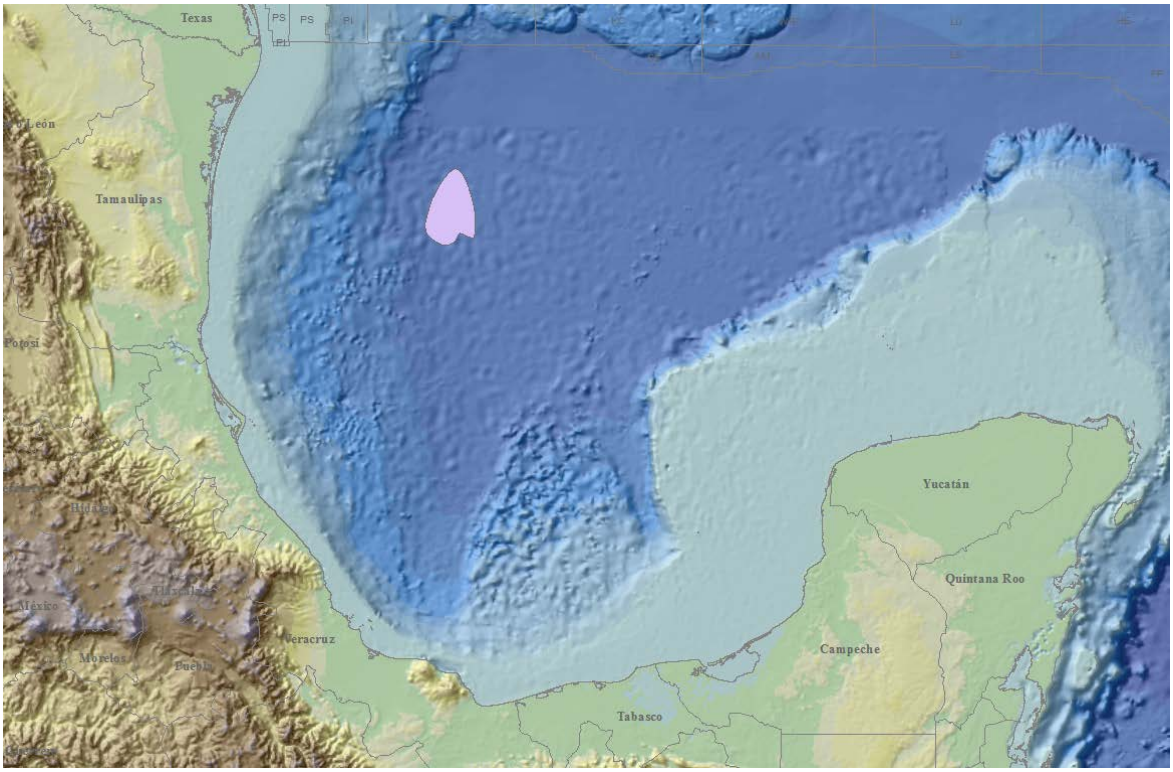

Figure 3.12. Map showing the location of the Upper Miocene SDAS Geobody 2

Table 3.5 Measurements of SDAS UM geobody 2

SDAS UM Geobody 2			
Vendor	**Lines**	**North to South**	**West to East**
PGS	14	100 Km	62 Km
YucatanSPAN™	100, 2500	23.5° to 23.9°	94.6° to 95.2°

Unlike SDAS geobody 1, this geobody is located 17 km from of a series of folds and seabed structures. The SDAS package is limited to the west by a 27 km width channel complex or submarine canyon facies (Figure 3.14). The SDAS transitions to LAC seismic facies to the east. In contrast with geobody 1, there is not an extended zone of thinning of the SDAS facies to the east.

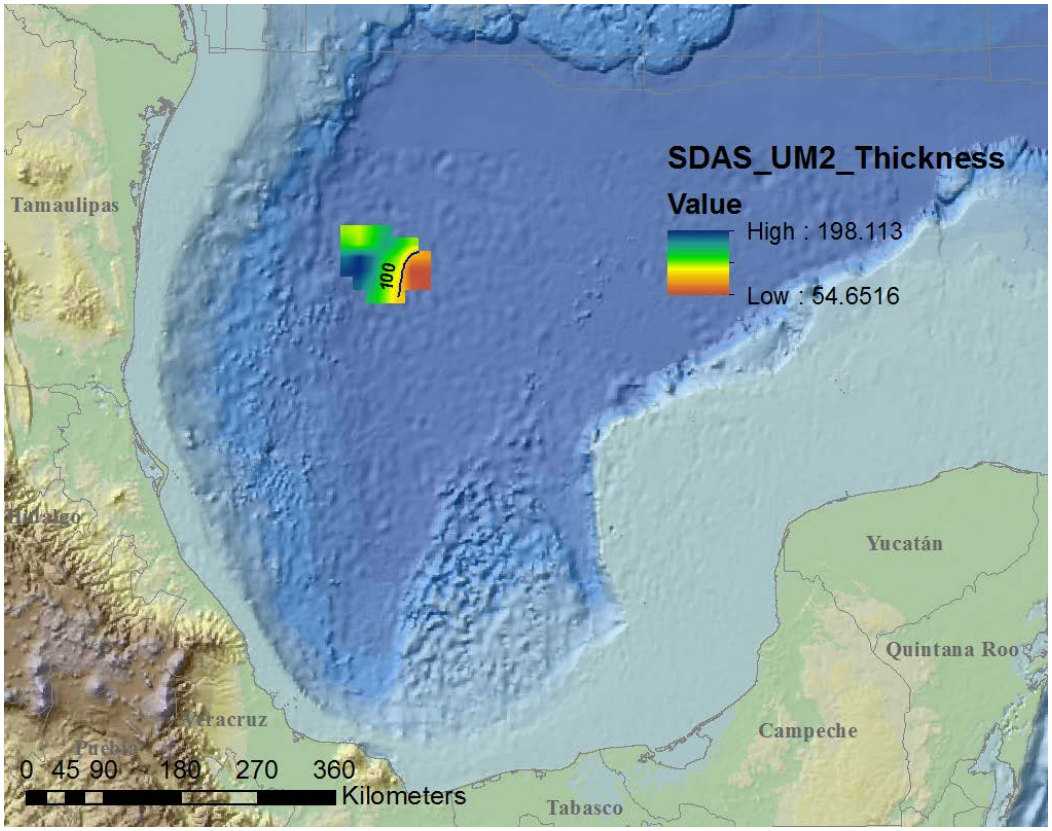

3.13 Isochron Map of the Upper Miocene Geobody 2, milliseconds (TWT).

The SDAS Geobody 2 is thicker on the west (nearly 150 ms TWT) and thins to the west. Below the SDAS body is a prominent high amplitude reflection that marks a sharp change to an underlying interval of MAC seismic facies. The SDAS package grades vertically into wavy seismic facies that continue until the seabed (3693 meters below sea level).

Geobody 2 is penetrated and cored in this area by DSDP leg 10 site 90 (Figure 2.7). Core 7 obtained samples of SDAS which indicated clay-rich sediments, though core recovery of sandy lithology was poor in this interval, due to the poorly consolidated section (DSDP Volume X, 1973).

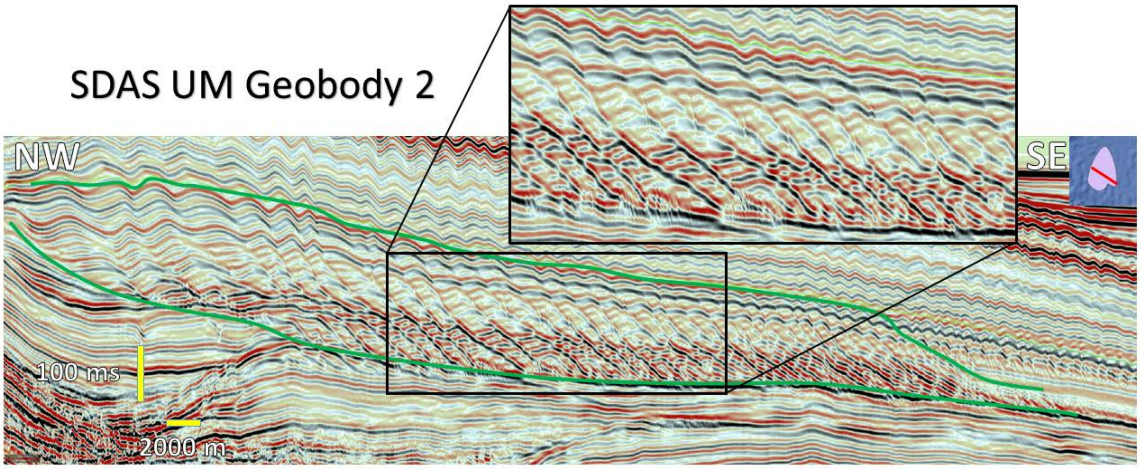

Figure 3.14 Seismic line showing SDAS UM geobody number two.

SDAS MIO-PLIOCENE (PB1) BODY #3

Seismic correlations indicate that SDAS facies geobody 3 was deposited during the Mio-Pliocene (PB1 unit; Figure 3.15).

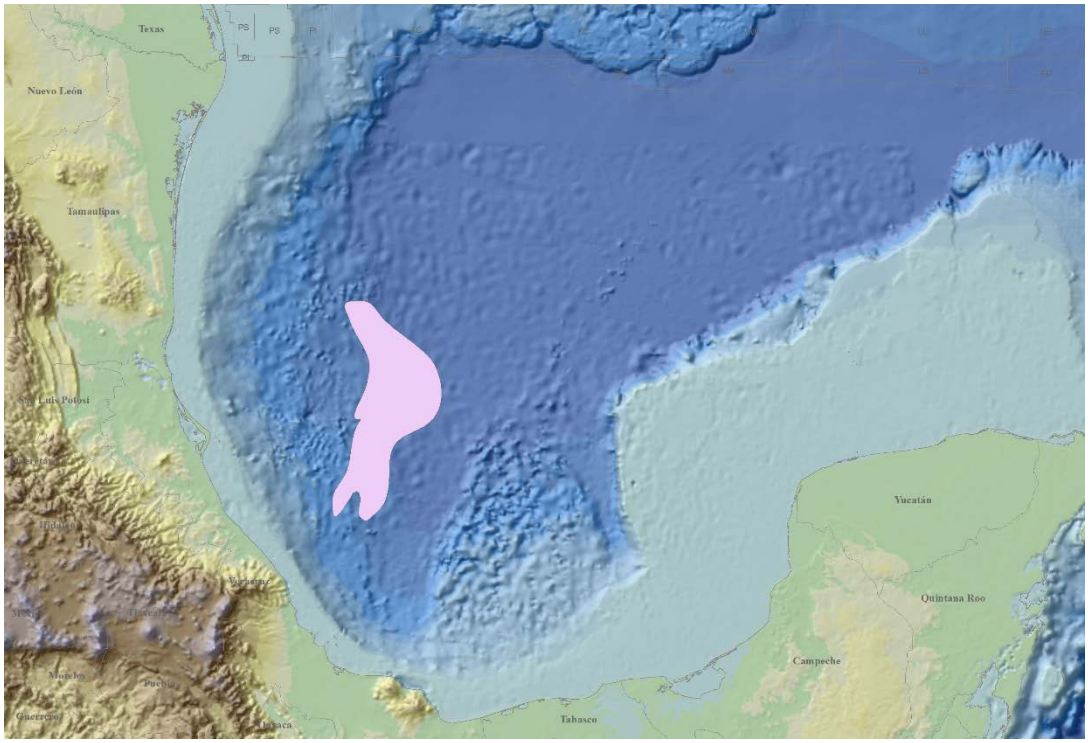

Figure 3.15. Map showing the location of the SDAS PB1 geobody 3.

Table 3.6 Measurements of SDAS PB1 geobody 3

SDAS PB1 Geobody 3			
Vendor	**Lines**	**North to South**	**West to East**
PGS	15, 19, 20, 23	285 Km	136 Km
YucatanSPAN™	4000, 3000, 3500, 250	20.5° to 23.1°	94.5° to 95.5°

Like SDAS Geobody 1, this geobody is located at the end of a long chain of Mexican ridge folds and tectonic structures, whose amplitude decreases gradually to the south. This geobody is limited to the west by MAC facies with smooth transition to SDAS facies. The SDAS geobody 3 is limited to the northeast, transitioning to MAC facies and to the southeast with HAD facies that become LAD facies trending to the south.

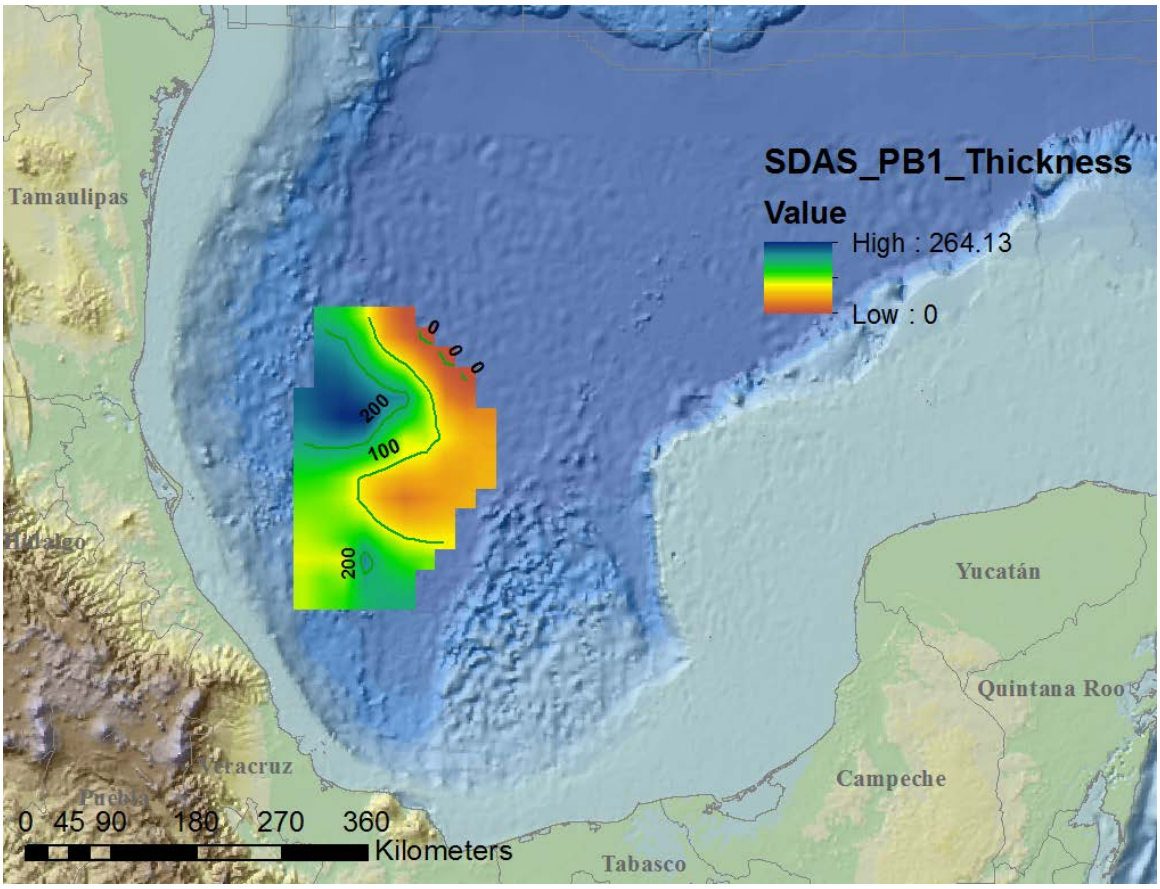

Figure 3.16 Isochron Map of the PB1 age geobody 3, milliseconds (TWT).

Above the north part of the SDAS geobody 3 is a MAC facies, above the central part is SDAS PGa seismic facies and above the southern part is MAW seismic facies. Below the north part of the SDAS geobody 3 is LAC seismic facies while below the central and south part is SDAS UM seismic facies (Figure 3.17).

The SDAS geobody 3 varies in thickness from north to south, from 200 ms TWT on the north, 80 ms TWT in the central part and on the south has a range from 150 to 330 ms TWT (Figure 3.16).

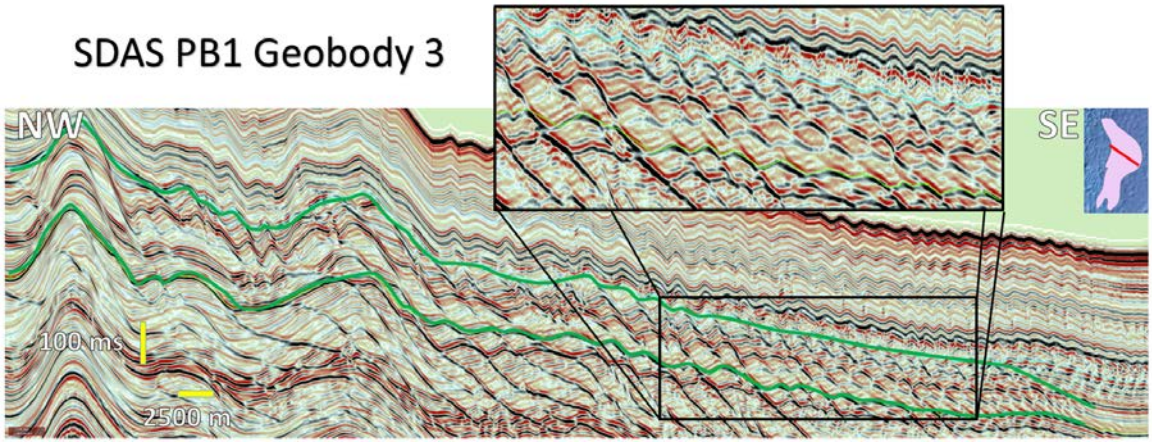

Figure 3.17 Seismic line showing SDAS geobody number three.

SDAS PLIOCENE BODY #4

This SDAS geobody number 4 is the most western SDAS geobody (Figure 3.18). As with geobodies 1 and 3, it is located at the eastern end of a chain of folds and seabed structures. At the northwest end, it is limited by five Mexican Ridges seabed structures. The number of seabed structures reduces to four at the southwest end.

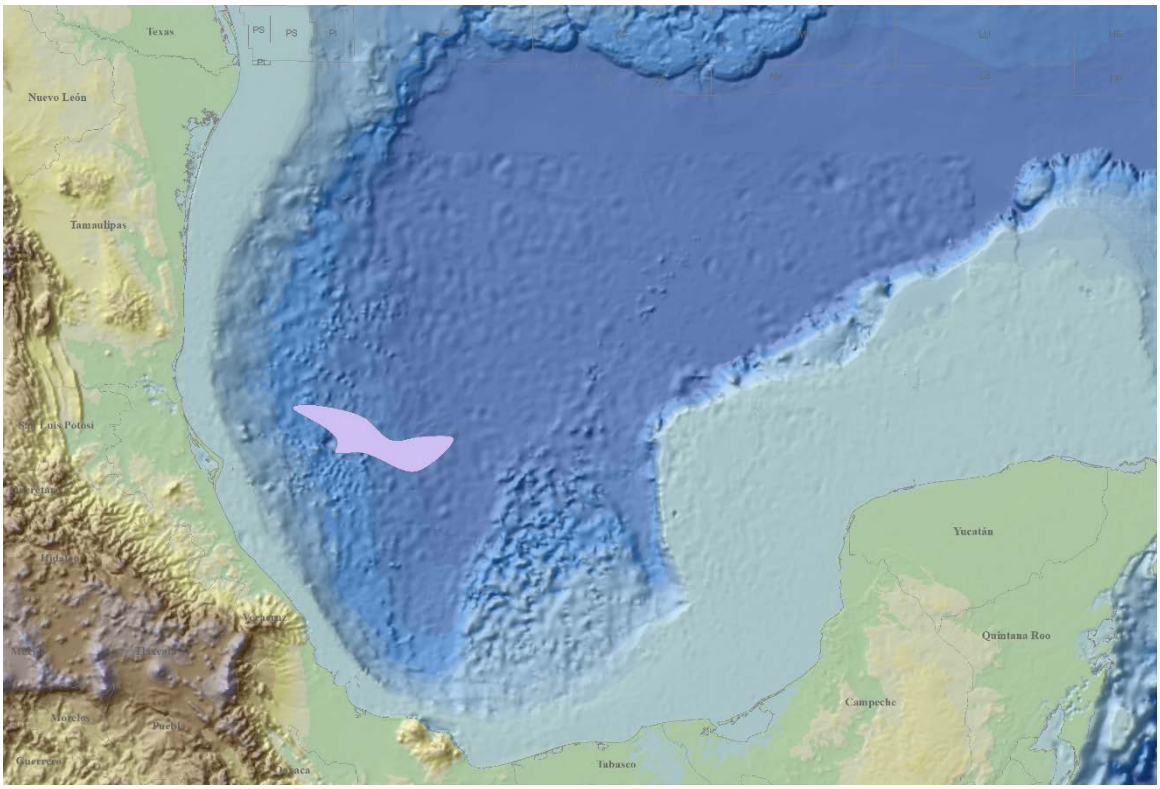

Figure 3.18. Map showing the location of the SDAS PB1 body.

Table 3.7 Measurements of SDAS PB1 geobody 4

SDAS PGa Geobody 4			
Vendor	**Lines**	**North to South**	**West to East**
PGS	23, 19	84 Km	183 Km
YucatanSPAN™	3000, 3500	21.4° to 22.1°	95.2° to 96.4°

The SDAS geobody 4 is limited at the northwest area by transition to MAC seismic facies and at the west end with transition to LAD seismic facies. This geobody terminates to the east with LAC facies and to the southwest with MAC seismic facies.

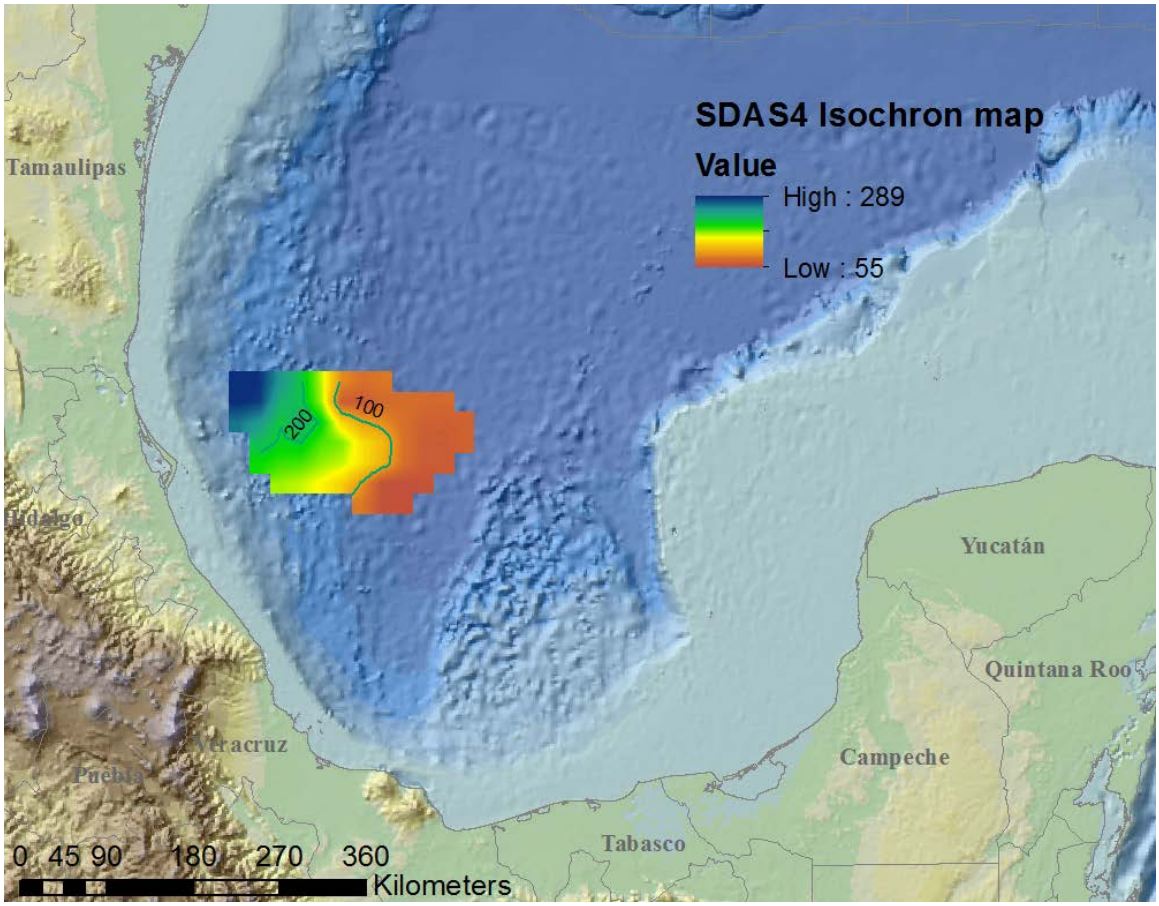

Figure 3.19 Isochron Map of the PB1 age geobody 4, milliseconds (TWT).

Above the SDAS geobody 4 is a MAC facies in the north that grades into MAW in the south of the body (Figure 3.20). Below the geobody is a LAD seismic facies on the western half and eastern areas have a contact with the MAC facies. The SDAS geobody 4 has an almost uniform thickness, with a limited range from 190 to 230 ms TWT (Figure 3.19).

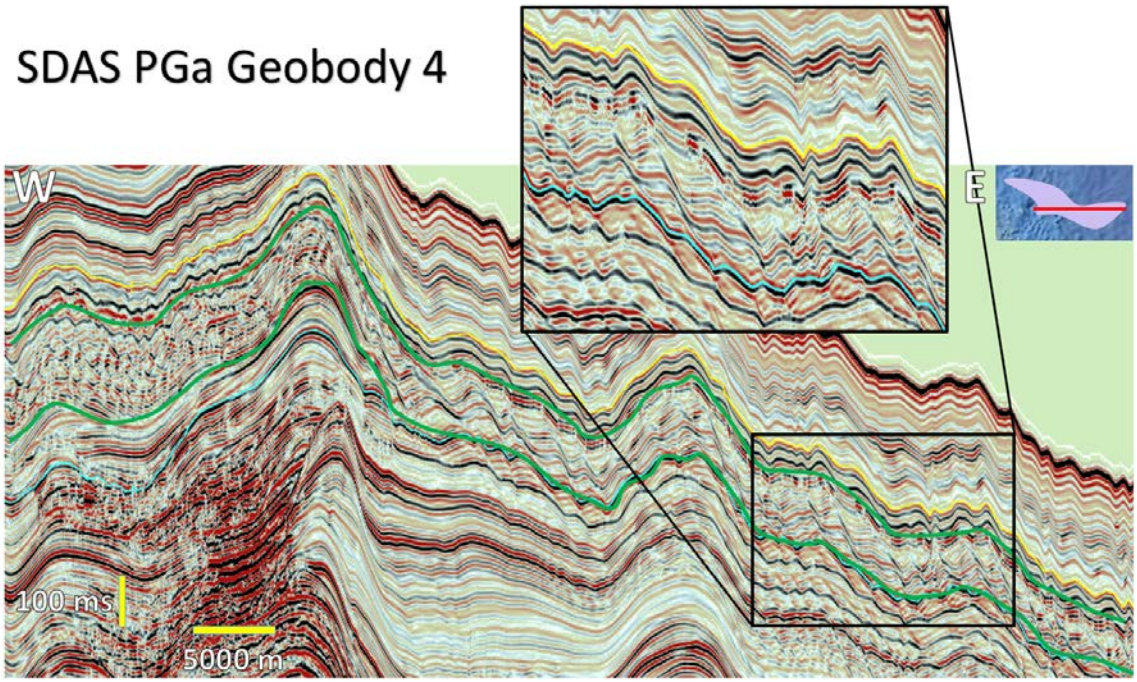

Figure 3.20 Seismic line showing SDAS geobody number four.

Chapter 4: Interpretation

A series of hummocky, oblique, and shingled to parallel seismic clinoform reflections were deposited during the Upper Miocene, Mio-Pliocene and Pliocene intervals. These geobodies are referred as Seaward Dipping Accretion Surfaces (SDAS). These downlap onto the underlying intervals. Within the Pliocene section these are relatively thin but are thicker in the Upper Miocene (Figure 4.1).

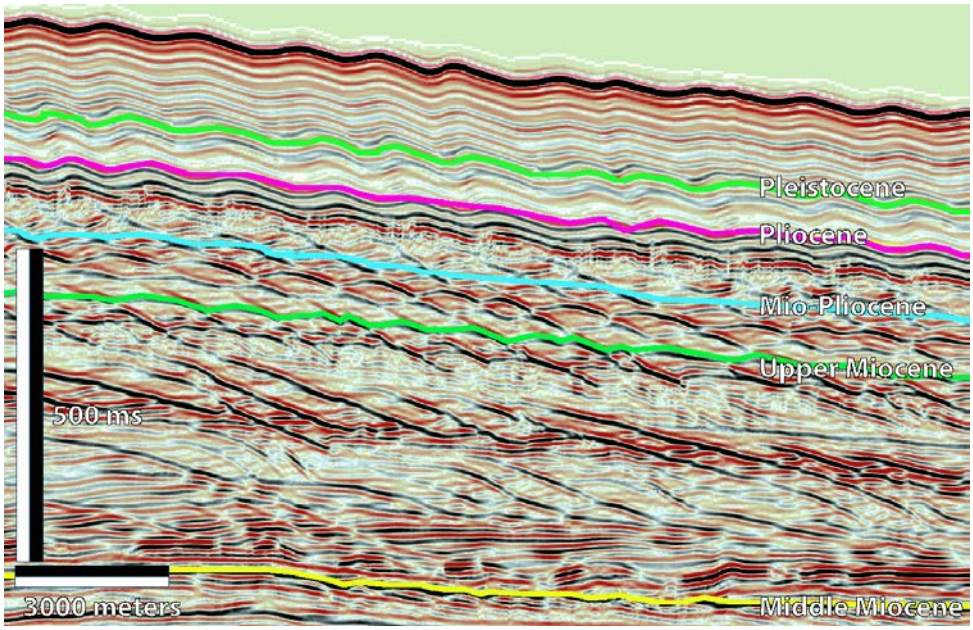

Figure 4.1 Cross-section were the SDAS are found from the Upper Miocene until the Pliocene.

These SDAS are located in the range from 45 to 142 mi (73 to 230 km) from the mapped coeval shelf-edge (Figure 4.2). Paleo water depths in this area are likely to have been bathyal (>1500 ft.; 450 m) at this time (Ambrose et al., 2005; Rodriguez, 2011; Snedden et al. 2012). In these paleo-deepwater depths, there are three main sedimentary processes that could be responsible for depositing this bedded seismic facies: bottom

currents, hemipelagic settling, and turbidity currents (Figure 4.3). This classification excludes mass transport deposits which rarely generate bedforms of this scale and form.

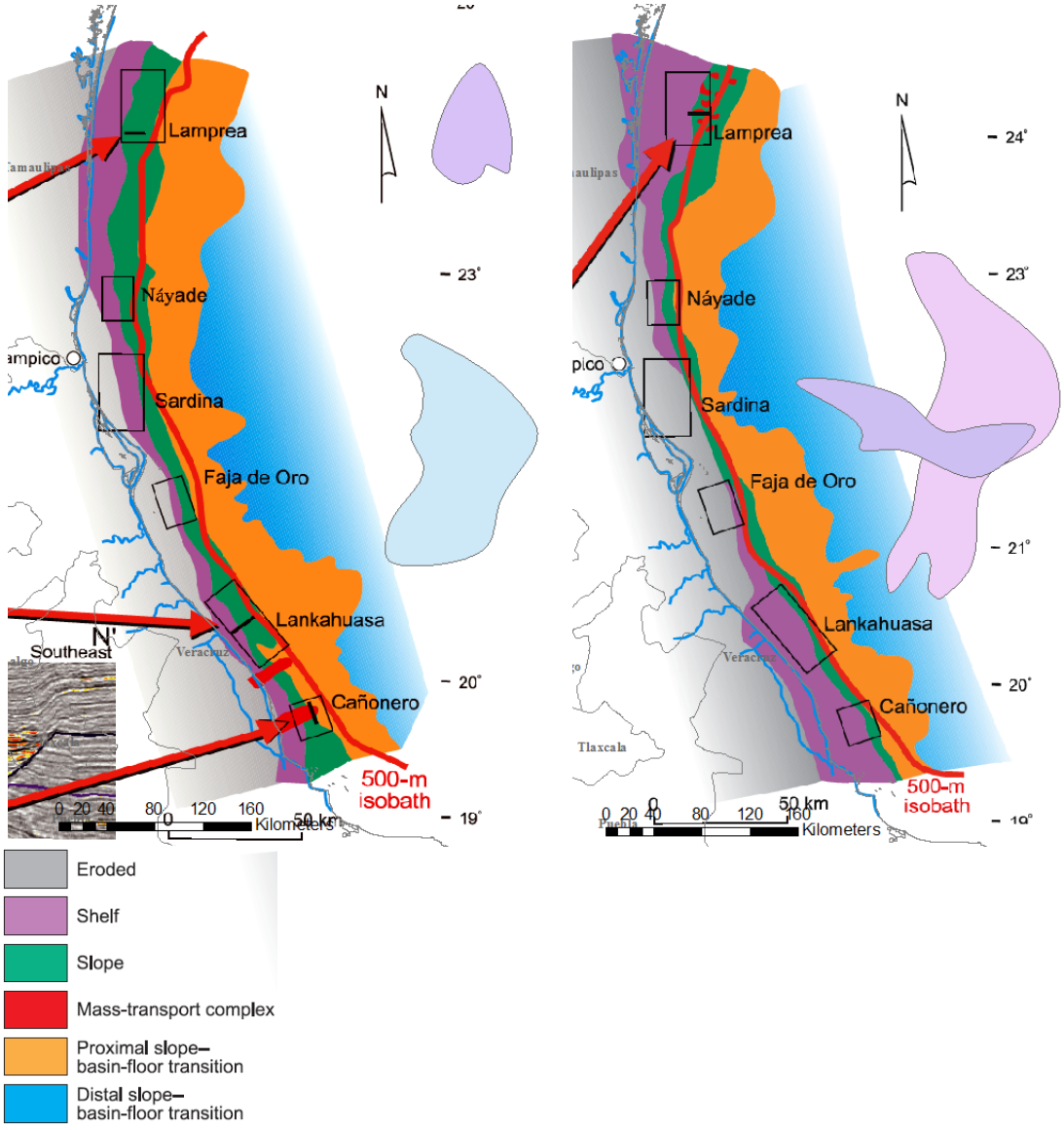

Figure 4.2 Progradation of the shelf from the Upper Miocene to Upper Pliocene (Ambrose et al., 2005). Note location of 500 paleo-isobath.

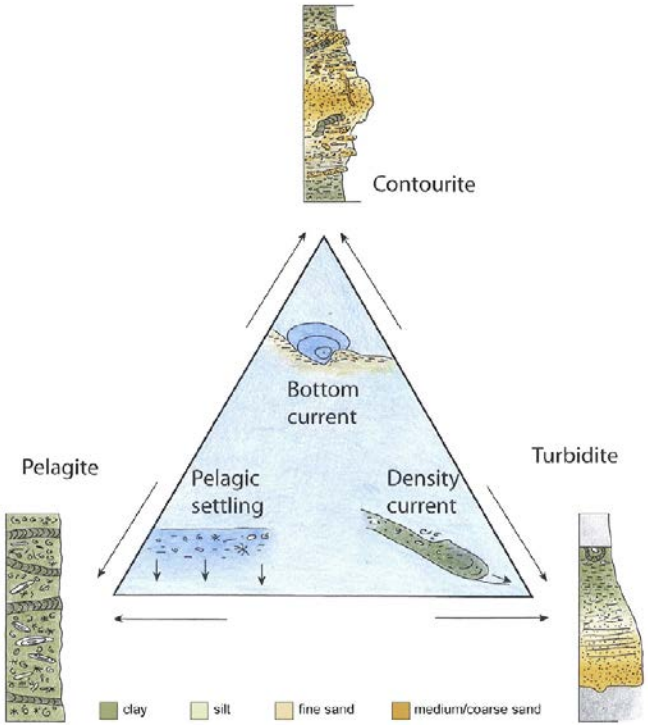

Figure 4.3 Conceptual diagram showing the three main types of sedimentary processes operating in the deep sea and the facies model of the respective depositional products. (Rebesco et al., 2014)

Depositional Models

Evaluation of seismic and well data, leads one to propose two possible mechanisms forming the genesis of Seaward Dipping Accretion Surfaces (SDAS) seismic facies:

1. Along slope-flowing bottom currents.
2. Downslope-flowing (unconfined) turbidity currents.
3. Levee-overbank over-spilling turbidity flows.

1. ALONG SLOPE-FLOWING BOTTOM CURRENTS

Persistent bottom-current systems strongly affect the seafloor in some areas, creating erosional moats and depositing large accumulation of sediments, known as contourite drifts (Rebesco et al., 2014). Contourite drifts have along-slope elongated mounded geometry almost parallel to the margin and an adjacent concave moat. (Figure 4.4). These drifts can extend from the upper shelf to the abyssal plains. They can extend to more than 100 km in width, are hundreds of kilometers long, and up to 2 km thick. Areal dimensions range from 100 km^2 to 100,000,000 km^2. Contourites drifts act as a petroleum reservoirs and also can be sealing rocks if particularly fine-grained. The main difference between sandy and muddy contourites depends on bottom current energy and proximity of sand-rich areas prone to sweep by contour currents.

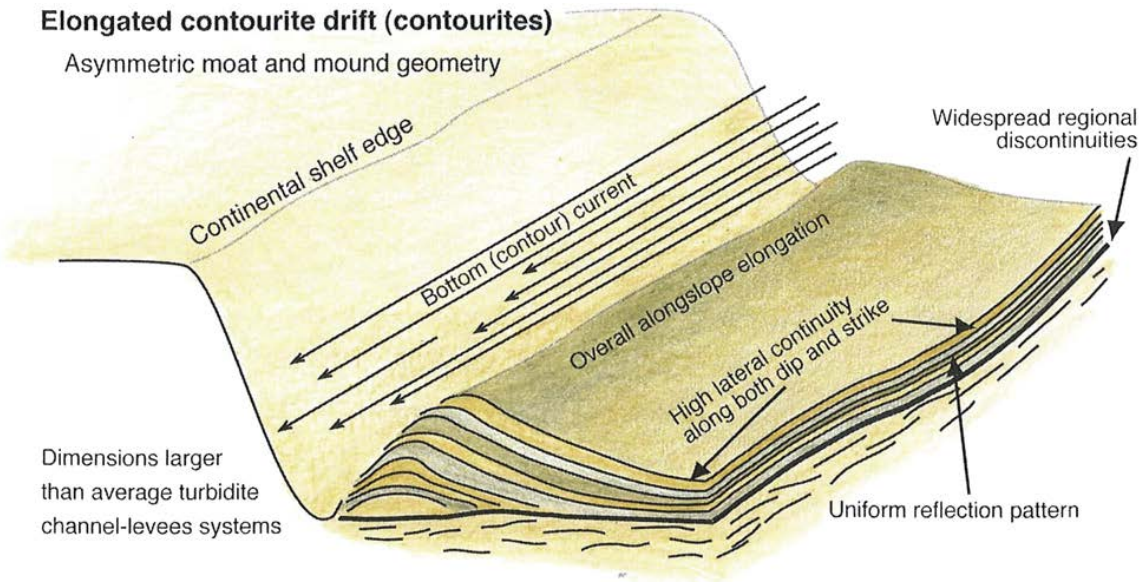

Figure 4.4 Schematic model showing the ideal contourite drift (Rebesco et al, 2014).

The SDAS seismic facies were originally identified on older vintage 2D UTIG seismic data (Snedden et al. 2012; Figure 1.10) and interpreted as attached to a submarine fan system coming out of the Cañonero Canyon system earlier identified by Ambrose et al. (2005). Modification of this submarine fan by northerly-flowing deep-water bottom currents possibly generated this seismic facies. The model of Snedden et al. (2012) suggested that SDAS were related to accelerated deep-water contour currents associated with closure of the equatorial seaway between North and South America (Figure 4.5). The Miocene is a well-known time period of changing oceanographic conditions as a function of closing oceans gateways (Potter and Szatmari, 2009).

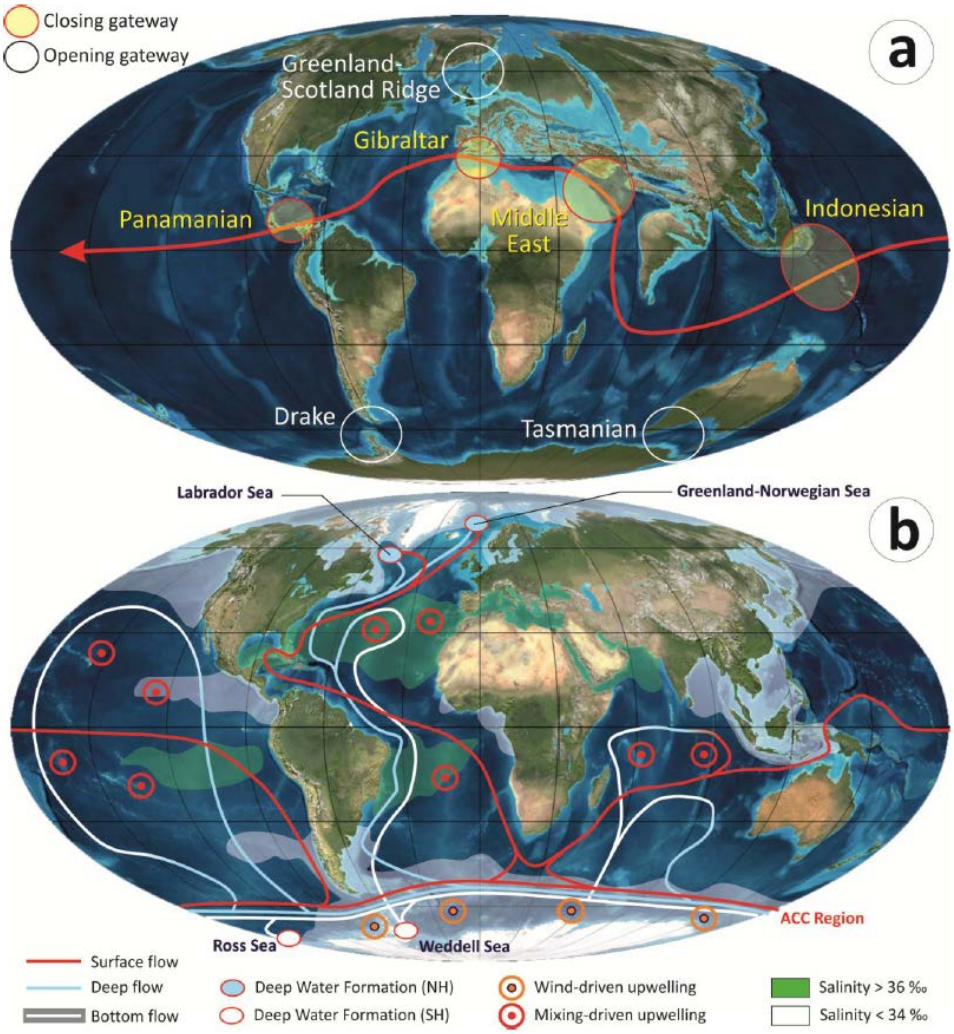

Figure 4.5 Differences between the global currents before and after the closure of the equatorial gateways (Potter and Szatmari, 2009)

Bottom current velocities tend to accelerate when encountering small-scale bathymetric features like submarine canyons or ridges due to confinement (Bernoulli effect). Such a velocity increase can keep particles in suspension for longer periods. Bottom current interaction with the Mexican Ridges could have strengthened bottom flow in some areas. These bottom currents could modify and, in fact, build thick and extensive contourite drifts deposits (Figure 4.6).

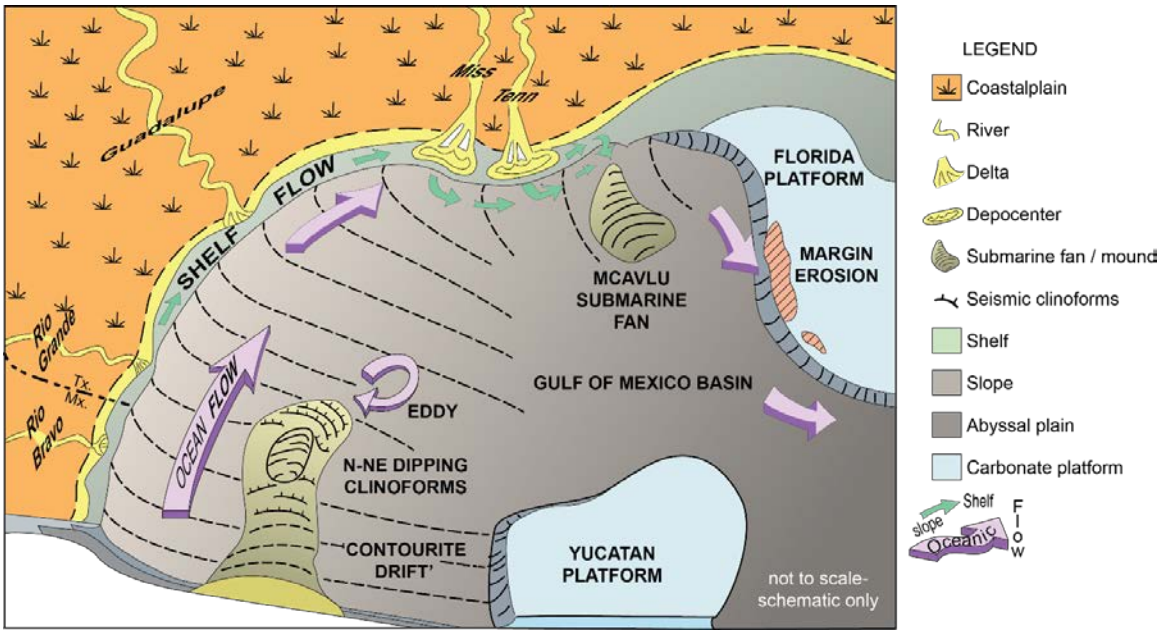

Figure 4.6 Diagram showing Miocene contourite drift in Mexico (from Snedden et al. 2012).

The source of sediments for those contourite deposits would be the submarine fans deposited during the Miocene in deep waters of the Gulf of Mexico, reaching their maximum extension during the Upper Miocene as is shown by Snedden et al. (Figure 4.7). This would also apply to the SDAS geobodies 1, 3 and 4 that are limited to the west by the Mexican Ridges (Figure 4.8). However, is common to find contourites deposits interbedded with other deepwater facies types so other sedimentary processes need to be considered.

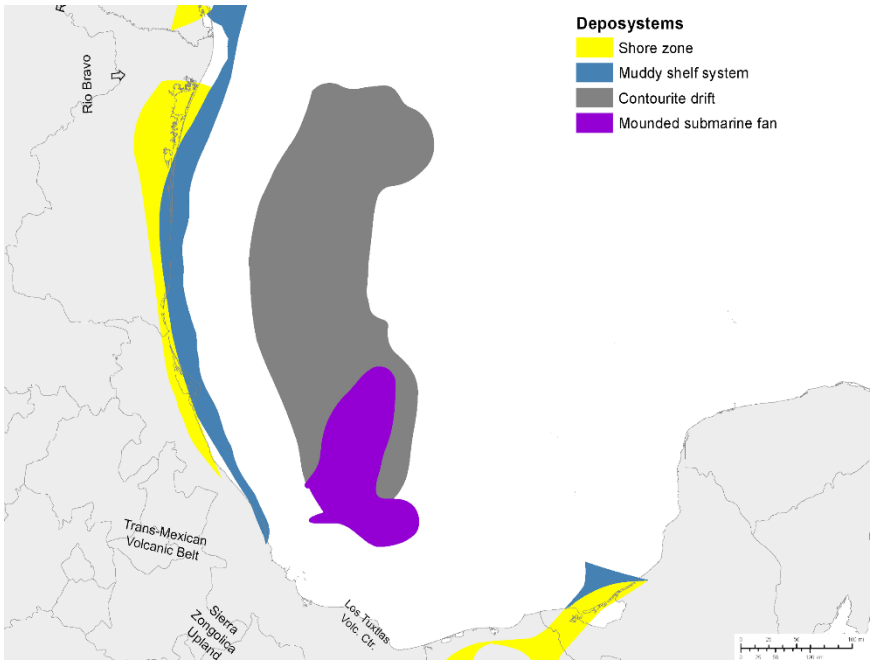

Figure 4.7 Map showing the maximum extent of the contourite drift during the Upper Miocene (Snedden et al. 2012).

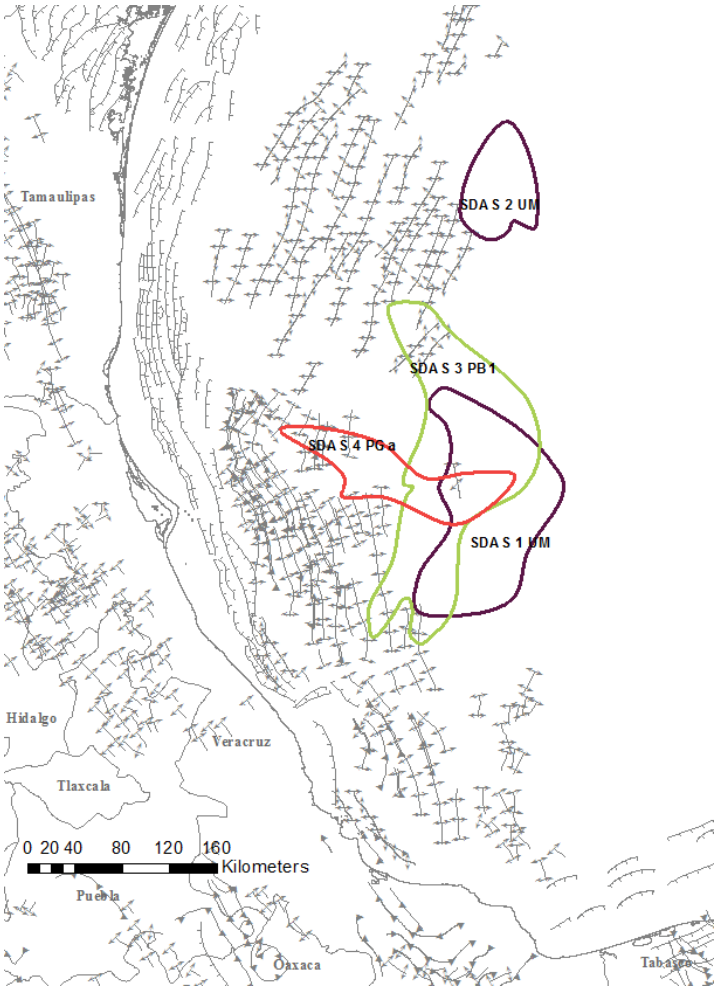

Figure 4.8 Location of the SDAS geobodies, Mexican Ridges and nearby onshore basins and tectonic features (modified from Yarbuh and Contreras, 2015).

It is possible that the sediment drift type that we observe in these geobodies represent elongated, mounded drifts in one or two different forms (Figure 4.10). Separated drifts are associated with steeper slopes and are bounded by a distinct erosional moat. Or these could be detached drifts, with pronounced elongation that deviates from the adjacent slope against which it first began to form (Figure 4.9). These drifts would be of the type of bottom-current reworked sands from previous turbidity deposits from the submarine fans. These deposits are characterized by smaller scale sand-mud rhythmites,

double-mud layers, climbing ripples, mud-draped ripples, alternation of parallel and cross-lamination, representing variable deposition by traction load or suspension load (Figure 4.10). Paleocurrent orientations are a good way to differentiate between contourites and turbidite deposits, as along slope trends suggest contourites and downslope transport vectors are characteristic of turbidites. However there is no unique facies sequence for contourites because most of the structures are also present in other deepwater deposits, so there is no general agreement on ways to differentiate between contourites from turbidites (Rebesco et al., 2014).

Recently acquired, higher resolution 2D seismic data by PGS and reprocessed UTIG data (marketed as YucatanSPAN), permits reevaluation of the SDAS seismic facies as cyclic steps bedforms generated by downslope easterly-flowing turbidity currents. This model, and its implication for the regional depositional history is described in the next section.

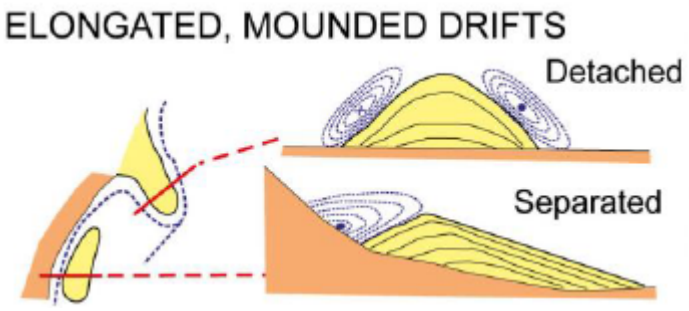

Figure 4.9 Sediment drift type and inferred bottom-current paths (Rebesco et al., 2014)

.

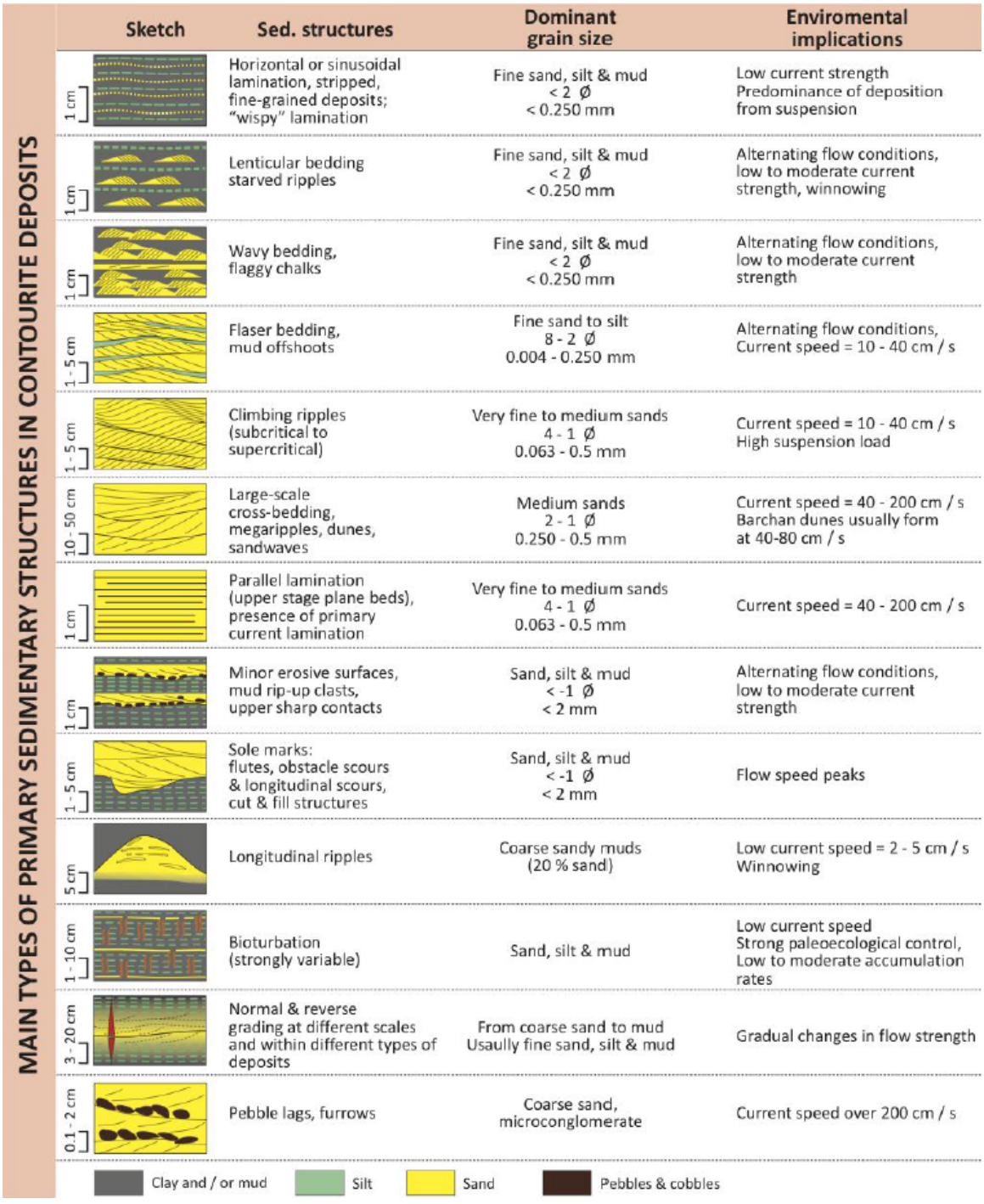

Figure 4.10 Main types of sedimentary structures in contourite deposits (Rebesco et al., 2014)

2. HIGH DENSITY TURBIDITY FLOW CYCLIC STEPS HYPOTHESIS

Sedimentary structures observed in core photographs of the nearby Kunah-1 well include dish and fluid escape structures, Bouma sequence Ta-Tb-Tc-Td-Te bed divisions, sharp basal contacts, and other structures consistent with deposition by turbidity flows (Appendix). In fact, many beds and bedsets of these Miocene-age cores show upward-fining (normal) grain size trends as well as decreasing sand percentages, consistent with both high density and low density sediment gravity flows.

Recent work with both modern data and experimental simulations of sedimentation indicate deepwater turbidity flows can produce bedforms called "cyclic steps" (Kostic, 2011). Covault et al. (2014) describes submarine cyclic steps as morphodynamic features characterized by a cyclic series of long-wave, upstream-migrating bedforms. The average wavelength of cyclic step bedforms is a factor of 10 x the turbidity flow thickness (Kostic, 2011). Using this Kostic proportion (Table 4.1), average turbidity flow thickness is estimated in Table 4.1. The ratio of bedform wavelength to flow thicknesses in marine environment has been estimated to be between 1 and 7 (Allen, 1982a)

Table 4.1 Average Wavelength and Thickness per geobody

Geobody	Average Wavelength [m] (Crest to crest)	Average Flow Thickness [m] (Wavelength/10)
1	2581	258
2	186	18
3	1904	190
4	1808	180

The bedforms are classified as cyclic steps if each bedform in the series is bounded by a hydraulic jump in an overriding turbidity current, which is Froude-supercritical (Froude number >1) over the lee side of the bedform and Froude-subcritical (Froude number <1) over the stoss side where deposition would occur (Figure 4.11). If we superimpose the Covault et al. (2014) model on the SDAS seismic facies, a similar geometric fit for asymmetrical cyclic steps can be inferred.

Three facies types that characterize three different flow conditions and lithologies associated with cyclic steps are:

1) Structureless sands (supercritical flow at the hydraulic jump)

2) Cross-stratified sands (subcritical flows)

3) Parallel laminated sands (Froude numbers just below 1.0)

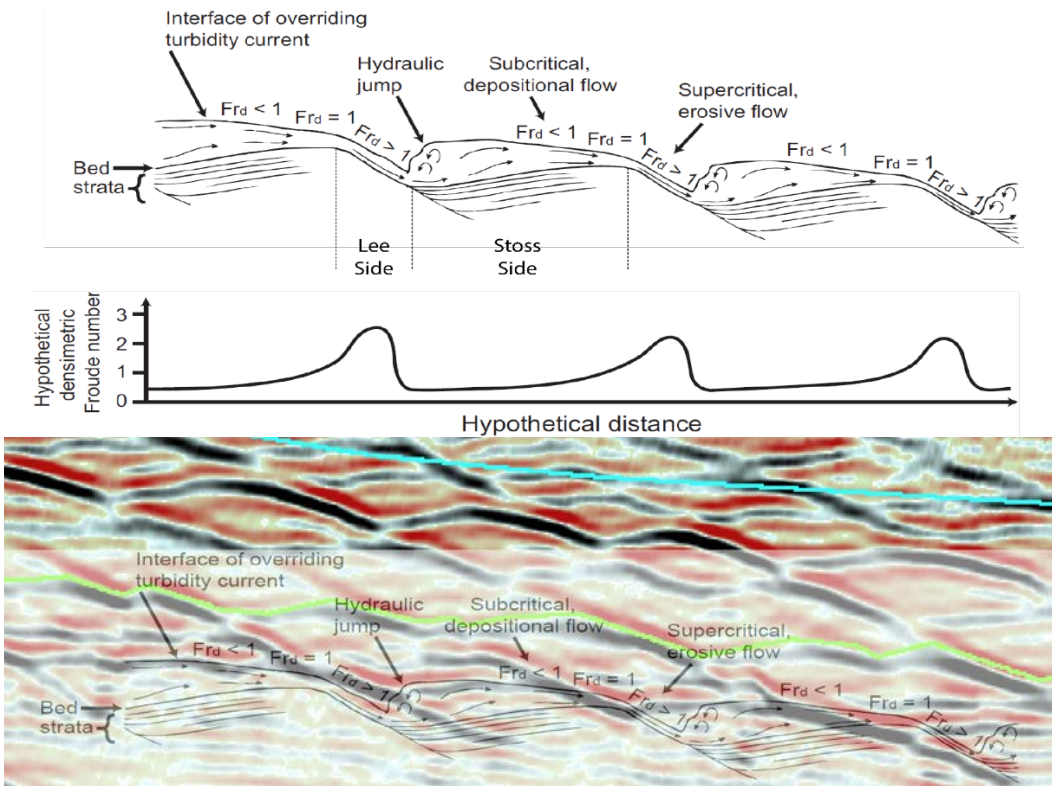

Figure 4.11 Schematic drawing of a series of down-slope asymmetrical cyclic steps (downstream from left to right) and hypothetical densimetric Froude number (Fr) variability. Modified from Covault et al. (2014). Below. Superimposition of Covault et al. (2014) schematic figure on the SDAS facies in the study yields some geometric similarity.

Cartigny et al., (2011) suggests that the geometry of up-slope migrating sediment waves geometry can be symmetrical, asymmetrical upsloping facing crests or asymmetrical with the crest facing downslope (Figure 4.12).

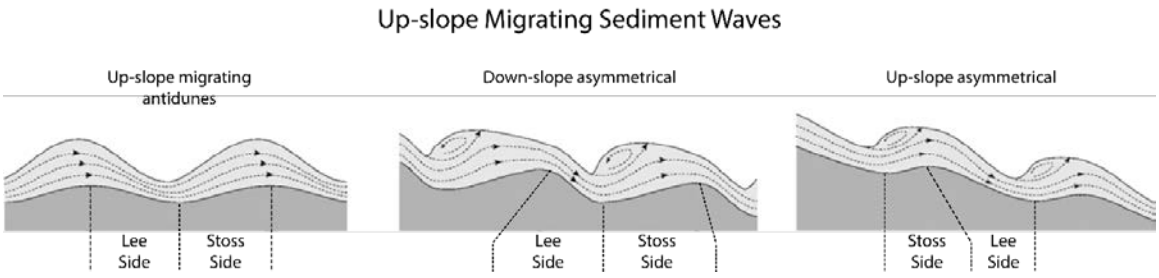

Figure 4.12 Different geometries of the up-slope migrating sediment waves and how their stoss and lee sides can vary. (Modified from Cartigny, 2011)

Sediment-laden, high-velocity turbidity flows form these supercritical bedforms. The migration direction (trace of the crests) is useful to distinguish cyclic steps from subcritical bedforms, as dunes migrate down flow while supercritical cyclic steps migrate up flow. Internal structures of supercritical flow in stoss side bedforms are unique to cyclic steps and hold the clearest evidence to distinguish supercritical flow cyclic steps from large scale subcritical regime dunes (Cartigny et al. 2011). Cyclic steps can exhibit erosional truncation on the lee side, which under conditions of high deposition, produces down flow "back-sets" (Cartigny et al. 2011) or dipping accretion sets separating the aggrading stoss side bedforms (Figure 4.11).

Cyclic steps are, in general, one order of magnitude larger than antidunes. It is therefore improbable to form antidunes and cyclic step of the same scale in a single train of sediment waves. Experiments show that there is a gradual transition between antidunes and cyclic steps (Cartigny et al. 2009). Kubo and Nakajima (2002) proposed that cyclic steps can result from antecedent topography on the seafloor. Cyclic steps initiate by breaking antidunes, leading to a gradual transformation from antidunes into larger cyclic steps.

Turbidity current-generated cyclic steps can be fine-grained or coarse-grained. Fine- grained cyclic steps consist of mud to fine sand, with the coarser grain sizes deposited on the stoss side. Cyclic steps can be found in areas where turbidity currents flow unconfined, such as on the back slopes of channel-levees (Normark et al. 2002). Cyclic steps have been observed where turbidity flows exit canyons into less confined down flow areas (Cartigny et al., 2011). Lengths of fine-grained sediment waves range from 1 to 7 km with heights up to 80 m (Table 4.2). Dimensions are closely related with slope and distance from the source area, with shorter length and less aggradation in the downslope direction (Normark et al. 2002). This pattern can be observed in Figure 3.14.

Table 4.2 Range of Length and Height of Cyclic Steps. From Cartigny et al. (2011).

Range of Size of Cyclic Steps							
Fine Grained Cyclic Steps				Coarse Grained Cyclic Steps			
Length		Height		Length		Height	
1 km	7 km	0 m	80 m	0 km	1 km	0 m	10 m

Coarse-grained cyclic steps consist of fine to coarse sand deposited on the stoss side due to the effect of rapid flow deceleration and instantaneous deposition of coarser sediments just after the hydraulic jump. These are often located in the proximal part of the submarine fan systems, such as in canyons, channels, and channel-lobe transitions. Wavelengths of coarse-grained sediment waves reach up to 1 km with wave heights up to 10 m (Table 4.2). The downslope facing asymmetric geometry is more common in coarse-grained sediment cyclic steps bedforms. (Cartigny et al., 2011). Downslope facing asymmetries seem to characterize confined, high-energy settings, while the upslope-facing asymmetries are apparently more representative of fine-grained sediment waves in

unconfined, low energy environments (Cartigny et al. 2011). The only bedforms that displays such wide range of symmetries are cyclic steps.

The cyclic steps formed by turbidity currents are initiated by a slope instability or some type of sea bottom roughness. Cyclic steps structures can be created in deep-water channels and canyons (Smith, et al. 2005), on levee-overbanks (Normark et al. 1980; 2002), and on submarine fans by more unconfined flow (Flood et al. 1995).

Examples

Geobody number 2 is located 17 kilometers east of the last of the Mexican Ridges (Figure 4.13). Here the SDAS are associated with a large channel complex or small canyon implying that the cyclic steps formed as part of levee-overbanking flows. However, the ratio between SDAS facies to channel complex is >3:1, though part of the section may be oblique to flow. This geobody is one of the smaller geobodies as the average wavelength (Table 4.1) is only one tenth of the size of the other SDAS bodies. The ratio of the ratio of channel complex to overbank deposit seems unusually high (>3:1) but more data is needed to distinguish cyclic steps levee-overbanks and SDAS unconfined flow deposits in the case of this geobody.

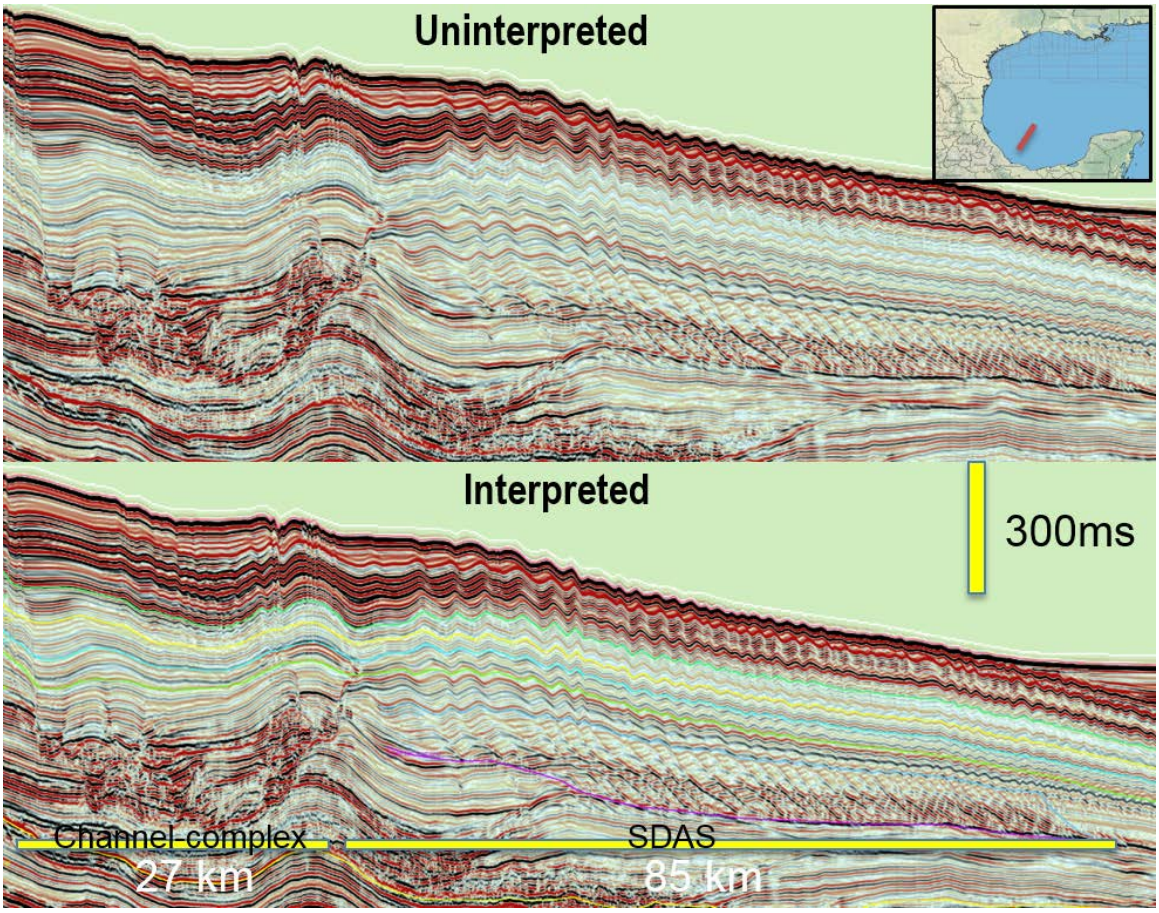

Figure 4.13 Seismic line across SDAS body 2.

SDAS bodies 1, 3 and 4 (Figure 4.8) are located just east of the Mexican Ridges, but, distant from mapped channel-complexes or canyons. Early forming ridges could have created a slope and sea bottom roughness (Figure 4.14) to generate the necessary flow instability initiating supercritical turbidity currents that deposited these cyclic steps bodies in a more unconfined flow here. Cyclic steps in this area could have been created by submarine fans in unconfined flow settings as is described by Flood et al. (1995).

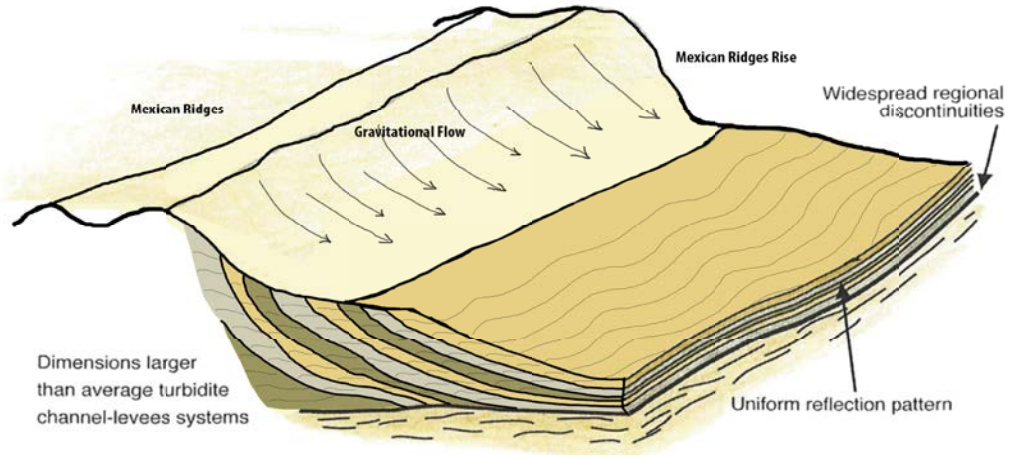

Figure 4.14 Cyclic steps model for study area.

Regional Context for SDAS Deposition

The Neogene strata of eastern Mexico exhibit features of a tectonically active, divergent margin setting. Active plate subductions at the Pacific Plate margin and the passage of the Chortis continental block to the south resulted in long-lived Tertiary orogenesis and volcanism in the hinterland. Sediments were deposited along narrow shelves and steep slopes (Figure 4.15) dominated by siliciclastic deposits, linked to tectonically active coastlines affected by uplift and erosion of adjacent volcanic and carbonate terrains (Ambrose et al., 2005). Associated loading and subsequent gravitational sliding in the Quetzalcoatl extension is linked with the compression in the Mexican Ridges fold belt. Uplift in eastern Mexico resulted in deep incision and canyon formation along a narrow shelf and slope leading to delivery of large volumes of coarse-grained sediments to the basin floor (Ambrose et al., 2005; Figure 4.15).

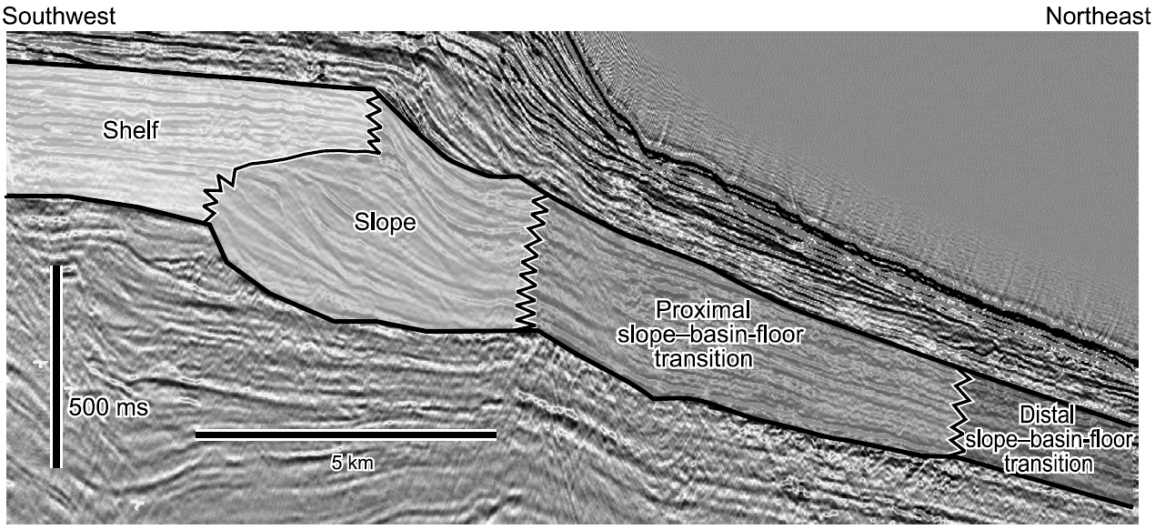

Figure 4.15 Seismic line showing present-day and inferred Neogene narrow shelf-slope-basin profile in eastern Mexico (from Ambrose et al. 2005).

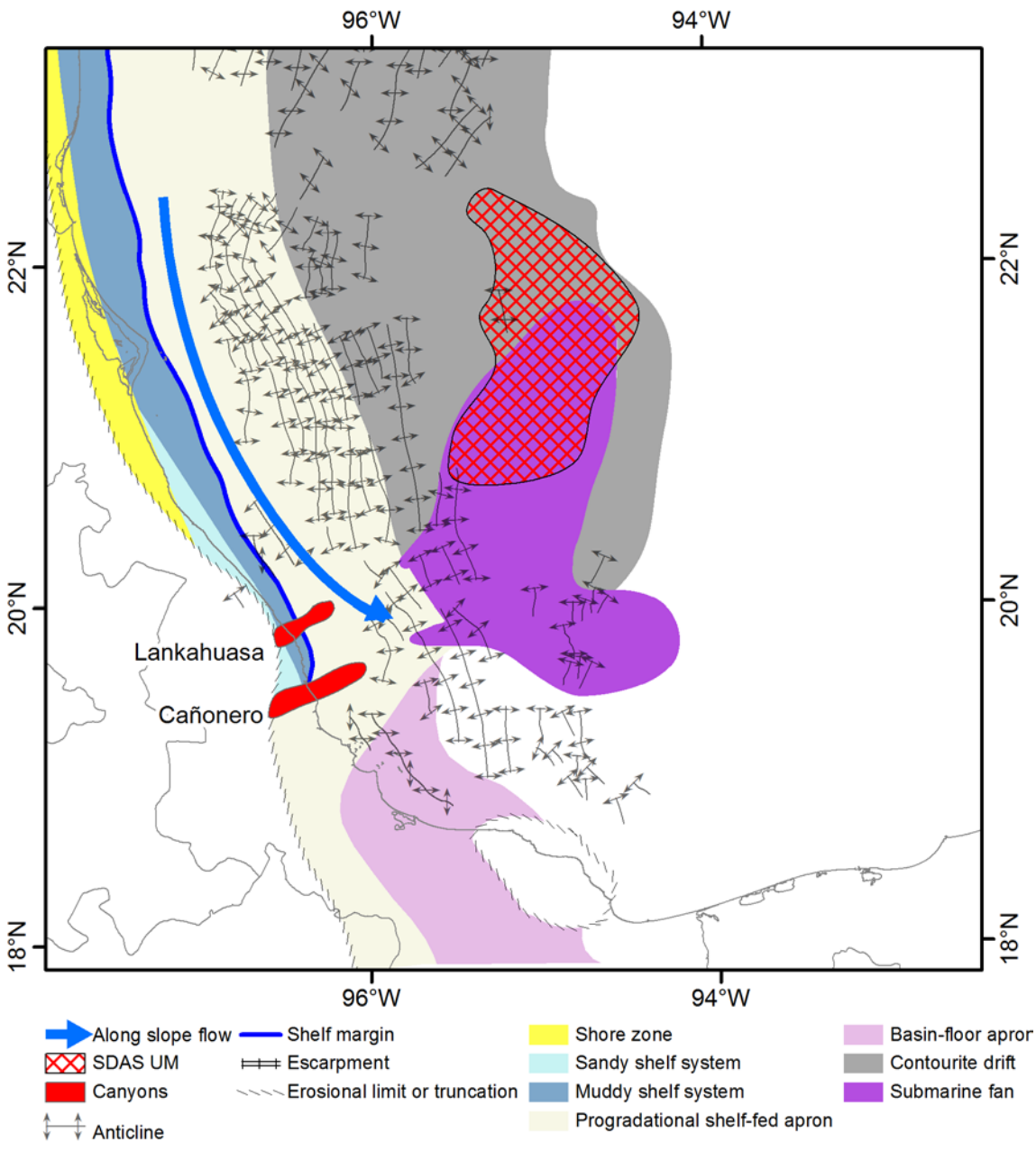

Figure 4.16 Upper Miocene canyon systems related with SDAS UM geobody 1. (GBDS paleogeography and adapted from Ambrose et al. 2005).

Neogene strata in eastern Mexico are part of an overall progradational, offlapping succession. The upper Miocene shelf edge was located eastward of the modern coastline and shelf deposits were likely deeply dissected by channels and canyons (Figure 4.16). Upper Pliocene slope deposits are almost at the same location of the modern shelf break (200 m water depth). The Upper Pliocene is interpreted to be more eroded and consist of several shelf successions intercalated with inner slope slump deposits (Ambrose et al., 2005). Geobody number 3 appears to be located at the transition of two different margin settings. Contemporaneous slopes were mud-dominated at that time. A few well developed submarine canyons graded distally into basin floor fan deposits (e.g. Cañonero Canyon). Those basin floor fan deposits consist of bright-amplitude zones of wavy, subparallel to mounded reflections. These reflect individual episodes of lowstand-derived submarine-canyon and basin-floor-fan development tectonically driven by the uplift of the Sierra Madre Oriental (Ambrose et al., 2005).

Neogene channel systems on the slope have complex routing directions, within an overall trend to the east-northeast. During the Upper Miocene, in the area south of Geobody 1, turbidite systems were steered into a confined area between the uplifting Mexican Ridges and the Catemaco Fold Belt (Figure 4.16). There is published seismic evidence for the presence of coarse-grained sediment turbidites systems between those fold belts (Arreguín-López et al., 2011). It is expected that those channel systems evolved basinward into more unconfined deposition in the Veracruz Trough. These basin floor fans could have long run-out distances that perhaps reflect the interplay among active orogenic processes in the continent, narrow shelf and frequent seismically triggered slope failures. Those sedimentary systems were steered by developing structural relief continuing until the Pliocene.

A seismic line that goes from north to south through Geobodies 1, 2 and 3 illuminates the spatial and temporal association with mound-like (double downlapping) features earlier interpreted as a submarine fan (Figure 4.17). This suggests that SDAS bodies are contemporaneous with and transition from submarine fan deposits. One hypothesis that be offered is that SDAS facies represents a deceleration of unconfined turbidity flows on the margin of these submarine fans. The observed basinward thinning trend would support this notion. However, seismic resolution on available YucatanSPAN seismic data is insufficient to map the exact basinward transition over the extent of these geobodies.

Structural Controls

Prominent Neogene orogenic activity in Mexico and the associated narrow shelf to slope profile probably accentuated transport of terrigenous sediments through coeval canyons directly to the basin (Figure 4.16). Is proposed that Cañonero canyon was particularly important for sediment bypass to the Veracruz Trough. The contemporaneous Mexican Ridges may also played a role by forcing south-flowing longshore flow and along slope flow into the Cañonero Canyon.

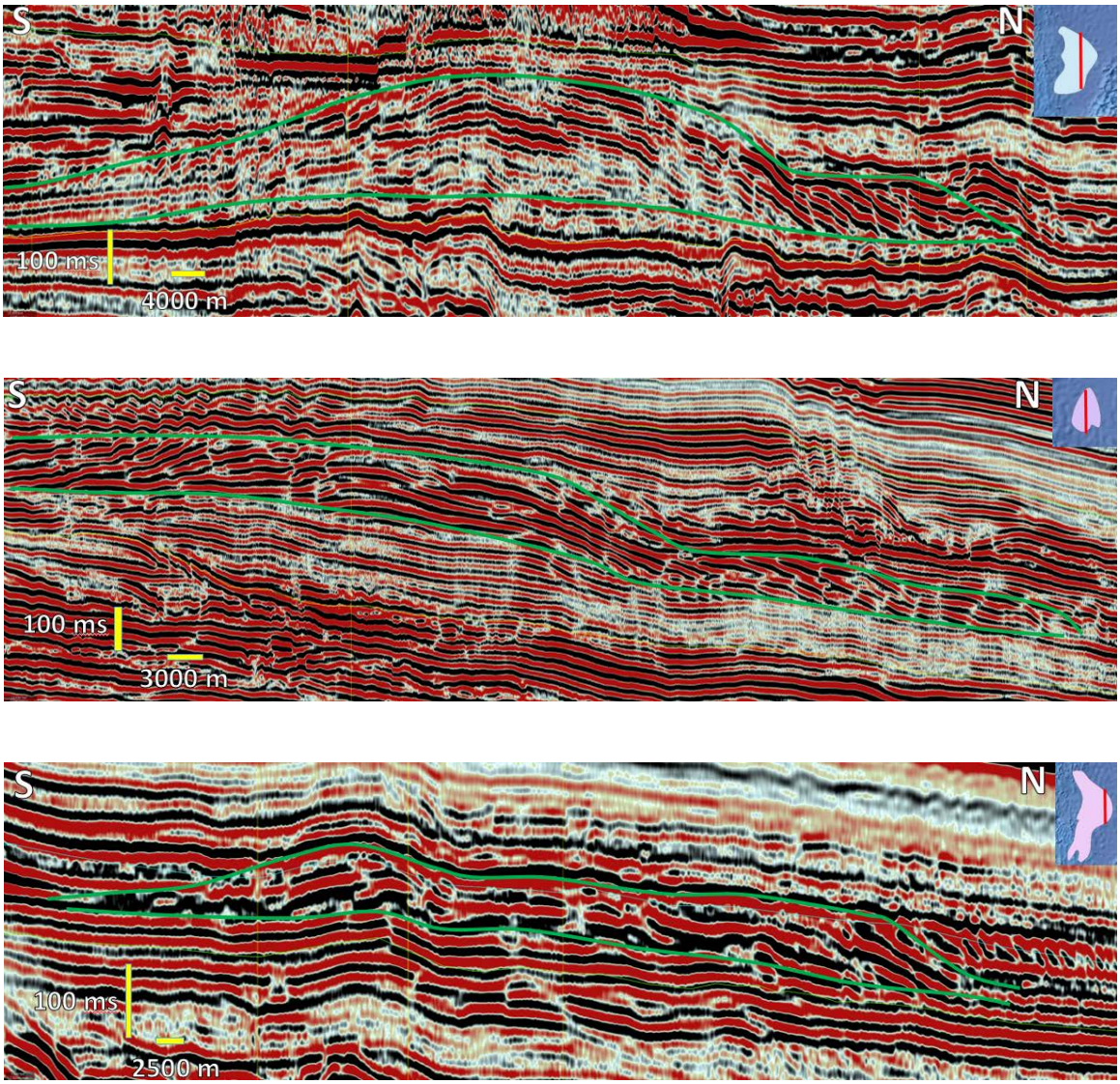

Figure 4.17 Cross-section of the SDAS geobodies 1, 2 and 3 showing spatial and temporal association lobe shape bodies interpreted as submarine fan mounds.

Analog

In some respects, the west margin of the Neogene Gulf of Mexico is very similar to the central Japan Sea where long Toyama deep-sea channel (TDSC) submarine conduits descend from the steep rifted margin (> 1000m relief), transporting sediments from the mountain range and bypassing the narrow shelf (<4km) and steep slope (> 15 degrees) to the basin floor (Figure 4.17).

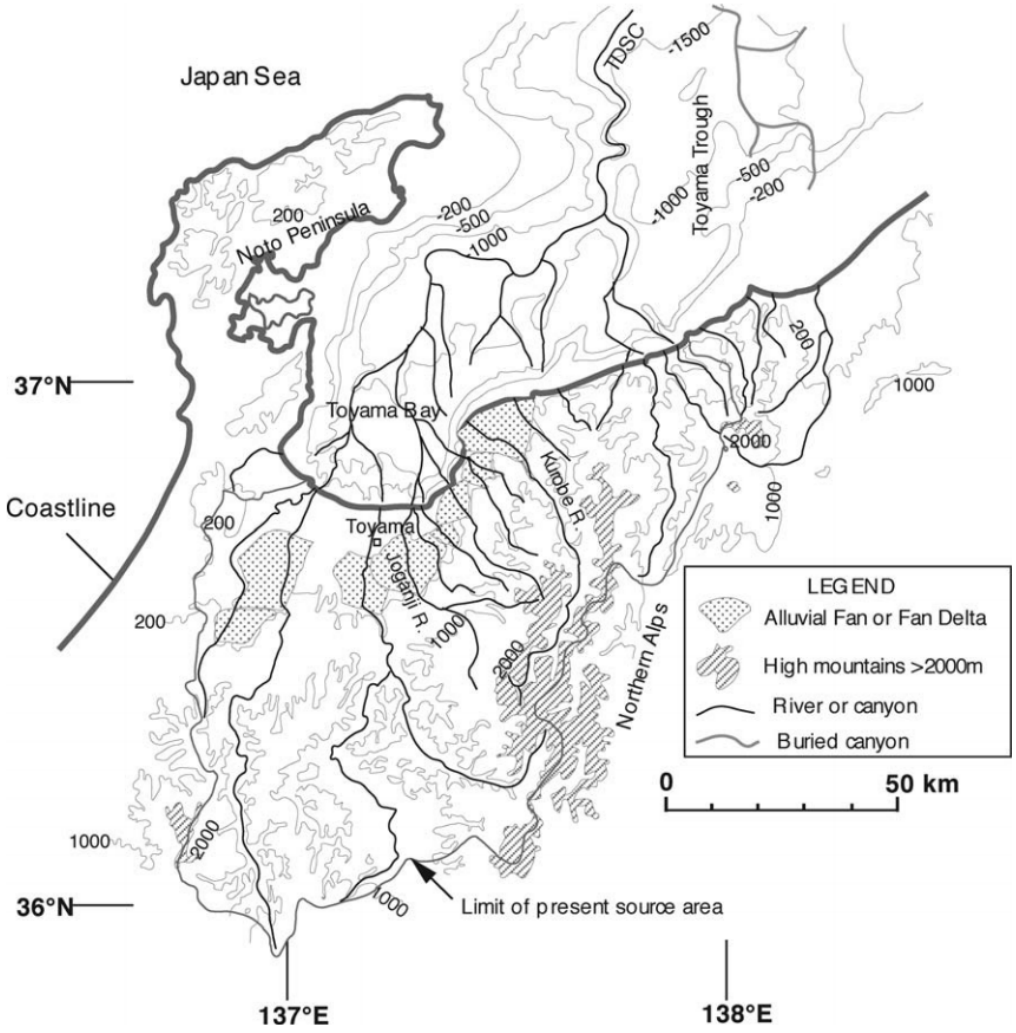

Figure 4.18 Topographic map of the Toyama Deep-Sea Channel system (Nakajima, 2006).

Here, episodic hyperpycnal flows from delta mouths produce a whole range of rhythmic bedding types in the terminal fan zone (Nakajima, 2006). There are seaward dipping reflections with wavelengths from 0.2 to 3.6 km and amplitudes from 2 to 44 km, similar to what we have in Gulf of Mexico. These interpreted as overbanking turbidity currents formed by flows 30 to 500 m thick just as our flows for Geobody 2.

In Japan the acceleration of turbidity currents on the steep slope probably increase their mass, momentum and thickness, akin to what is inferred for the southern Gulf of Mexico. Frequent hydrologic events such as floods may generate density underflows such as observed in the Japan Sea. Cyclic steps are believed to reflect variable flow behavior and hydrographic pattern of river floods, combined with the varying impact of the deltaic or basin-margin slope. In Japan, 700-km long runout hyperpycnal currents are linked to frequent extreme floods, with estimated duration of 10 to 24 days, generated almost every 5 to 7 years (Nakajima, 2006). Such frequent extreme floods could also have been the stimulus for formation of compound sets of SDAS bedforms in the Neogene strata of deep-water Mexico.

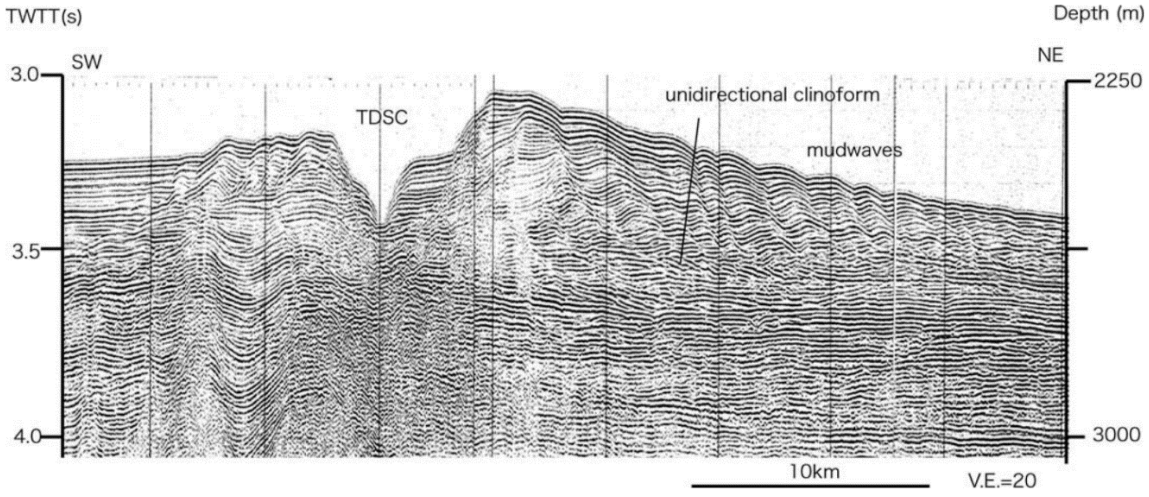

Figure 4.19 Seismic reflection profile across the TDSC. Modified from Nakajima, 2006.

5. CONCLUSIONS

The shingled seismic clinoforms previously identified by Snedden et al. (2012) were analyzed in this project as Seaward Dipping Accretion Sets (SDAS). The SDAS were present in four geobodies, two of Upper Miocene age, one in the PGa and another in the PL1 genetic sequence. These three intervals were mapped using new or reprocessed 2D seismic lines. Time structure maps of these genetic intervals show progressive infill of the deep-water Veracruz Trough from the southwest. SDAS bodies are located in distal and deepwater areas at the east of the Mexican Ridges. Isochron maps show how these geobodies thin basinwards, paralleling observed trends of adjacent submarine fans. Regional mapping further suggests that the SDAS seismic facies are associated with and form distal portions of previously identified submarine fans for the most part.

Snedden et al. (2012) interpreted these SDAS as contourite drift deposits but recently acquired seismic shows a series of internal bedforms climbing upwards that can be interpreted as cyclic steps bedforms deposited by high-velocity turbidity flows. Cyclic steps are thought to form under supercritical flows that exceed most bottom current magnitudes. Seismic observations and dimensions of the SDAS geobodies are consistent with the definition that these are morphodynamic features characterized by a cyclic series of long-wave, upstream-migrating bedforms.

The cyclic steps are products of high-density, high velocity turbidity currents that may have originated as density underflows at adjacent river mouths (hyperpycnal flows). Cyclic steps can also form when sediment-laden turbidity flows transition from confined settings (e.g. canyons) to unconfined environment. This is likely for geobodies 1, 2 and 3. Geobody 2 is associated with an adjacent channel complex and may be a product of unconfined, levee overbanking flows, although 2D seismic data here is sparse.

The deep-water geobodies 1, 2 and 3 formed during an episode of high precipitation, modulated by contemporaneous tectonics (e.g. uplift of the Trans-Mexican Volcanic Belt). Paleogeographic mapping depicts a narrow shelf and slope that may have allowed frequent bypass of sediments to the basin. Development of the Mexican Ridges foldbelt linked to the contemporaneous Quetzalcoatl extensional system, may have steered both longshore and along slope flow into the nearby Cañonero Canyon. It is proposed that the Cañonero canyon was a zone of sediment bypass, diverting turbidity flows to the east. The early forming Mexican Ridges may have created a steep slope gradient and bottom roughness that facilitated local development of hydraulic jumps, a prerequisite for generation of cyclic steps bedforms. Identification of these unique bedforms in Pliocene and Miocene strata of deepwater Mexico represents one of first documented occurrences in subsurface settings, complementing previous models built on observations from modern systems and experimental models.

APPENDIX

Kunah-1 Well

Core N2a: Upper Miocene

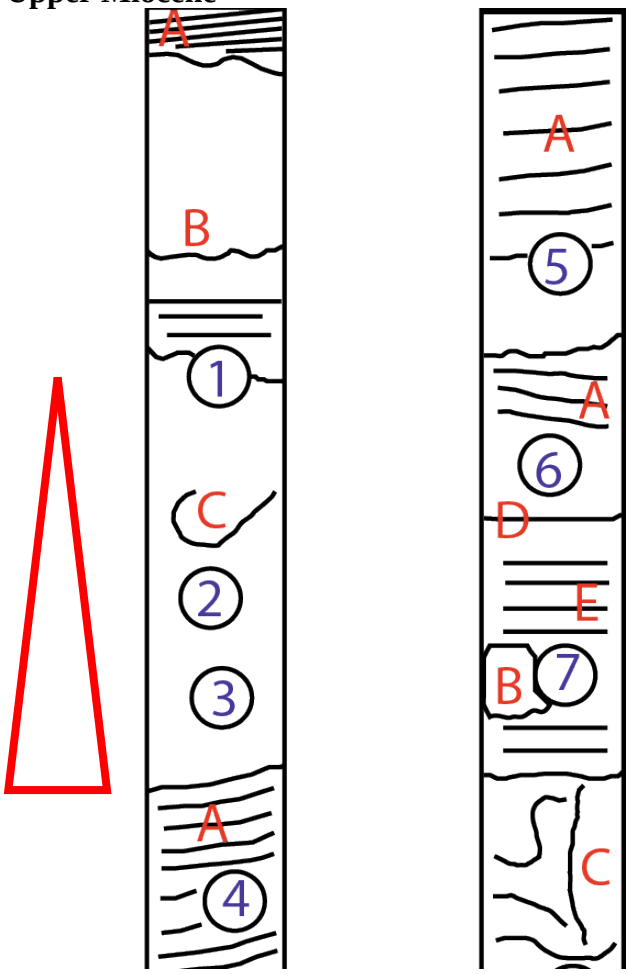

Structures:

A = Inclined Laminations (Tb or Tt turbidites)

B = Core disturbance

C = Fluid escape (dish) structure (Ta turbidite)

D = Sharp or scoured contact

E = Horizontal laminations (Tb turbidite)

Grain analysis:

1: Folk Av. GS = 12 microns; SS = 13.5%;

2: Folk Av. GS = 48 microns; SS = 52.8%;

3: Folk Av. GS = 51 microns; SS = 57%;

4: Folk Av. GS = 9 microns; SS = 9.1%;

5: Folk Av. GS = 5 microns; SS = 1.4%;

6: Folk Av. GS = 38 microns; SS = 43.4%;

7: Folk Av. GS = 8 microns; SS = 6.1%;

Core N2b: Upper Miocene

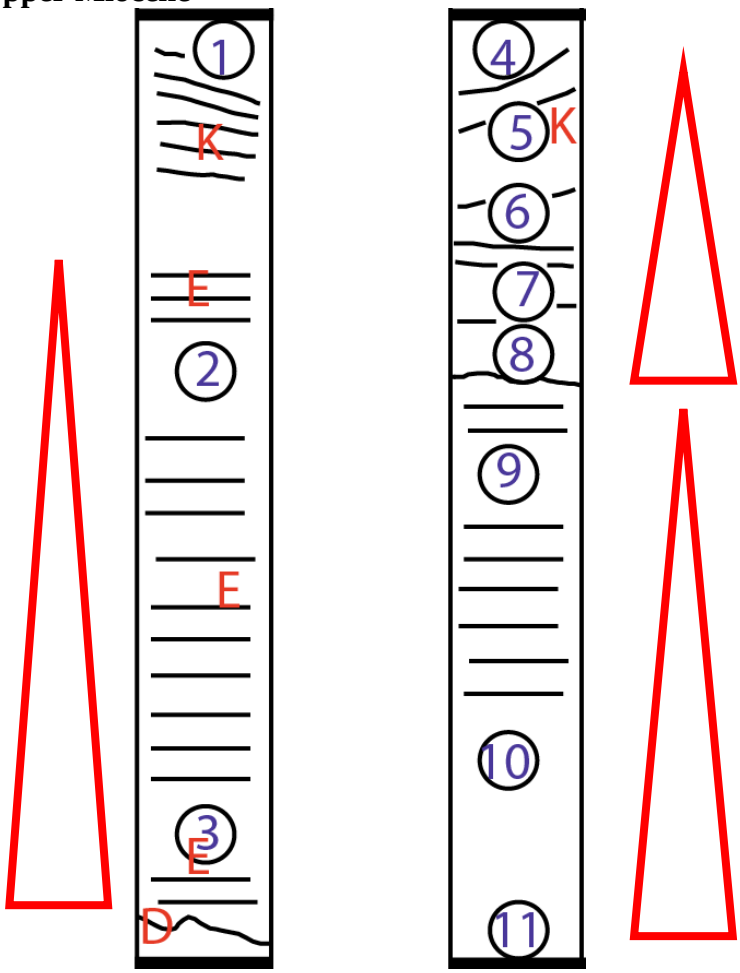

Structures:

K = Cross lamination

D = Sharp or scoured contact

E = Horizontal laminations (Tb turbidite)

Grain analysis:

1: Folk Av. GS = 41 microns; SS = 46.6%;

2: Folk Av. GS = 7 microns; SS = 2.2%;

3: Folk Av. GS = 12 microns; SS = 6.2%;

4: Folk Av. GS = 9 microns; SS = 2.1%;

5: Folk Av. GS = 29 microns; SS = 31.9%;

6: Folk Av. GS = 44 microns; SS = 46.8%;

7: Folk Av. GS = 35 microns; SS = 41.9%;

8: Folk Av. GS = 11 microns; SS = 11.5%;

9: Folk Av. GS = 12 microns; SS = 10.2%;

10: Folk Av. GS = 9 microns; SS = 7.6%;

11: Folk Av. GS = 40 microns; SS = 45%;

Core N3: Middle Miocene

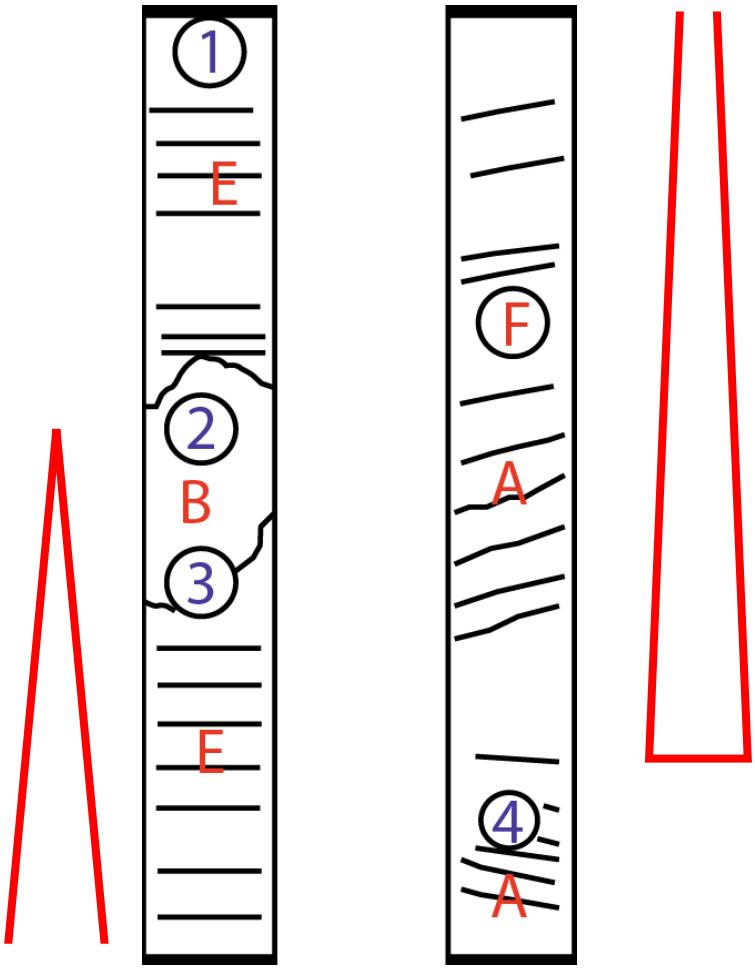

Structures:

A = Inclined Laminations (Tb or Tt turbidites)

B = Core disturbance

E = Horizontal laminations (Tb turbidite)

Grain analysis:

1: Folk Av. GS = 221 microns; SS = 84%

2: Folk Av. GS = 156 microns; SS = 78.2%

3: Folk Av. GS = 194 microns; SS = 82.3%

4: Folk Av. GS = 96 microns; SS = 62.3%

Core N4a: Lower Miocene

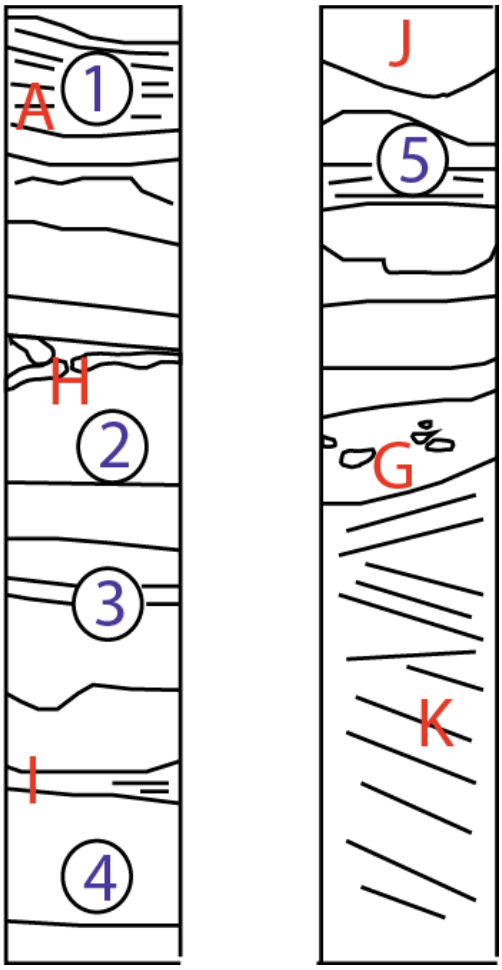

Structures:

A = Inclined laminations (Tb or Tt turbidites)

H = Burrows

I = Ripples

J = Load structure

G = Shale clasts

K = Cross lamination

Grain analysis:

1: Folk Av. GS = 14 microns; SS = 51%

Core N4b: Lower Miocene

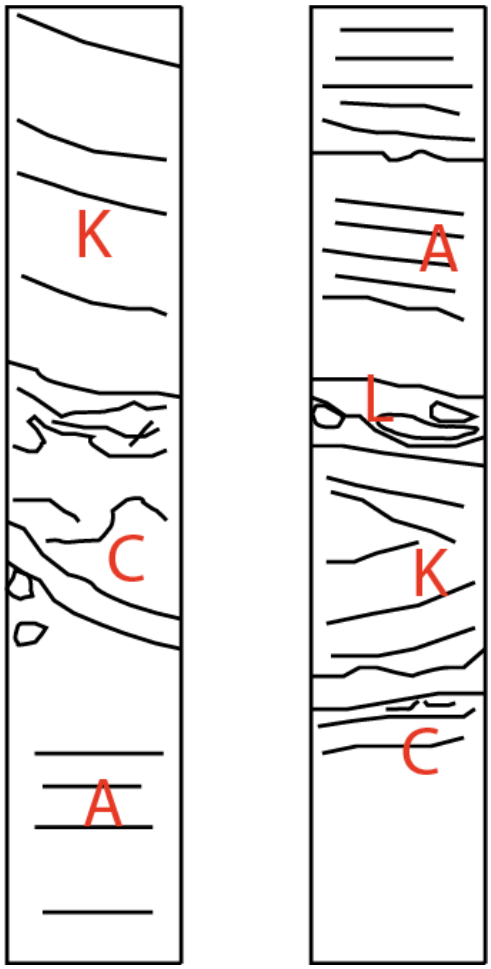

Structures:

A = Inclined Laminations (Tb or Tt turbidites)

B = Core disturbance

C = Fluid escape (dish) structure (Ta turbidite)

D = Sharp or scoured contact

E = Horizontal laminations (Tb turbidite)

REFERENCES

Allen, J.R.L. (1982a) Sedimentary Structures: Their Character and Physical Basis. Development in Sedimentology: 30, part I. Elsevier, Amsterdam.

Arreguín-López, M. A., G. Reyna-Martínez, H. Sánchez-Hernández, A. Escamilla-Herrera, and A. Gutiérrez-Araiza, (2011), Tertiary turbidite systems in the southwestern Gulf of Mexico: Gulf Coast Association of Geological Societies Transactions, v. 61, p. 45–53.

Ambrose, W. A., K. Fouad, S. Sakurai, D. C. Jennette, L. F. Brown Jr., E. H. Guevara, D. B. Dunlap, T. F. Wawrzyniec, S. C. Talukdar, M. A. Garcia, U. H. Romano, H. R. Ruiz, R. C. Hernández, J. A. Vega, and E. M. Zamora, (2005), Neogene tectonic, stratigraphic, and play framework of the southern Laguna Madre – Tuxpan continental shelf, Gulf of Mexico, in C. Bartolini and J. R. Román Ramos, AAPG Bulletin, v. 89, no. 6, pp. 725– 751

Cartigny, M.J.B., van den Berg, J.H., Mulder, J., Postma, G., (2009). Stability and morphodynamics of bedforms of the upper flow-regime. Proceedings 33rd IAHR Congress Vancouver.

Cartigny, M. J. B., G. Postma, Van den Berg, Jan H., Martbergen Dick R. (2011). A comparative study of sediment waves and cyclic steps based on geometries, internal structures and numerical modeling. Marine Geology 280 (1-4): 40-56.

Cserna, Z. de, (1989), An outline of the geology of Mexico: The Geology of North America – An overview: Vol. A, The Geological Society of America, p. 233-264.

Covault, J.A., Kostic, S., Paull, C.K., Ryan, H.F., Fildani, A., (2014). Submarine channel initiation, filling and maintenance from sea-floor geomorphology and morphodynamic modelling of cyclic steps. Sedimentology 61 (4), 1031–1054.

Moran-Zenteno, Dante J., Martini, B., Tolson, G., (2000). Geocronología y características geoquímicas de las rocas magmáticas terciarias de la Sierra Madre del Sur. Boletin de la Sociedad Geologica Mexicana LIII: 27 - 58.

Feng, J., (1995), Post mid-Cretaceous seismic stratigraphy and depositional history, deep Gulf of Mexico: Ph.D. dissertation, University of Texas at Austin, Austin, Texas, 253 p.

Feng, J., R. T. Buffler, and M. A. Kominz, (1994), Laramide orogenic influence on late Mesozoic–Cenozoic subsidence history, western deep Gulf of Mexico basin: Geology, v. 22, p. 359–362.

Ferrari, L., Orozco-Esquivel, T., Manea, V., Manea M., (2012). The dynamic history of the Trans-Mexican Volcanic Belt and the Mexico subduction zone. Tectonophysics 522-523: 122-149.

Ferrari, L., Tagami, T., Eguchi, M., Orozco-Esquivel, Ma. T., Petrone, Chiara M., Jacobo-Albarran, J., Lopez-Martinez, M., (2005). Geology, geochronology and tectonic setting of late Cenozoic volcanism along the southwestern Gulf of Mexico: The Eastern Alkaline Province revisited. Journal of Volcanology and Geothermal Research 146(4): 284-306.

Flood, R.D., Piper, D.J.W., Klaus, A., (1995). Proceedings of the Ocean Drilling Program Initial Report, vol. 155 (1233 p.)

Galloway, W. E., Ganey-Curry, P.E., Li, X., Buffler, Richard T., (2000). Cenozoic depositional history of the Gulf of Mexico Basin. AAPG Bulletin 84(11): 1743-1774.

Guzman, E. and Cserna, Z., (1963). Tectonic History of Mexico. American Association of Petroleum Geologists 2: 113 - 129.

Gomez-Cabrera, P. T., and Jackson, M. P. A., (2009), Regional Neogene salt tectonics in the offshore Salina del Istmo Basin, southeastern Mexico, in C. Bartolini and J. R. Román Ramos, eds., Petroleum systems in the southern Gulf of Mexico: AAPG Memoir 90, p. 1–28.

Hudec, Michael R., Norton, Ian O., Jackson, Martin P. A., Peel, Frank J. (2013). Jurassic evolution of the Gulf of Mexico salt basin. AAPG Bulletin, V. 97, No. 10, PP. 1683-1710.

Jacobo A., J., Garduño, M., Innocenti, F., Manetti, M., Pascuaré, G., Tonarini, S., (1992), Datos sobre el vulcanismo geogénico-reciente del Complejo Volcánico de Los Tuxtlas, Edo. De Veracruz, México: Evolución petrológica y geovulcanológica: 11 Convención Geológica Nacional, Veracruz, Libro de Resúmenes, p. 97-98

Kostic, S. (2011) Modeling of submarine cyclic steps: controls on their formation, migration, and architecture. Geosphere, 7, 294–304.

Kubo, Y., Nakajima, T., (2002). Laboratory experiments and numerical simulation of sediment-wave formation by turbidity currents. Marine Geology 192 (1–3), 105–121.

Nakajima, T., (2006) Hyperpycnites deposited 700 Km away from river mouths in the central Japan Sea. Journal of Sedimentary Research. V. 76, PP. 60 – 73.

Normark, W.R., Hess, G.R., Stow, D.A.V., Bowen, A.J., (1980). Sediment waves on the Monterey Fan levee: a preliminary physical interpretation. Marine Geology 37 (1–2), 1–18.

Normark, W.R., Piper, D.J.W., Posamentier, H., Pirmez, C., Migeon, S., (2002). Variability in form and growth of sediment waves on turbidite channel levees. Marine Geology 192 (1–3), 23–58.

Padilla, R. (2007). Evolución geológica del sureste mexicano desde el Mesozoico al presente en el contexto regional del Golfo de México. Boletin de la Sociedad Geologica Mexicana LIX (1): 19 - 42.

Potter, P. E., Szatmari, P., (2009), Global Miocene tectonics and the modern world: Earth Science Reviews, v. 96, p. 279–295.

Rebesco, M., Hernandez-Molina, F. J., Van Rooji, D., Wahlin, A., (2014) Contourites and associated sediments controlled by Deep-water circulation processes: State-of-the-art and future considerations. Marine Geology 352 PP. 111 – 154

Rodriguez, A. B., (2011). Regional structure, stratigraphy, and hydrocarbon potential of the Mexican sector of the Gulf of Mexico. Jackson School of Geosciences. The University of Texas at Austin.

Rodriguez, A. B., and P. Mann, (2011), Origin of the Mexican Ridges passive margin foldbelt based on seismic and well integration from the shelf-slope-deep basin and structural restoration: American Association of Petroleum Geologists Search and Discovery

Salomon-Mora (2011). Tectonics, Structure, and Hydrocarbon Potential of the Mexican Ridges Fold Belt, Western Gulf of Mexico.

Salvador, A. (1987). Late Triassic-Jurassic Paleogeography and origin of Gulf of Mexico Basin. The American Association of Petroleum Geologists Bulletin 71(4): 419-451.

Schaaf, P., Moran-Zenteno, D., Hernández-Bernal, María del S., Solís-Pichardo, G., Tolson, G., Kohler, H., (1995). Paleogene continental margin truncation in southwestern Mexico: Geochronological evidence. Tectonics 14(5): 1339-1350.

Smith, D.P., Ruiz, G., Kvitek, R., Iampietro, P.J., (2005). Semiannual patterns of erosion and deposition in upper Monterey Canyon from serial multibeam bathymetry. Geological Society of America Bulletin 117 (9–10), 1123–1133.

Snedden, John W., Galloway, William E., Whiteaker, Timothy L., Ganey-Curry, Patricia E. (2012) Eastward Shift of Deepwater Fan Axes during the Miocene in the Gulf of Mexico: Possible Causes and Models. GCAGS Journal, V. 1 (2012), p. 131 – 144.

Vazquez-Meneses, M. E. (2005). Gravity Tectonics, Western Gulf of Mexico. Department of Geology, Royal Holloway University of London.

Yarbuh, I., Contreras, J., (2015). The interplay between deformation, erosion and sedimentation in the deep-water Mexican Ridges foldbelt, western Gulf of Mexico basin. EAGE Basin Research PP. 1 – 19.